The Biochemical Energy Balance of the Coral Symbiosis

Johanna Howes

December 2015

This thesis is submitted in fulfilment of the requirements for the degree of Doctor of Philosophy in Science

Aquatic Photosynthesis Group

Climate Change Cluster

School of Life Sciences

University of Technology Sydney

Certificate of Original Authorship

I certify that the work in this thesis has not previously been submitted for a degree nor has it been submitted as part of requirements for a degree except as fully acknowledged within the text.

I also certify that the thesis has been written by me. Any help that I have received in my research work and the preparation of the thesis itself has been acknowledged. In addition, I certify that all information sources and literature used are indicated in the thesis.

Date:

Acknowledgements

There are too many people to count that I need to thank for their invaluable assistance, but I'm going to try. A huge thank you needs to go to the technical support staff for both the department of Chemistry and C3 with a specific thank you to Paul Brooks, Ronald Shimmon and Linda Xiao. Sutinee Sinutok, Katherina Petrou and Ross Hill provided vital assistance with experimental design, experimental execution and a biology crash course that I desperately needed. A huge thank you also to Milán Szabó for his incredible literature searching skills and encyclopaedic knowledge of photosynthetic function.

A special thanks goes to Olivia Sackett for being amazing, travelling to Wisconsin and providing much-needed advice and encouragement. Thanks also to the IR beamline staff at both the Synchrotron Radiation Center in Madison, WI and the Australian Synchrotron in Melbourne. Specifically Julia Sedlmair for looking after us in Wisconsin and Keith Bambery for help with data processing. Phil Heraud and Carol Hirschmugl also gave me amazing ideas and direction for tricky imaging data at WIRMS 2013 and beyond. This work was made possible by funding provided by C3, as well as the International Synchrotron Access Program (ISAP) through the Australian Synchrotron.

Thank you to my fellow C3 PhD candidates for the countless emergency coffee runs and for listening to my experimental woes. Similar thanks goes to my fellow first year chem tutors for (safe) laboratory shenanigans. Thank you to my best friend, Camille and Sarah, who surprised me with my "Cheer Squad Box" filled with encouraging messages from friends and family. Thank you to my incredible Mum, Dad and sister, for putting a roof over my head when I needed it, endless encouragement, love and unwavering support. And thanks for listening to me vent when you didn't understand a word I was saying.

And finally, thank you to my amazing supervisors, Peter Ralph and Barbara Stuart. None of this would have been remotely possible without your encouragement, advice, excitement, experimental help, red-pen-covered thesis edits, pushing me to achieve my best, fighting for me when I needed it and commiserating when things didn't go the way I wanted them to. I have no words to tell you both how much I have appreciated this opportunity and your help.

Table of Contents

List of Figures

List of Tables

Abbreviations

ANOVA	Analysis of variance
ATP	Adenosine triphosphate
ATR	Attenuated total reflectance
BSA	Bovine serum albumin
CD	Circular dichroism
Chl *a*	Chlorophyll a
DNA	Deoxyribonucleic acid
EMSC	Extended multiplicative scatter correction
FPA	Focal plane array
FTIR	Fourier transform infrared
GBR	Great Barrier Reef
GC-MS	Gas chromatography – mass spectrometry
HCA	Hierarchical clustering analysis
Hsp	Heat shock protein
IR	Infrared
IRENI	Infrared environmental imaging
LHC	Light harvesting complex
MS	Mass spectrometry

NMR	Nuclear magnetic resonance
OEC	Oxygen evolving complex
PAM	Pulse amplitude modulated
PCA	Principal component analysis
PCP	Peridinin-chlorophyll-protein
PLS	Partial least squares
PLSDA	Partial least squares discriminant analysis
PSI	Photosystem I
PSII	Photosystem II
rmANOVA	Repeated-measures analysis of variance
RMSEP	Root mean square error of prediction
SEM	Standard error of the mean
sp.	Species
SRC	Synchrotron Radiation Center
SST	Sea surface temperature
TEM	Transmission electron microscopy
XRD	X-Ray diffraction

Abstract

Over the last three decades, coral reefs around the world have declined by an estimated 51%. This has largely been caused by anthropogenic climate change resulting in increases in ocean acidification and sea surface temperatures. At their core, corals are a symbiotic relationship between a microscopic algae of the genus *Symbiodinium* known as “zooxanthellae”, the cnidarian coral host and associated bacterial communities. Under severe environmental stress, the coral will expel the algae. This results in the host losing its major source of organic carbon.

Extensive research into tolerance of the algae, have revealed a large genetic diversity within the genus *Symbiodinium* and it is thought that macromolecular content (carbohydrates, proteins, lipids and phosphorylated compounds) have an effect on biochemical processes responsible for energy acquisition and repair of photosynthetic membranes within the cells. Metabolomics, the study of macromolecular compounds within a biological system, has been applied in various forms, to describe individual compounds such as fatty acids or sterols, contained within different clades of *Symbiodinium*.

In this study, two clades of *Symbiodinium* sp. were chosen based on their differing tolerance to environmental stress, and analysed to investigate macromolecular changes in the face of fluctuations in light and temperature. Under normal growth conditions, clades of *Symbiodinium* sp. differed in protein and lipid structure. This is the first time this has been reported to date.

In order to further explore these differences in macromolecular content and structure, the cells were subjected to sub-lethal light and temperature treatments. Under these conditions, it was found that both clades increased their β-sheet protein secondary

structure. When exposed to elevated light, lipid was stored and carbohydrate consumed whereas the opposite was found under elevated temperature. This has further implications for nutrient exchange *in hospite.*

Clades of *Symbiodinium* sp. were then exposed elevated temperature to simulate bleaching conditions. Under these high temperatures, clade A was found to exhibit the largest decline in maximum quantum yield of PSII indicating photodamage. This decline in F_v/F_m was linked to changes in lipid and protein secondary structure indicating a change in thylakoid membrane structure occurred under extreme stress. It was also proposed that the change in protein secondary structure was related to protein subunits associated with the oxygen evolving complex, and subsequently photodamage and PSII repair mechanisms.

Synchrotron FTIR spectroscopic chemical imaging was also used to further analyse these changes in *Symbiodinium* sp. from a single-cell perspective. Macromolecular compound groups (protein, lipid, carbohydrate and phosphorylated compounds) were shown to be distributed differently across the cells. Further to this, there appeared to be a difference in the regions in which α-helix and β-sheet protein structures clustered across the individual cells.

Chapter 1. General introduction

1.1 Introduction

Over the last century, scientists have been becoming increasingly concerned about the sudden and dramatic elevation in atmospheric carbon dioxide [1]. This rise has resulted in a global phenomenon known as climate change and has been consistently attributed to anthropogenic activities [2]. The effects of climate change are widespread and are predicted to be devastating; and these effects are most obvious in delicate, yet vital ecosystems such as tropical coral reefs.

Healthy coral reefs are flourishing pockets of biodiversity that exist in some of the oceans' most oligotrophic (low nutrient) waters. Sometimes known as the oceans' rainforests, coral reefs are home to a diverse array of organisms and are estimated to harbour a third of the world's fish species [3]. Many coastal communities rely on the coral reefs for their survival while the ecosystems provide a source of food, clean water, storm protection and building materials [3]–[5].

Under the effects of global anthropogenic climate change, Great Barrier Reef (GBR) coral cover has been estimated to have declined by 51% over the last 30 years [6]. This decrease has been directly attributed to a rise in catastrophic bleaching events largely caused by an increase in sea surface temperature (SST) and solar irradiance [7]. Model predictions for the future health of the reefs are concerning, with these events predicted to occur with increasing frequency and severity over the next 10-15 years [2]. However, these predictions are difficult to quantify given the vast complexity of these ecosystems, both biologically and physically [8].

This thesis aims to provide vital information about macromolecular content of reef-building scleractinian corals using vibrational spectroscopy. The purpose of this introductory chapter is to provide a background for this thesis, covering basic

physiology, genetic diversity of the symbiotic dinoflagellates, and vibrational spectroscopy and its applications.

1.2 The coral symbiosis

Tropical coral reefs generally occupy small pockets of flourishing biodiversity within a high irradiance environment [9]. For nearly 200 million years, the backbone of these reef structures has been formed by the scleractinian corals [7]. These corals are largely responsible for the abundance of life found in these ecosystems as they form the physical structure of the reef. Without them, numerous species would not exist. In order to halt the decline of reefs worldwide, an understanding of how the two symbiotic organisms work in isolation and in partnership is required.

1.2.1 Basic physiology

Scleractinian corals are made up of a community of polyps that cover a calcium carbonate skeleton. These corals are also sometimes referred to as "reef-building" or "hermatypic" corals denoting the gradual build-up of their calcium carbonate deposits, resulting in the reef structures seen around the world. The coral polyps are essentially two different layers of tissue separated by collagen fibrils collectively known as "mesoglea" (Figure 1.1). Each layer of epithelial cells, the ectoderm and endoderm, have different roles; the ectodermis protects the polyp with cnidoblast 'stinging' cells, and the calicoblastic epithelium (endodermis) provides attachment and synthesises the calcium carbonate skeleton [3], [10].

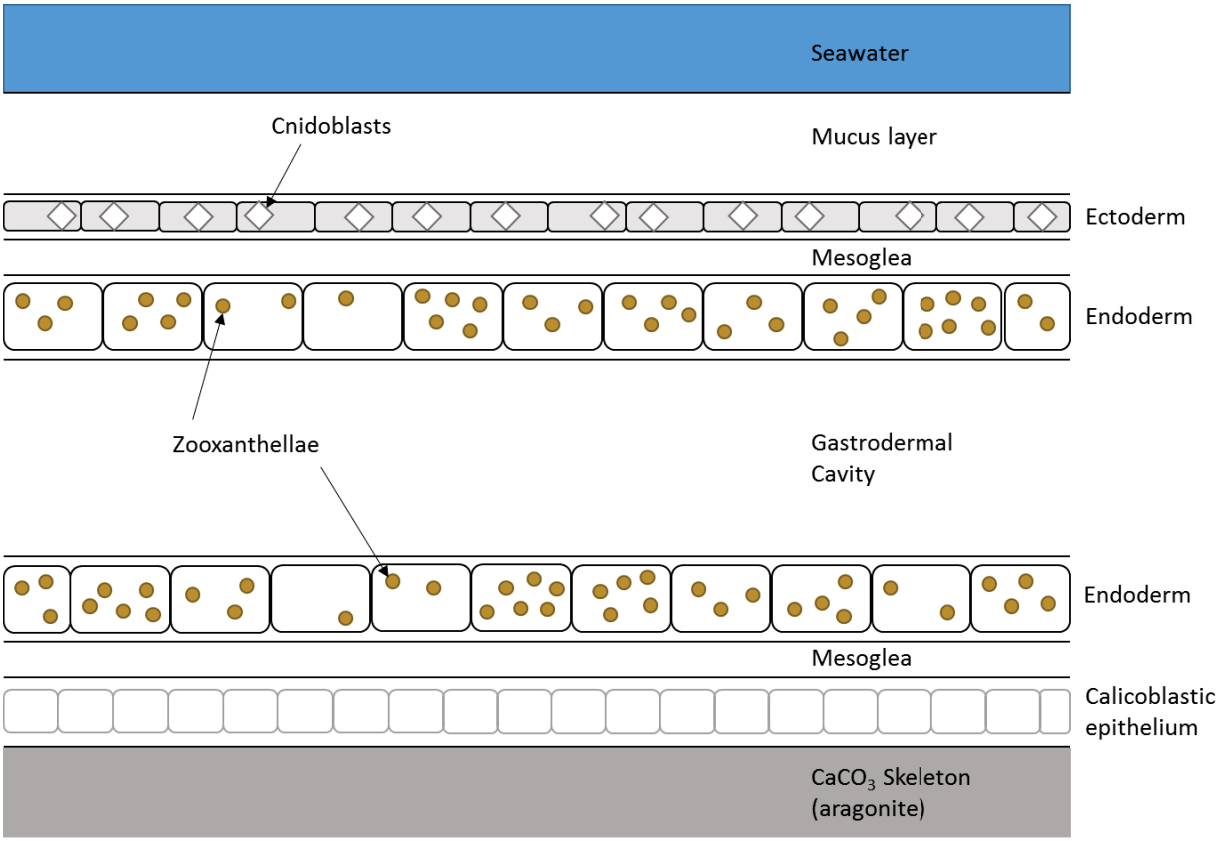

Figure 1.1: Cross-section of a coral polyp [11]–[13].

In the centre of the polyp is the gastrodermal cavity where zooplankton and bacteria are digested. This is lined by another layer of epithelium called the endoderm. These cells are home to between one and six symbiotic, dinoflagellate microalgae known as "zooxanthellae" [10], [12].

Due to the mixotrophic nature of the coral-zooxanthellae symbiosis, there is a large amount of nutrient exchange occurring; see Figure 1.2 as a schematic representation of this exchange [10], [12], [14]–[18]. Corals require a large amount of organic carbon that cannot be obtained entirely from heterotophic feeding sources [19]. So the coral host must rely on the photosynthetic algae for up to 90% of its daily carbon needs [12]. Photosynthate is transported from the zooxanthellae to the host mostly in the form of glycerol, but also lipids, fatty acids and organic and amino acids [20]. In turn, the

zooxanthellae receive dissolved inorganic nitrogen, carbon and phosphate from the host, which they would normally acquire directly from the surrounding waters were they not encased in coral tissue. And so the algae recycles the coral's waste products, urea, CO_2, ammonium and polyphosphates [8].

This nutrient exchange between the two organisms is a delicate balance that is inextricably linked to their surrounding environmental conditions. Any shift in either of the host or symbiont's function due to environmental changes, affects the whole organism [19]. It is little wonder that this partnership is facing such dire consequences in the face of global climate change.

1.2.2 Photosynthesis and photoinhibition

Observations made over recent decades have indicated a concerning increase in "mass bleaching events", where multiple species of corals over wide areas of the ocean lose their zooxanthellae and/or their photosynthetic pigments are degraded. An overall decrease in scleractinian coral cover has been reported for the Great Barrier Reef and other reef systems around the world [12]. Decreases of this nature have wider social and economic implications as well as the devastating loss of ecosystems and biodiversity. Given the complexity of this delicate symbiotic relationship, an understanding of the underlying mechanism of bleaching and coral mortality is still elusive despite the extensive literature on this subject [12], [21]–[26].

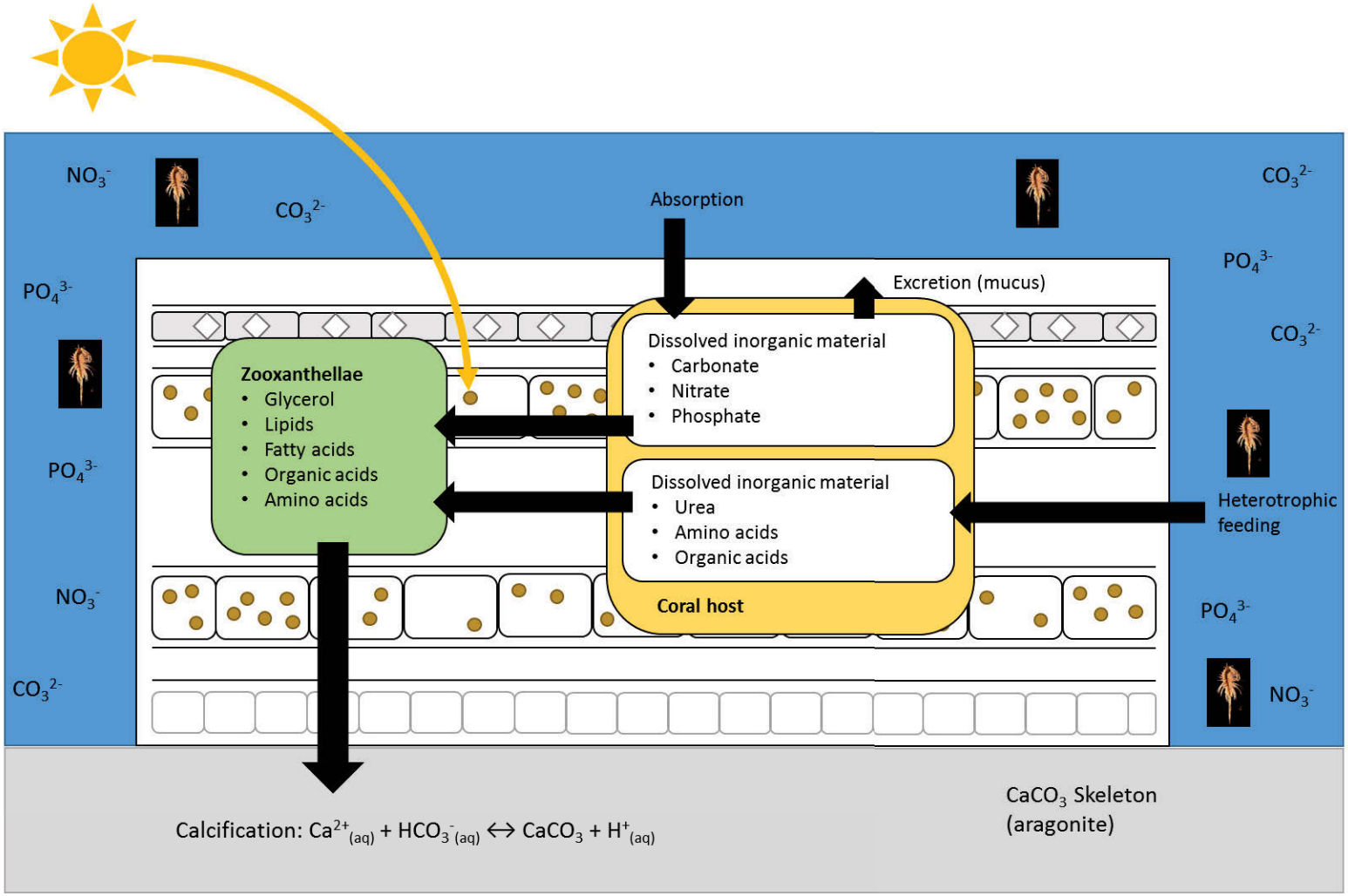

Figure 1.2: Schematic representation of the metabolic products exchanged within the coral symbiosis.

The delicate and complicated energy balance within the coral symbiosis can be severely affected by changes in temperature, salinity, pH and light intensity, all inducing coral bleaching [27], [28]. The specific mechanism of coral bleaching is not yet known, however, there is a consensus amongst scientists that bleaching involves a disruption of the symbiotic relationship between the zooxanthellae and their coral host [9]. Under stress, the coral will expel their symbiotic algae, resulting in a loss of pigment, hence the coral is said to have been "bleached" [22], [29], [30].

The zooxanthellae have long been thought to hold the key to the trigger of the bleaching process [12]. This is largely due to these organisms' photosynthetic processes that have been known to breakdown under increasing environmental pressure [23]. At the centre of the zooxanthellae cells is an organelle common to all photosynthetic organisms, called the chloroplast. This contains the thylakoid membranes, stacked grana housing large protein complexes called photosystems. These complexes are responsible for generating the energy required to fix organic carbon, which is the main source of energy transferred to the host from the symbiont [21], [31], [32].

Of the two photosystems, I and II (PSI and PSII), PSII is thought to be the site of initial damage within the zooxanthellae [33][34]. This protein complex begins the chain of light-dependent reactions culminating in the formation of ATP which goes on to energise the Calvin cycle and carbon fixation [32]. PSII also generates oxygen through the Oxygen Evolving Complex (OEC). At the centre of the OEC is a metalloprotein complex made up of calcium and manganese [35], [36].

The OEC has recently been proposed to be a site of photodamage causing a process known as photoinhibition [21], [33], [37], [38]. The thylakoid membranes are susceptible to excess light and a build-up of reactive toxic oxygen species and so it

contains a number of repair mechanisms [21]. These include dissipation of excess light as heat and disassembly and subsequent repair of the PSII D1 protein centre. If these repair mechanisms cannot keep up with the rate of damage, then cells will enter a photodamaged state where net productivity of the cells is significantly diminished as the electron transport driving carbon fixation declines [21].

The exact molecular trigger for photoinhibition and ultimately coral bleaching, is still somewhat elusive. What is becoming increasingly apparent is the importance of the zooxanthellae's role in causing and mitigating bleaching. These processes rely on a number of macromolecular compounds (proteins, lipids, carbohydrates and phosphorylated compounds such as amino acids and DNA). A breakdown in function of one of these components has a direct effect on the productivity of the cells [21], [32], [33]. Hence, the study of metabolic function and biochemistry of these cells is vital to gain a comprehensive map of how these organisms behave under environmental stress.

1.3 Analysis of *Symbiodinium* sp.

For many years, zooxanthallae ("zoox" for animal and "xanth" for yellow [39]), were thought to belong to a single species of algae. This species was first described by Hugo Fruedenthal in 1962 [40]. Since that time, these symbiotic algae have been classified into a number of different, unique species, as well as genetic clades of the same species, *Symbiodinium* [41].

In a review published in 2012, Fernando Gomez compiled a comprehensive list of currently known dinoflagellate species. He found that twenty one species, less than 1% of the total list of dinoflagellates were endosymbiotic. Fifteen of these symbiotic species were of the genus *Symbiodinium* [42]. These algae have been found in symbiosis with a wide array of organisms including anemones, giant clams,

foraminifera, sponges and cnidarian corals [39], [41]. Since it was found that zooxanthellae differed in their biochemistry and response to stress [43], research into the genetic diversity amongst *Symbiodinium* has been extensive.

1.3.1 Genetic diversity and tolerance

Until the 1970s, and the advent of more complex molecular analysis techniques, not much was known about the genetic diversity within this specific type of dinoflagellate. Figure 1.3 shows the nine clades of *Symbiodinium* sp. currently identified and their associated host organisms [39], [44]–[46]. Within these clades, an additional layer of diversity has also been noted; for example clades F and C can be specifically split into multiple sub-clades [44], [47].

Symbiodinium sp. is sometimes called a "key-stone" species, due to its wide array of associations with different symbiotic organisms [41]. These cells are not only spread across different symbiotic hosts, but also distributed across different geographic regions [41], [45]. Available literature covering this topic, ranges from global distribution patterns to diversity within small reef communities [48], [49]. Depth gradients within a reef system have also been known to cause a pattern in symbiont diversity [50] and some organisms can also harbour a number of different clades of *Symbiodinium* sp. [41]. One possible reason for these distribution patterns is their tolerance to specific environmental conditions. *Symbiodinium* exhibit varying degrees of plasticity, both metabolically and in their photosystem repair [51], [52].

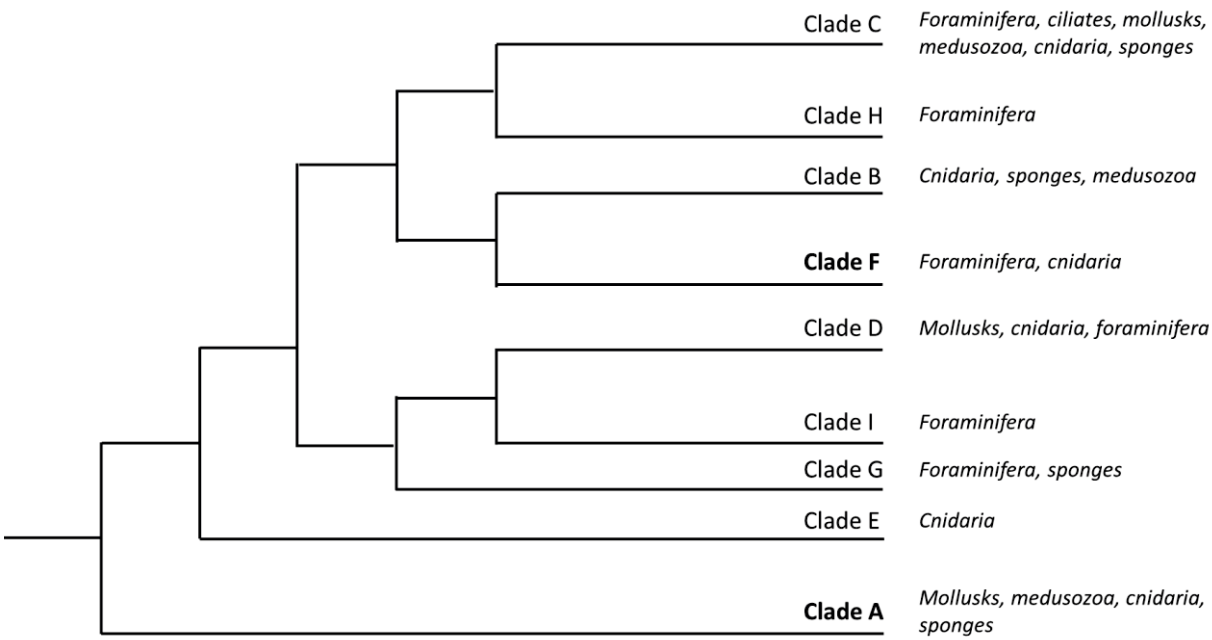

Figure 1.3: Genetic clades of *Symbiodinium* sp. and their associated hosts. Clades used for this thesis are in bold. Phylogenetic tree adapted from Coffroth and Santos (2005).

A large amount of research has revealed a marked difference in tolerance between genetic clades of *Symbiodinium*, indeed sometimes even between sub-clades. Corals housing different clades exhibited differences in bleaching tolerances [9], [48]. Studies investigating photoinhibition have also discovered clades exposed to thermal stress appear to experience impairment of photosynthetic function at different sites within the chloroplast [52].

Comparisons of thylakoid membrane structures in cultured and freshly isolated *Symbiodinium* clades CS-157 and CS-21 found that there was a difference in PSII melt temperatures [53]. This was considered to be a clear indication that different clades appeared to have different tolerances to thermal stress, even though the temperatures needed to induce irreparable damage to these membranes was extremely high (>35 ^{o}C).

Studies of this nature have served to highlight the incredible complexity of these organisms [23]. *Symbiodinium* cells *in hospite* add an extra layer of intricacy with some

clades showing signs of adaptation to different environments depending on their host species [52], [54]. In order to gain a more complete understanding of these differences in response to stress, research has been turning towards physiological parameters such as macromolecular structure and content, as it relates to photosynthetic function [46], [51], [55], [56]. It is becoming increasingly clear that the link between macromolecular content, structure and photosynthetic function must be established in order to gain a full understanding of how these organisms function.

1.3.2 Macromolecular analysis of *Symbiodinium* sp.

Over recent years, the study of the macromolecular content of *Symbiodinium* sp. has gained increasing interest within the coral research community [20]. The development and improvement of common methods has enabled the analysis of these complex organisms and the components making up these cells. The thylakoid membranes within the symbionts have been known to have varying degrees of fluidity in lipid structure. Given that this is where photosynthetic processes occur, chemical changes to the thylakoid membrane might have some bearing on thermal tolerance [53], [55]. Fatty acid analysis of thylakoid membrane lipids found that they differed significantly in degree of saturation. Specifically, in the ratio between the unsaturated Δ6,9,12,15-*cis*-octadectetraenoic (18:4) acid and the saturated Δ9-*cis*-ocatadecatetraenoic (18:1) [55]. It was proposed that this ratio could provide an indication of thermal tolerance. While this study has been criticised for its experimental bleaching regime, it precipitated further research into this area.

Further to this, fatty acid composition of five different species of *Symbiodinium* grown at different temperatures confirmed that stability of photosynthetic membranes was species-specific, linking photosynthetic function with macromolecular content [53].

Isolation of the thylakoid membrane, the location of all photosynthetic processes, and analysis of the lipid content revealed a number of interesting trends. Although there were significant differences in specific fatty acids (linoleic acid in particular) between clades, thermally tolerant species showed no change in fatty acid with elevated temperature. It was also found that the previously promising ratio between C18:1 and C18:4, was not a reliable indication of whether a clade was thermally tolerant or not [53]. Comparisons of membrane melting temperatures did not correlate with saturation ratio values. For example, two of the least tolerant species analysed, C1 and A1 gave significantly different values for lipid saturation. The authors concluded that fatty acid saturation could be used as an indication of exposure to stress, however they could not determine if a species was thermally tolerant using the ratio of C18:1 and C18:4 alone.

One of the most comprehensive analyses of the macromolecular content of various clades of *Symbiodinium* sp. to date was able to separate a number of specific compounds [51]. These included individual fatty acids, sugars and sterols. Under normal growth conditions, clades were able to be distinguished based on their sterol and sugar content. Multivariate statistical analysis of different clades grown at different temperatures indicated that clades differed significantly in inositol; a cyclic compound largely responsible for phosphorus storage [51]. The authors of this study note that the methods of analysis cannot be specific for the more particular cellular mechanisms driving these changes in macromolecular content.

It has also been proposed that, although some symbiont types may be more thermally tolerant, they are not always energetically beneficial for the coral host. In a study comparing storage lipids between clade types C and D, it was found that the endemic clade C contained 26% more stored energy than D [57]. *In hospite*, the nutrient assimilation of these clades reflected this trend; clade C was found to fix more inorganic

carbon and nitrogen than their more thermally tolerant counterparts, suggesting that while clade D appears to be more robust, clade C might be a faster growing symbiont [26], [58].

This pattern could be related to work analysing the metabolic compounds stored as energy within different clades of *Symbiodinium* sp. such as lipids and carbohydrates [59]. Some more tolerant clades were found to contain higher lipid content, whereas the less tolerant contained more carbohydrates. Lipids were also found to be significantly altered by the host. Analysis of fatty acid chains revealed once more that the level lipid saturation was highest in the more thermally tolerant clades [55], [59]. Research into polyunsaturated lipids within higher plants has found that as the saturation of lipids within membranes increases, the energy available to the organism as lipid decreases [57]. It is therefore generally thought that high levels of saturation results in a decreased tolerance to environmental changes and has some bearing on nutrient exchange within the coral symbiosis.

All of these studies have added significant information towards the analysis of metabolic function within and between clades of *Symbiodinium* sp, both in culture and *in hospite*. However, the majority of these studies seemed to focus on the content of one particular biochemical family, usually fatty acid content [51], [53], [55], [59]. The use of a technique able to analyse the entire macromolecular content simultaneously, along with important information about structure of certain groups of compounds, would lend invaluable information to the understanding of these undeniably complex organisms. Vibrational spectroscopy, specifically Fourier transform infrared (FTIR) spectroscopy, could provide this information.

1.4 Metabolomics and vibrational spectroscopy

Over the last decade, there has been a marked increase in research focusing on what has been called “omics” technology. Genomics and metagenomics have been gaining ground as an in-depth tool to analyse the genetic makeup of individual organisms and ecosystems. Along with these techniques, a third “omics”, metabolomics, has been increasing in interest [20]. Specifically, environmental metabolomics is the “study of the interactions of living organisms with their natural environments at a metabolic level” [60]. This area of study employs techniques common in analytical chemistry to measure the whole macromolecular content of a cell or specific compounds [20], [60].

Nuclear magnetic resonance (NMR) spectroscopy and Mass spectrometry (MS)-based techniques dominate the literature [51], [53], [55], [60], [61]. This is likely due to their sensitivity; however, as with all techniques, there are advantages and disadvantages.

FTIR spectroscopy is a form of vibrational spectroscopy that is becoming increasingly popular amongst the metabolomics community [62]–[65]. It has disadvantages, specifically the absorption of water; however, its ease of use and the simple sample preparation, and therefore minimal chance of contamination, have contributed to its recent rise in popularity. FTIR spectroscopy is an extremely versatile analytical technique that can be used to analyse both organic and inorganic components of a wide range of systems and thus provide a snap-shot of the whole biochemical composition of a given organism [66].

Due to the development of a wide array of sampling techniques, FTIR spectroscopy allows researchers to study a diverse range of biological organisms. However, FTIR spectroscopy does pose a significant challenge for the analysis of biological systems. The O-H bond in water is highly polar and as such shows an intense absorption in the

infrared part of the spectrum; sample preparation techniques must take this into account. Freeze-drying samples or desiccating algal colonies can remove water with little disturbance to the chemical structure and make this technique the method of choice, due to its ability to measure the whole biochemical composition of a sample simultaneously.

Conventional FTIR spectroscopy measurements usually require the sample in question to be homogenised in some way. However, when cellular structure and distribution is important then coupling of a microscope to a FTIR spectrometer allows heterogeneous samples to be analysed whilst maintaining cellular integrity. This technique also significantly reduces the quantity of sample needed for analysis, allowing microscopic algae and bacteria to be examined [62], [67]–[69]**.** Several studies into the effect of nutrients on plankton and bacteria have also been undertaken using this technique. Using micro-FTIR spectroscopy, algae can be separated into individual taxa and identified using the "fingerprint" region of a spectrum; the lower wavenumber region which has a unique combination of peaks for a given compound [66], [70].

Micro-FTIR spectroscopy has also been used to detect changes in composition of algal samples exposed to differing levels of nutrient stress. The amide I (C=O stretching) and II (N-H bending) bands have been of use in these types of studies as they correspond to different bond vibrations within the protein structure [71]. The amide I band in particular depends on secondary structure of proteins and is often used to detect protein degradation, as well as conformation and hydrogen bonding within the protein [71].

While FTIR spectroscopy can provide detailed qualitative information on structure, it is not well suited to providing quantitative changes in concentration. However, ratios of intensity or area of bands in a spectrum can show relative changes in content. This technique has been applied to the study of nutrient changes in algae and cyanobacteria

where researchers showed changes in the relative content of carbohydrates, lipids and proteins with variations in nutrient availability [62], [63], [65], [72]–[74].

This technique has been gaining recognition within the phytoplankton research community over recent years and has been used to successfully monitor macromolecular changes in response to nutrient limitation [70], [72], [74]–[76], identify and classify species of algae [66], [73] as well as calculate growth rates [63].

FTIR spectroscopy is also used in conjunction with multivariate statistical analyses methods known as chemometrics. Spectra can contain thousands of data points and so it is useful to reduce the complexity, whilst maintaining information integrity which can be an incredibly powerful analysis tool. Common chemometric methods include clustering analyses such as Partial Least Squares regression (PLS) and Principal Component Analysis (PCA). In both of these methods, spectra are reduced to a single point in multi-dimensional space and then compared with other samples. Similar spectra will cluster closer together and so groups can be observed within sample sets. Use of a combination of supervised classification methods, as well as regression techniques can provide a comprehensive analysis of the entire data set. These methods have previously been employed in analysis of various biological systems including diatoms [65] and for calculating cultured algal growth rates [63].

FTIR spectroscopy can also be carried out in conjunction with a specific type of detector, known as a Focal Plane Array (FPA) detector in an imaging instrument. The technique can be used to produce a multi-dimensional picture of the biochemical properties of a sample. A large number of detector elements are read during the acquisition of spectra and this allows thousands of interferograms to be collected simultaneously and then transformed into infrared spectra. The spectra can then be used

to generate false colour images in which intensities are used to effectively map the biochemical content across a sample [75]. Due to effective resolution limitations, regular laboratory instruments using the commonplace globar light source can only generate images with a pixel size as low as 10 x 10 μm. Given that *Symbiodinium* sp. cells are generally about 10 μm in diameter [12], use of this conventional technique to investigate cellular components would seem futile.

Recent advances in synchrotron technology have culminated in the development of FTIR spectroscopic imaging techniques. The use of synchrotron radiation reduces the effective pixel size to 0.54 x 0.54 μm [77]. This highly specialised method has been used previously to analyse algal macromolecular content [75]. It has the potential to provide vital information about spatial distribution of macromolecular compounds within a cell.

Recent efforts in identifying macromolecular changes using metabolomics have outlined a number of disadvantages to this technique. In a mass spectroscopic analysis of *Symbiodinium* sp. metabolites, Kleuter et al (2015) mention that their results could not isolate areas of change or outline specific macromolecular processes and mechanisms within the cells. At the moment, metabolomics can only identify the compounds present and in what quantities [51]. This information is undoubtedly vital; however, often inconclusive and limited in its ability to be interpreted.

FTIR spectroscopy, while still unable to be conclusive in terms of identifying specific biochemical processes, can add a certain depth to studies of macromolecular content. Most metabolomics techniques will only investigate one or two types or families of macromolecule such as lipids, carbohydrates or proteins [51], [55], [59], [78]. And so the scope of these techniques, although they are detailed, are limited. FTIR

spectroscopy can be used to analyse the whole metabolic profile of biological organisms simultaneously. While it cannot provide the same level of detail as, say, mass spectrometry, the ability to measure lipids, proteins, carbohydrates and phosphorylated compounds all together can provide critical information about interactions between these groups which would be missed otherwise. The use of these spectra in combination with chemometric analysis can provide a detailed picture of the whole metabolome of different clades of *Symbiodinium* and how they respond to environmental stress.

1.5 Thesis outline

To begin, **Chapter 2** is an outline of the methods repeated throughout the experimental chapters of this thesis. Initial comparisons of the two chosen clades of *Symbiodinium* are presented in **Chapter 3.** It was found that there was a significant difference in macromolecular composition of two un-stressed clades of *Symbiodinium* sp. with distinct thermal tolerance limits. Specific structural differences are found to be present within the protein and lipid content of these two ecotypes.

In order to determine whether these differences in structure had any bearing on the cells' response to changes in environment, the second of three experiments is presented in **Chapter 4.** Two clades of *Symbiodinium* sp. were further subjected to various combinations of light and temperature in order to assess their macromolecular response to non-lethal stress. Not only did the protein and lipid structure change between clades, their response to different combinations of environmental stress was different.

This experiment only subjected cells to sub-lethal environmental change and so, the experiment presented in **Chapter 5** subjected these cells to extreme changes in temperature. For the first time, photosynthetic function and macromolecular structural differences in lipids and proteins, are correlated using chemometric analyses. **Chapter 6**

is a preliminary study in which these samples, analysed in Chapter 5, were further investigated using Synchrotron Chemical Imaging FTIR spectroscopy. This is the first study of this nature to be reported and shows clusters of macromolecules across the cells; however the chapter concludes that there is much method development still to be done before this is a viable method of analysis. In **Chapter 7** a discussion of these experiments as a whole and the implications for further research is presented.

Chapter 2. General methods

2.1 Introduction

Over the course of this thesis, a number of methods were utilised that were common to all experimental chapters. These are presented below and should be referred to throughout the thesis. Multivariate statistics have been largely omitted from this common section as they differed depending on dataset. Refer to the methods sections of those particular chapters for further details.

2.2 Sample preparation

Two specific types of *Symbiodinium* sp. were used throughout this thesis. The sample preparation of the cells in culture are outlined in the following section. All cultures were grown in F/2 media modified for dinoflagellate growth to minimise interference from nutrient depletion effects [79]. They were maintained at 25 ^{o}C with a 12:12 hour light: dark cycle with 25 μmol photons m^{-2} s^{-1} in incubators fitted with 18W "cool white" fluoro, 4000k lights. Four biological replicates were maintained for each clade.

Cultures were allowed to reach the exponential growth phase; ~18-20 days after innoculation before being subjected to different light and temperature treatments. Table 2.1 shows the conditions for each separate experiment. These conditions were derived from Summer field data for the Heron Island Lagoon (Australian Bureau of Meteorology) but also from previous research [80]. Aliquots were removed at noon daily for six days and the cultures replenished with fresh F/2 media in equal volume to the amount removed.

Maximum quantum yield of PSII (F_v/F_m) was measured using a Water PAM (Walz GmbH, Effeltrich, Germany) on cell suspensions that were dark-adapted for 10 minutes. Cell counts were taken using a Haemocytometer (Naebauer) with a light microscope.

Table 2.1: Light and temperature regimes for the experiments.

	Light (µmol photons m^{-2} s^{-1})	**Temperature (ºC)**
Control	25	25
High Temperature	25	31
High Light	100	25
High Light + Temperature	100	31
Temperature ramp	25	+ 2 ºC/day (24 to 34)

Lugol's iodine (1µL mL^{-1}) was added according to the method of Giordano et al., (2002). This aliquot was centrifuged at 4000 rpm for 4 minutes and the supernatant discarded. Washing was performed as described by Heraud et al. (2006) to remove residual culturing media.

2.3 FTIR spectroscopy

2.3.1 Attenuated Total Reflectance (ATR)-FTIR spectroscopy

After rinsing the sample in isotonic saline solution and centrifuging, the pellets of CS-73 and CS-156 were dried in an oven at 60 ºC for 48 hours or until mass remained unchanged. The dry weight of the pellet was recorded and the samples were stored in a desiccator until analysis. Spectra were collected using a FTIR-ATR (Agilent Technologies Cary 630) spectrometer with a pseudo-replication rate of 4 for each sample to account for differences in beam penetration. Resolution was 4 cm^{-1} and 128 scans were co-added.

2.3.2 Micro-FTIR spectroscopy

For the studies that would culminate in the analysis of single cells by chemical imaging, it was decided that instead of employing ATR as a sampling method as with previous

experiments, bulk cultures would be analysed in a similar manner to the chemical images for comparison purposes. Micro-FTIR spectroscopy was used to analyse macromolecular content of the whole culture.

After rinsing, cells were resuspended in 2 mL of isotonic saline solution and deposited onto 12 mm diameter and 0.5 mm thick CaF_2 slides (Crystran, Dorset, UK) using a cytospin centrifuge (Hettich, Australia). This ensured an even cell deposition across the window and a good signal for FTIR spectroscopy.

Spectra were collected using a spectrometer (Nicolet 6700) coupled to a IR microscope (Nic-Plan). Spectra were acquired in transmission mode and were collected at 4 cm^{-1} resolution with 128 co-added scans. Spectra were collected with a pseudo-replication rate of 4 to ensure even deposition across the CaF_2 windows.

2.3.3 Synchrotron chemical imaging FTIR spectroscopy

Samples of the two *Symbiodinium* cultures were taken to the Synchrotron Radiation Center (SRC) in Madison, Wisconsin, USA for analysis. The SRC has since been decommissioned; however, before it was closed, it was the only Synchrotron in the world with the capability for chemical imaging using infrared light at the Infrared Environmental Imaging (IRENI) beamline.

During the limited experimental time available at this beamline, it was found that even with the increased resolution of the synchrotron, clade A cells were too small to be analysed (<10 μm in diameter). It was therefore decided to focus on clade F as they were generally 10 μm in diameter or larger. Dilute concentrations of the culture were deposited onto CaF_2 windows (Crystran, UK) and dried in the oven to remove interference from water.

Images were collected using an IR microscope (Bruker Hyperon 3000) coupled with a 128 x 128 pixel Focal Plane Array (FPA) detector. The added power of Synchrotron radiation allowed the effective pixel size to be as small as 0.54 x 0.54 μm. Each pixel was a spectrum collected at 4 cm^{-1} resolution and 128 co-added scans. 4096 spectra were collected simultaneously for each image. Light microscope images were collected at the same time for comparison.

2.4 Macromolecular content calculations

For samples collected by ATR FTIR spectroscopy, pre-processing of the spectra was performed by applying a 9-point Savitsky-Golay smoothing function and baseline correction. ATR distortion of the "fingerprint" region (1800 – 800 cm^{-1}) was corrected using the in-built ATR correction algorithm [81]. The relative macromolecular content was calculated by integrating the area under the bands as shown in Table 2.2. The total area was added together and used to estimate the percent composition of the carbohydrates, lipids, proteins and phosphorylated compounds.

Table 2.2: Integrated regions for the estimation of macromolecular content.

Macromolecular pool	**Integrated region(s) (cm^{-1})**
Lipid	1760-1705
Protein	3500-3000, 1705-1300
Phosphorylated compounds	1300-1200, 1130-1070
Carbohydrates	1070-800, 1190-1130

Lipid saturation, branching and membrane disorder were measured by comparing macromolecular ratios of band absorbance intensities outlined in Equations 2.1-2.3 [82].

Equation 2.1

$$Degree\ of\ saturation\ = \frac{= CH_2}{v_{as}CH_2 + v_sCH_2} = \frac{3012\ cm^{-1}}{(2925\ cm^{-1} + 2850\ cm^{-1})}$$

Equation 2.2

$$Lipid\ branching = \frac{v_{as}CH_3}{(v_{as}CH_2 + v_sCH_2)} = \frac{2960\ cm^{-1}}{2925\ cm^{-1} + 2850\ cm^{-1}}$$

Equation 2.3

$$Membrane\ disorder = \frac{v_{as}CH_2}{v_sCH_2} = \frac{2925\ cm^{-1}}{2850\ cm^{-1}}$$

Sample collected using micro-FTIR transmission spectroscopy and Synchrotron radiation were analysed in the same manner with minor variations. In order to determine whether or not the observed changes in macromolecular ratios and lipid structure were statistically significant, various ANOVA methods were used. Repeated measures ANOVA (rmANOVA) was used to assess changes in content over time within samples. If the Mauchly sphericity test statistic was significant (<0.05), then conditions of sphericity were not met and the data was transformed using the natural log. Tukey's post hoc test was used to determine which time groups were significantly different. To test the significance of any differences observed between clades and between treatments, a mixed model ANOVA was used. Data was also transformed using either the natural log or arcsine functions if conditions of sphericity were not met. Tukey's post hoc analysis was again used to determine where differences were occurring between clades or between treatments.

2.5 Spectra pre-processing and statistical modelling

Spectra were pre-processed using statistical software (The Unscrambler 10, Oslo, Norway). Second derivatives were calculated using a Savitsky-Golay function with 9 smoothing points. Bands associated with biological components were identified and isolated using the range function and the Extended Multiplicative Signal Correction (EMSC) function for scatter correction was applied to remove any scattering effects [83]–[85].

A number of different approaches were taken for statistical modelling and these were found to be specific to each sample set. Each of these methods are described at the beginning of each of the four subsequent experiments (Chapters 3-6).

2.6 Image processing

2.6.1 Chemical images

Chemical images were generated using CytoSpec. 2nd derivatives were generated for all spectra using a Savitsky-Golay 9 point smoothing method. These derivatives were then vector normalised to account for differences in cell width. The following trough intensities were used to build the images; α-helix (~1655 cm^{-1}), β-sheet (~1620 cm^{-1}), lipid (~1730 cm^{-1}), carbohydrates (~1020 cm^{-1}) and phosphorylated compounds (~1080 cm^{-1}).

2.6.2 Statistical images

Hierarchical Clustering Analysis (HCA) was used to assess the groupings of similar spectra within the chemical images. HCA images were built with a Euclidean distance

method and average linkage clustering. Average spectra were generated for each cluster displayed in the images.

Chapter 3. Macromolecular composition variation between genetic clades of symbiotic dinoflagellates (genus *Symbiodinium)*

3.1 Introduction

Before analysis could begin, a number of methodological considerations needed to be investigated. Appropriate clades of *Symbiodinium* would need to be chosen and sampling methods optimised. In this series of experiments, FTIR spectroscopy was used to analyse two different clades of *Symbiodinium* (A, CS-73 and F, CS-156). Thermal tolerances of these two clades were investigated and the cells characterised. Chemometrics and ratios of important bands in the spectra were employed to verify the results of FTIR spectroscopy and to determine the effectiveness of this technique for discrimination between these two clades.

3.2 Initial assessment of *Symbiodinium* sp.

3.2.1 Investigation of tolerance

Drawing upon literature sources, the parameters of the experiments were tested for suitability including choice of genetic clade of *Symbiodinium*, method of spectra collection and macromolecular analysis methods using the spectra. Previous research has indicated *Symbiodinium* cells experiences significant photoinhibition and stress at temperatures above 30 ^{o}C with a number of papers showing complete cessation of photosynthesis at 34 ^{o}C [52], [53], [58], [86], [87]. In this study, it was necessary to expose the cells to environmental stress, but not lethal conditions. Prolonged and sustained stress was needed to monitor the response of the macromolecular composition of the cells over time (6 days).

In order to determine the lowest thermal limits of these cells, a pilot study was conducted and maximum quantum yield of PSII (F_v/F_m) was monitored. The cells were subjected to a gradual increase in temperature (2 ^{o}C/day) from 24 ^{o}C to 34 ^{o}C. Aliquots

of these cultures were removed, dark adapted for ten minutes and the maximum quantum yield of PSII was measured at 12 noon every day. Results of these measurements are shown in Figure 3.1.

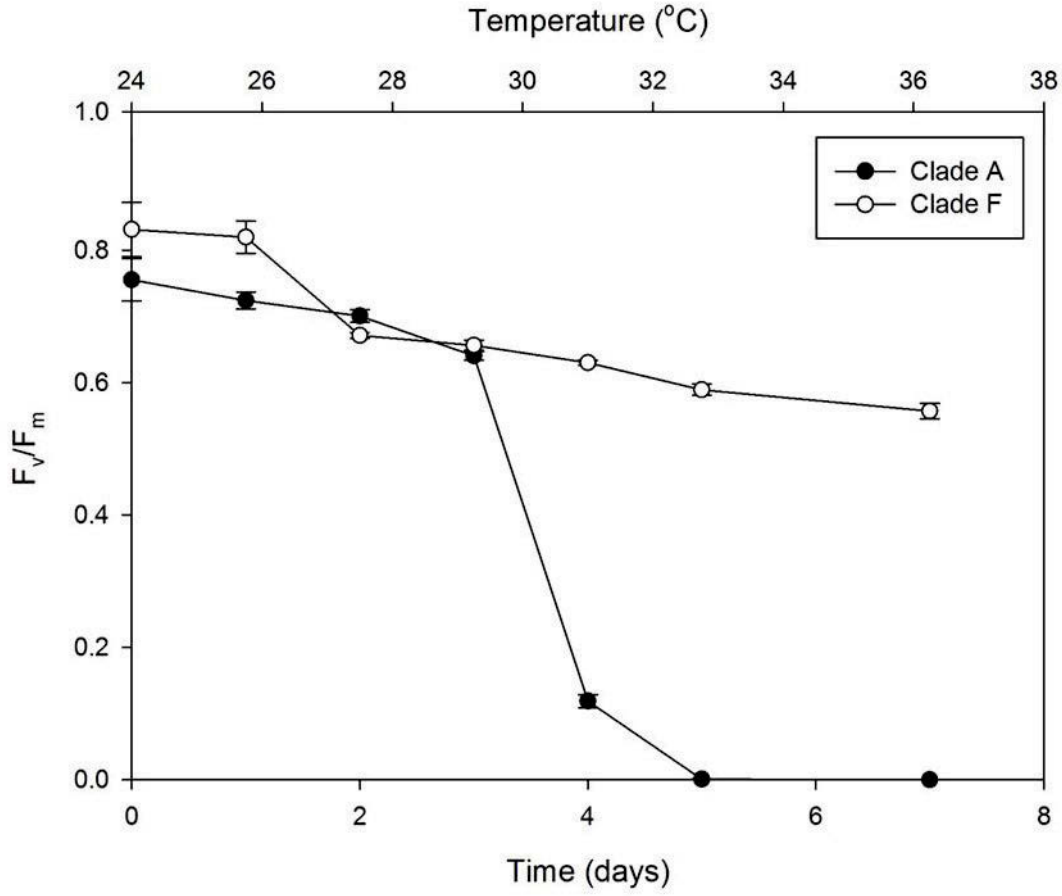

Figure 3.1 Maximum quantum yield for clades A and F exposed to elevated temperature. Data points are mean (n=4) and error bars are ± Standard error of the mean (SEM).

The clade A cells were less thermally tolerant than the clade F culture. This meant that the two cultures were suitable for this study and would provide a good comparison between a thermally tolerant, and more susceptible clade of *Symbiodinium*. Once these two clades had been chosen and their thermal tolerance tested, literature was published that re-identified CS-156 as *S. kawagutii*, a clade F1 type, not C as originally thought [46]. This will have further implications in terms of interpretation of results in later

chapters; however, since the two clades were found to have different thermal tolerances, this was not considered to be a setback.

Before analysis by FTIR spectroscopy was possible, it was necessary to fix and store the cells for further analysis. A number of methods for fixing cells were possible; however, FTIR spectroscopy is highly sensitive to the chemicals used in these processes. Lugol's iodine has previously been used to fix cells [74]. This solution was ideal as it quickly preserved the cell' macromolecular components without causing interference in the subsequent spectra. The cells were, however, required to be preserved further through drying or snap-freezing in liquid nitrogen. Light microscopy was used to ensure these processes did not rupture the cells.

3.2.2 FTIR spectroscopy

There are a number of different and suitable sampling methods with which to analyse biological samples using FTIR spectroscopy [70], [74]–[76]. In order to decide which methods were most appropriate to use for this thesis, a number of considerations needed to be assessed. Firstly, the cells needed to be dried as water absorbs strongly in the IR region and so obscures any macromolecular peaks [74], [88]. Previous research had revealed that biological samples could be dried in an oven at low temperature (60 ^{o}C) without damaging the macromolecular content [67], [89].

FTIR spectroscopy is also highly sensitive to interference by polar molecules, a number of which were included in the growth media used to maintain the cultures. This meant that initial spectra were contaminated by a large phosphate peak at ~ 1080 cm^{-1} (Figure 3.2). Subsequent washing with isotonic saline solution made up with milli-Q water was required to remove this contamination. Previous research has indicated that this must be

done at least twice [72]. In this study, the washing and centrifuging was performed three times.

ATR was chosen as the sampling method for FTIR spectroscopy. This has previously been used in the use of algal biomass and biological tissues [68], [90], [91]. However, in the case of the Synchrotron chemical images, samples for comparison were analysed using micro-FTIR spectroscopy in transmission mode.

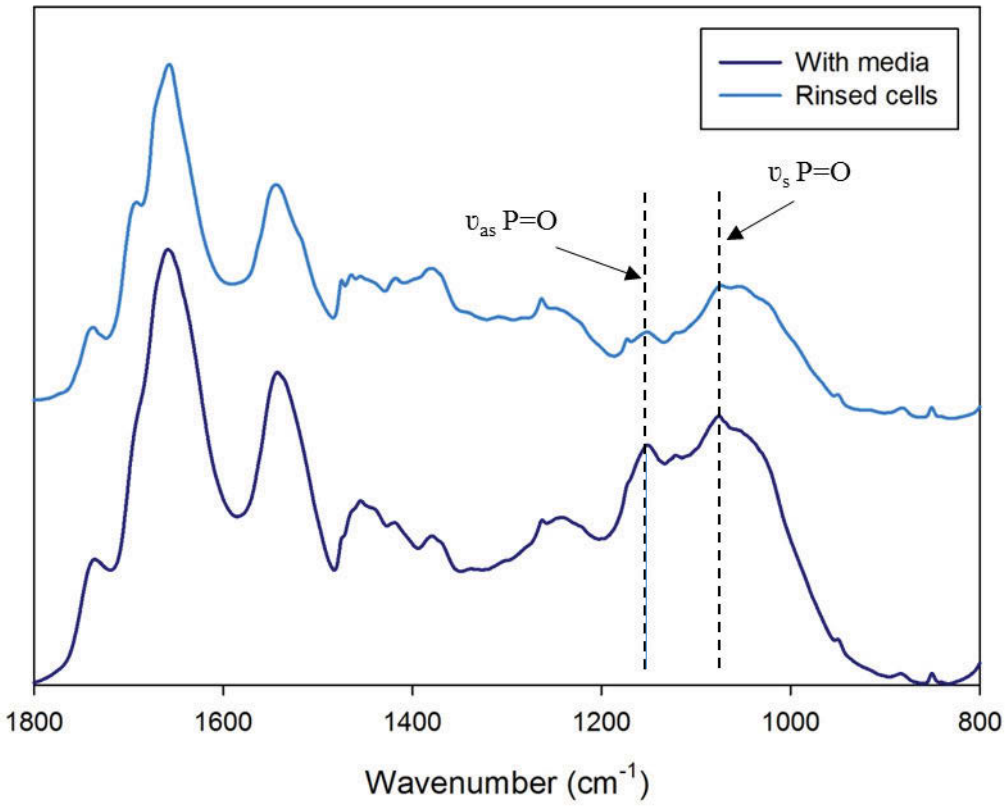

Figure 3.2: Comparison of typical *Symbiodinium* sp. spectra with and without rinsing. Dotted lines indicate area of media interference.

3.2.3 Spectral analysis

Once the spectra were obtained, a number of analysis possibilities were then considered. First of all, bands in each spectrum were assigned using literature sources but also three

standards; bovine serum albumin (BSA) for protein, starch for carbohydrates and palmitic acid for lipids. Band assignments are shown in Table 3.1 and a comparison of the standards and *Symbiodinium* sp. spectra are shown in Figure 3.3.

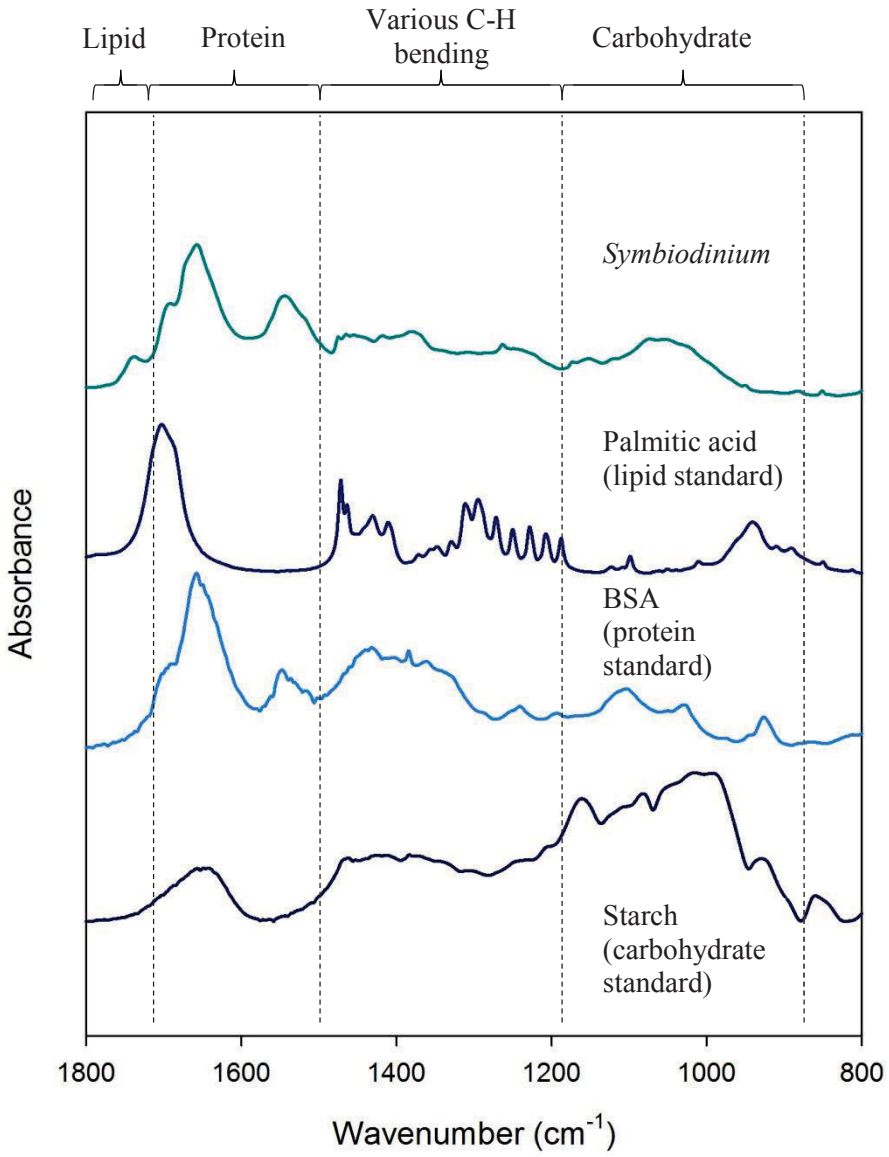

Figure 3.3: Comparison of spectra for band assignments. From top to bottom: representative *Symbidinium* sp. spectra, lipid standard, protein standard and carbohydrate standard.

Since these particular clades of *Symbiodinium* sp. were yet to be analysed in literature, it was necessary to compare them with standard spectra. A number of key problems arise when looking at these band assignments. First of all, according to literature, the C-H stretching region between 3100-2800 cm^{-1} contained vibrations due to both lipids and

proteins; however, standard spectra revealed that this was likely overwhelmed by lipids. The C-H bending vibrations between 1450 and 1415 cm^{-1} were likely a combination of lipids and proteins and so were discounted from any further analysis. However the region between 1000 – 900 cm^{-1} contained some vital and characteristic vibrations for both carbohydrates and phosphorylated compounds, which needed to be separated.

In order to address this issue, elemental composition of the spectra was initially investigated. The use of absorbance ratios to analyse relative changes in FTIR spectra is well-documented [62], [65], and is often used as a means of assessing changes in macromolecular content given that the absorbance in the infrared region of the spectra is proportional to the concentration of the assigned compounds [90].

Ratios of elements are commonly used in ecology to describe the changes in energy budget [19], [92], [93]. Given that the absorbance in the infrared region of the samples is proportional to concentration of the elements, the relative areas under the bands can be used to estimate elemental content. Using integrated areas outlined in Table 3.1, percentage composition was found to be approximately 80% carbon, 11% nitrogen and 9% phosphorus. There were no significant differences in percentage composition between the clades of *Symbiodinium*. This result does not wholly agree with previously reported values. For example Muller-Parker et al (1994) report C:N and N:P ratios of approximately 10:1 and 20:1 respectively. This is an indication of the technique's unsuitability for C:N ratios; however, it is likely that bands attributed to phosphorus are obscured in the spectra hence the phosphorus content is over-estimated.

Table 3.1: Integrated regions for the estimation of elemental pools.

Elemental pool	**Integrated region(s) (cm^{-1})**
Carbon	3000-2800, 1740-1600, 1400-1200
Nitrogen	3500-3000, 1500-1400
Phosphorous	1300-1200, 1140-1070

Table 3.2: Main infrared band assignments for *Symbiodinium* sp. (υ = stretching, δ = bending, as = asymmetric, s= symmetric).

Wavenumber (cm^{-1})	**Band assignment**	**Macromolecular assignment**
~ 3012	ν =CH_2	Unsaturated lipids
~ 2960	ν_{as} CH_3	Methyl groups of lipids and proteins
~ 2920	ν_{as} CH_2	Methylene groups of lipids and proteins
~ 2875	ν_s CH_3	Methyl groups of lipids and proteins
~ 2850	ν_s CH_2	Methylene groups of lipids and proteins
~ 1730-1740	ν C=O	Ester groups of lipids
~ 1650-1620	ν C=O Minor ν N-H and ν C-N	Proteins (Amide I)
~ 1530-1510	δ N-H	Proteins (Amide II)
~ 1450	δ_{as} CH_2 and CH_3	Proteins and lipids
~ 1415	δ_s CH_2 and CH_3	Proteins and lipids
~ 1380	ν_s C-O and COO^-	Proteins and lipids
~ 1300	ν C-N and δ N-H	Proteins (Amide III)
~ 1240	ν_{as} P=O	Nucleic acids and phosphorylated compounds
~ 1150	ν C-O-C	Cellulose
~ 1000 - 900	ν C-O-C ν_s P=O	Carbohydrates and phosphorylated compounds

It should also be noted that the relative size of the elemental pools measured here do not correspond to the commonly reported Redfield ratio of 106:16:1 (C:N:P) [94]–[96]. Results in this study were approximately 9:2:1 (C:N:P) for both clades A and F. Although Geider and La Roche (2002) suggest there is a level of plasticity in marine organisms in terms of this ratio, the differences between Redfield and our results are large. This is not wholly reason enough to discount this technique as a method for the determination of elemental stoichiometry. The complex nature of the spectra and the presence of overlapping or hidden bands, however, is a problem. For example, the amide I band at ~1650 cm^{-1} is known to be approximately 80% C=O stretching, but also 20% in-plane N-H bending [97]. This means that the use of this band as an estimation for carbon content is not accurate, as it contributes to both C and N pools as shown by the calculated percentage composition of the elemental pools. Thus, FTIR spectroscopy is not a straightforward method for elemental stoichiometry with *Symbiodinium* due to overlapping bands in the spectra. It was therefore decided to focus on the analysis of the macromolecular components of the spectra. Table 2.2 outlines the integrated regions for analysis.

A number of other analysis methods could add insight into the macromolecular content of the *Symbiodinium* cells. Prolific research into biological systems using FTIR spectroscopy have exploited the large-scale datasets by applying multivariate classification methods [63], [65], [98]. A combination of relative macromolecular content, structural analysis and multivariate statistics, would provide a deeper, more comprehensive analysis of the data obtained and will be employed over the course of this thesis.

3.3 Macromolecular content of *Symbiodinium* sp.

Two cultures of *Symbiodinium*, clades A and F, were grown as described in Chapter 2, before being sampled for comparison. Photosynthetic efficiency was not expected to change over the course of this experiment as no stress was provided and was only measured in order to show that no change in the photosynthetic condition occurred over the time of the sampling. Maximum quantum yield of PSII (F_v/F_m) was measured for the two genetic clades A and F, and was found to be 0.66 ± 0.01 and 0.63 ± 0.01, respectively. These values were compared and found to be consistent with other healthy cells [52][55].

3.3.1 Characterisation of cells by FTIR spectroscopy

Visual inspection of the average FTIR spectra for both clades show differences which are further resolved by second derivative spectra (Figures 3.4 and 3.5). Band assignments are outlined in Table 3.2 and were derived from previous spectroscopic studies of biological systems [74], [99], [100]. The amide I (predominantly due to the C=O bonds characteristic of proteins) band at ~1650 cm^{-1} shows differences in shape and maximum absorbance wavenumber. This is an indication of differences in the secondary structure, or the way the proteins are folded [71].

The band at ~1150 cm^{-1} is commonly attributed to the C-O stretching of cellulose carbohydrate [99], [101]. According to literature, it is unclear whether the cell walls of *Symbiodinium* contain cellulose; analysis of the ultra-structure of the cells have been inconclusive [40]. Cellulase digestion of isolated cell walls in *Symbiodinium* have been reported [102]; however, scanning electron microscopy also failed to demonstrate characteristic cellulose fibrils in *Symbiodinium* [103]. Conversely, a recent study using calcofluor staining to identify cellulose complexes in *Symbiodinium* thecal plates,

suggested the presence of cellulose [104]. It is possible that further analysis by imaging techniques may resolve the uncertainty in cellulose composition.

Finally, the large band at ~1020 cm^{-1} that is generally assigned to carbohydrates, is clearly present in *Symbiodinium* and shows a much higher absorbance in clade F than clade A cells, which suggests a corresponding difference in overall carbohydrate content.

3.3.2 Macromolecular content

The use of absorbance ratios to analyse relative changes in FTIR spectra is well-documented, and is often used as a means of assessing changes in macromolecular content given that the absorbance in the infrared region of the spectra is proportional to the concentration of the assigned compounds [62], [65].

Assigning the bands to specific macromolecular groups provides a more informative estimation of percent composition (Table 2.2). Macromolecular components as a percentage of the total integrated spectral band were found to be approximately 56% protein, 23% carbohydrates, 2% lipid and 18% phosphorylated compounds (a combination of deoxyribose nucleic acid (DNA), phospholipids and phosphorylated proteins). No statistically significant differences were observed between clades; however, the relative content seems to agree with other independent estimates of macromolecular content in the literature [105].

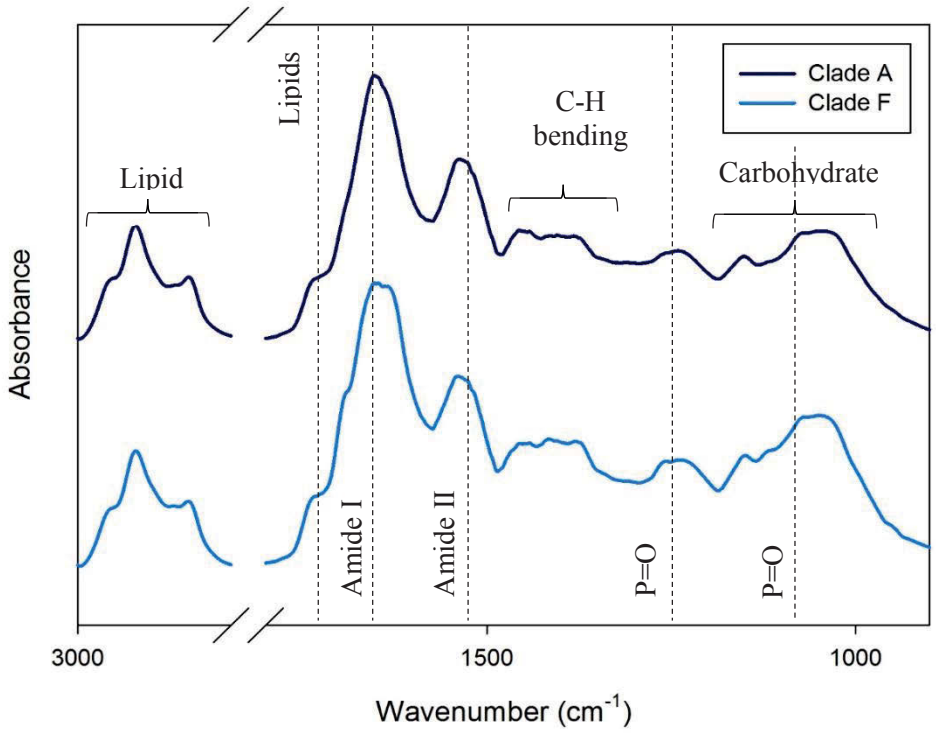

Figure 3.4: Total averaged spectra (n=20). Refer to Table 3.2 for band assignments.

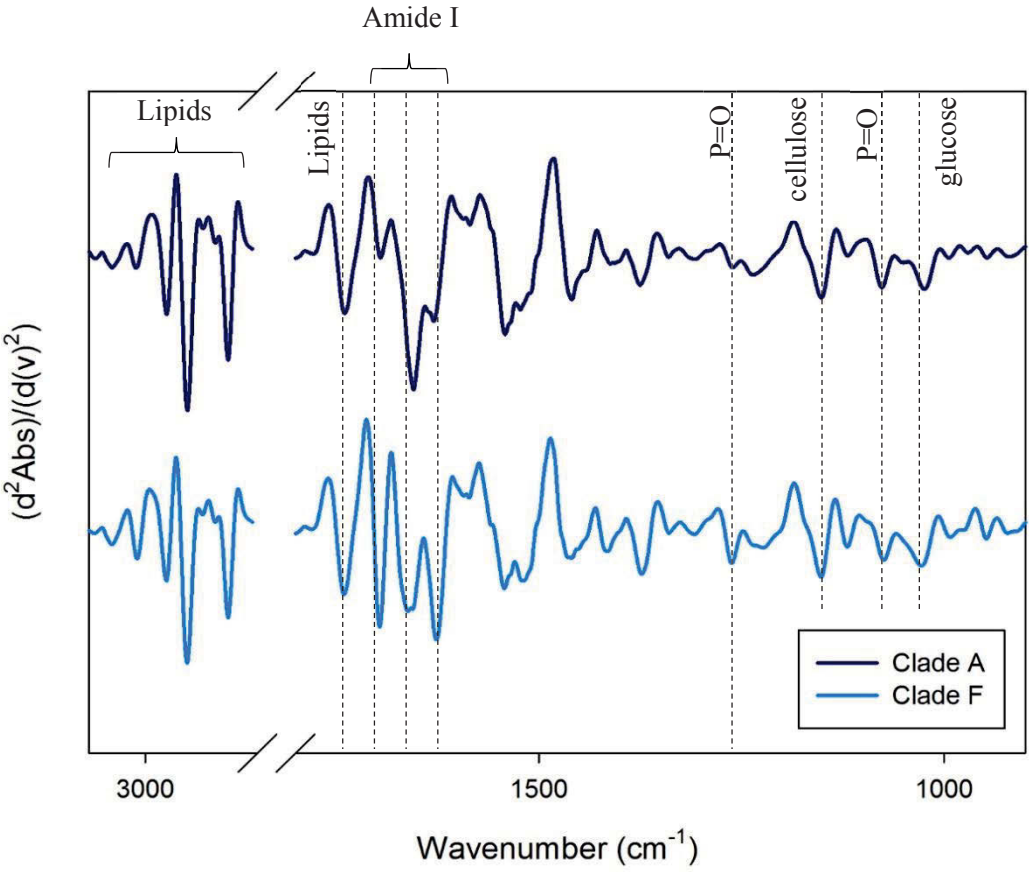

Figure 3.5: Total averaged spectra 2nd derivatives (n=20). Spectra are off-set on y-axis for comparison.

3.3.3 Statistical modelling

PCA with full cross-validation was performed in order to identify and remove outliers, as well as identify groups and clustering within the samples. No samples were removed from the clade A dataset, however, 20% of the clade F set were discarded based on leverage plots [65], [98]. If one spectrum was seen to have too much of an effect on the statistical model, as opposed to the rest of the group, it was considered an outlier. Once these had been removed, the EMSC function was re-applied to the raw second derivatives to be included in the final chemometric models.

Partial least squares discriminant analysis (PLSDA) was used to classify the spectra into two groups based on clade. The data was split into two sets; replicates 1-3 were put into the 'training' set and replicate 4 was assigned to the 'test' set. Clade A samples were assigned the Y-variable '0' and clade F '1'. Chemometric models with respect to clade A and F were generated and the specificity and selectivity of the models were calculated based specificity and selectivity parameters [106].

The percentage similarities between the two clades in terms of their macromolecular pools also seems to disagree with the differences observed in the spectra (see section 3.3.1). This suggests that there are no significant differences in terms of relative content, rather a difference in the structure of the components themselves. It is also clear, on inspection of Figure 3.4 that these are complex organisms and their spectra reflect this biochemical complexity. Overlapping peaks, for example, the overlap of the phosphate (1080 cm^{-1}) and glucose (1020 cm^{-1}), highlight the need for more sensitive analysis of the spectra.

Multivariate statistics was used to further investigate the apparent differences using the 2^{nd} derivative spectra. Figure 3.6 shows the scores and loadings for the chemometric

model developed with respect to clade A. The sensitivity and specificity of the model is a measure of how many samples were correctly classified [106]. With respect to clade A, any prediction score over 0.5 is classified as clade A and any score less than 0.5 is classified as clade F. The optimal statistical model developed for this dataset had a sensitivity and specificity of 94% and 95%, respectively, meaning that the majority of samples in the validation set were correctly classified.

The loadings for this model indicated that the majority of the separation occurred along factor 1. This factor's variation was mostly explained by the protein secondary structure which provides detailed information about the way the proteins within the cells fold. Figure 3.6 highlights the main peaks of interest. These were the α-helix (1655 cm^{-1}) and β-pleated sheet (1690 and 1620 cm^{-1}). Comparing scores and loadings helps identify which group contained more or less of the given secondary structure. Since 2nd derivatives were used, these observations needed to be reversed. So a positive loading meant that there was more of this component in clade F cells than clade A. The α-helix gave a negative loading and so clade A contained more of this type of structure than F. The β-sheet gave a positive loading and so clade F contained more of this structural type.

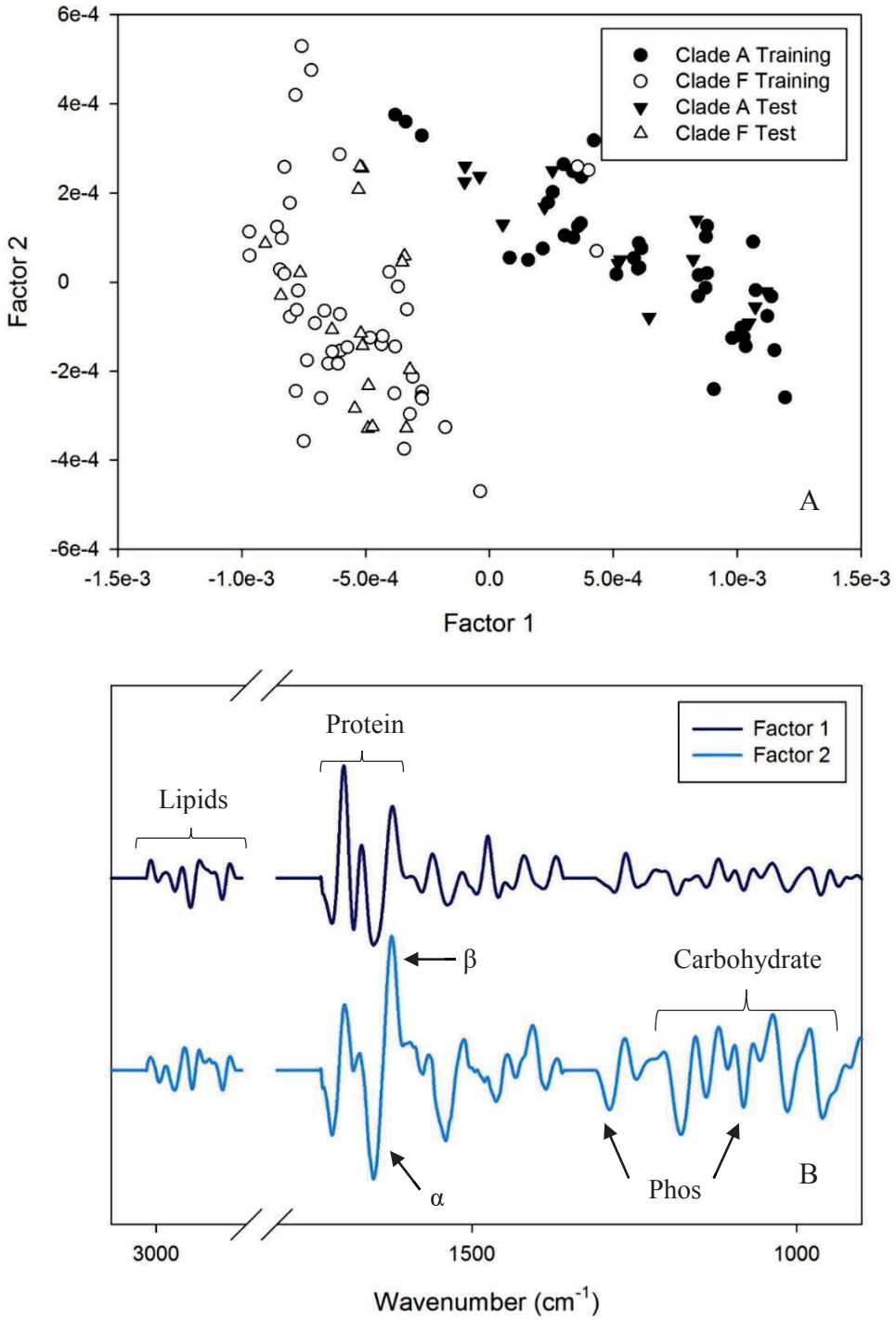

Figure 3.6: PLSDA model scores plot (A) and loadings (B).

3.3.4 Lipid structure

Characteristic bands in the region 3100 – 2800 cm^{-1} make it possible to observe changes in lipid structure within the cells. Comparing the ratios outlined in Equations 2.1 and 2.2, the degree of saturation and membrane disorder can be analysed. These were calculated for each replicate and an average taken for the total spectra collected. The degree of saturation was shown to be 0.33 ± 0.01 for clade A cells and 0.38 ± 0.01 for clade F. A student's t-test showed that these values were significantly different. "Membrane disorder" (or the ratio of asymmetric to symmetric CH_2 stretching vibrations) was also calculated and was shown to be 1.32 ± 0.03 and 1.27 ± 0.02 for clades A and F, respectively. A third value, lipid branching, was also calculated using the C-H stretching regions; however, these values did not differ significantly between the clades.

The PLSDA model discussed in section 3.3.3 included the 3012 cm^{-1} band attributed to the $=CH_2$ vibration. This peak gave a positive loading, indicating clade F gave a lower lipid saturation compared to clade A. Based on these values, and a comparison of the C-H stretching regions shown in Figure 3.7, clade A appears to contain a higher degree of saturated lipids than clade F. Clade A also appears to have a higher order (less asymmetric stretching vibrations) within the cells than clade F, which could indicate a higher membrane fluidity in clade F [82].

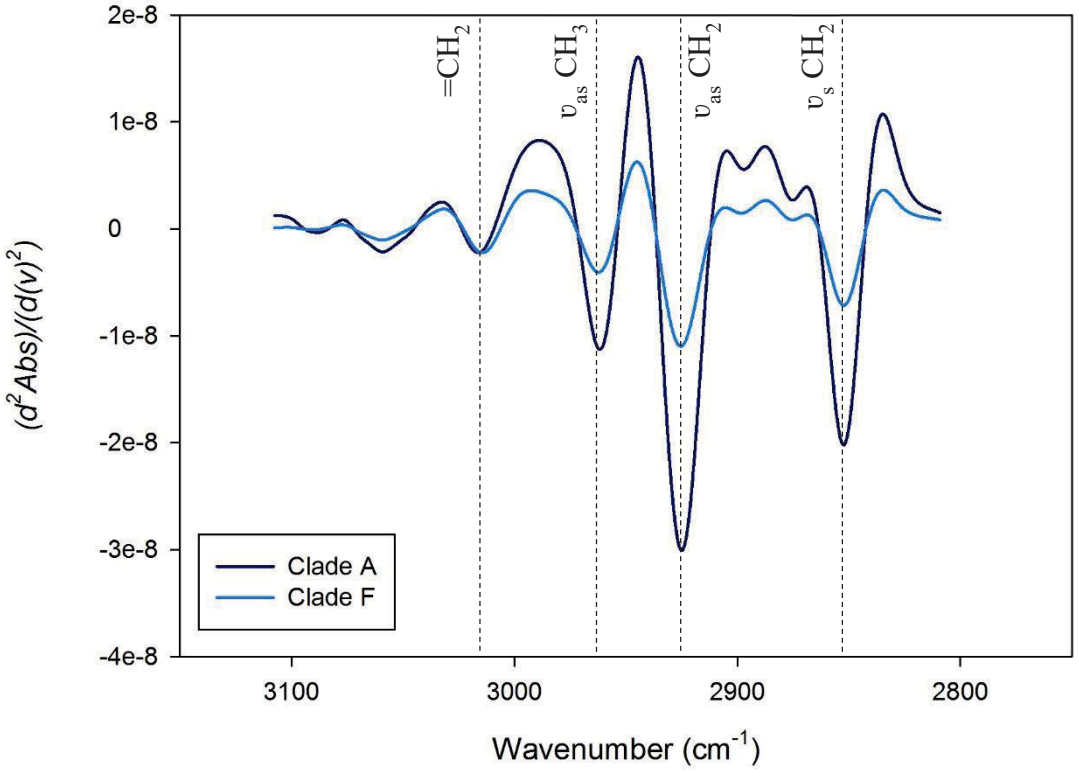

Figure 3.7: Lipid CH Stretching region (3100-2800 cm^{-1}). Spectra are averages (n=20) and are normalised to the $=CH_2$ band (3015 cm^{-1}) for comparison.

3.3.5 Protein secondary structure

The main source of variation from the more detailed statistical modelling was found to be the protein structure. FTIR spectroscopy can detect differences in secondary structures [71], [107], [108]. Bands appearing in the infrared spectra at ~1480-1350 cm^{-1} are assigned to CH_2 bending of methylene chains and can be partly attributed to amino acid side chains of proteins [107].

Second derivative spectra also show a difference in secondary structure between clades. The two prominent bands in the region ~1700-1450 cm^{-1} are a combination of a number of different bands very close together in the spectrum [97], [108]–[110]. These can be resolved using second derivatives and reveal important information about the proportions of α-helix and β-pleated sheets in the cells [71], [97], [108], [110]. Figure

3.5 shows the second derivative spectra for clade A and clade F. As shown, there are three prominent troughs between 1600 and 1500 cm^{-1}.

The trough (corresponding to a band in the underivatised spectra) at 1690 cm^{-1} corresponds to β-turns and is much stronger in clade F than A. The trough at 1625 cm^{-1} supports this observation, as this wavenumber is attributed to β-sheet structure and is again much stronger in clade F. The latter band is also assigned to a type of structure known as a β-strand or extended chain [111]. This is commonly found in protein complexes where there are linked sub-units as occurs in thylakoid membrane protein complexes [112]. The trough at ~1655 cm^{-1} (Figure 3.5) is more pronounced in clade A, indicating a higher concentration of the structurally ordered and stable α-helix conformation, than the cells of clade F.

As discussed in section 3.3.3, the main source of variation explained by the PLSDA models was found to be the bands at ~1690 cm^{-1}, ~1655 and 1625 cm^{-1} corresponding to two different protein secondary structures. The results of this particular model confirm that the clade A cells contain a higher proportion of the α-helix arrangement and that clade F contains more of the β-pleated sheet conformation.

3.4 Discussion

Macromolecular content is an important component of the energy budget of an organism as it is not in the elemental stoichiometry where cellular energy is bound, but in the chemical bonds within the lipids, proteins and carbohydrates [19], [93], [113], [114].

The results presented in this chapter found, using ratios of band intensities, that there were no significant differences in total macromolecular content. However, given the PLSDA models were able to accurately predict clade, it is clear that the spectra

exhibited significant differences. These differences can be attributed, therefore, to structural changes rather than content. Use of the second derivative spectra to resolve hidden bands is essential, due to the complex nature of the spectra. Development of such chemometric models has the added benefit of the simultaneous analysis of a large number of samples, which is particularly useful in datasets used to describe environmental systems [65], [72], [98], [115]. These chemometric models, along with a more detailed analysis of the C-H stretching region, revealed a number of significant differences in lipid and protein structure between clades.

The implications of these significant differences in structure are difficult to determine. The majority of literature on lipid content within *Symbiodinium* focuses mostly on the change in total lipids over time, under changes in environmental conditions. Increases in temperature have been shown to have an effect on membrane fluidity and induce desaturation of membrane lipids in higher plants [53]. Saturation of lipids have been the focus of a number of studies. Results have varied with values for the ratio of unsaturated: saturated fatty acids found to be in the range of 0.25 – 2.70 [55], [116], [117]. The results found here are within this range. The differences in saturation have previously been linked to possible differences in energy storage strategies [59]**,** as well as thermal tolerance [55]**.** It is therefore possible that the increased unsaturated fatty acid content in clade F cells could contribute to this clade's thermal tolerance.

It should be noted that our results here seem to contradict those of previous work [55]. However, this variation is likely due to the methodological differences. FTIR spectroscopy measures the total lipid content and cannot differentiate between the individual fatty acid chains. GC-MS is a method where this is possible; however, since the interest here was in assessing the whole metabolic profile of the cell, and not just the membranes, FTIR spectroscopy was an appropriate choice. Further investigation using

synchrotron-based light sources and spectroscopy, could reveal more detailed information about where these lipids occur within the cell.

The implications of the structural differences in protein and their arrangement in space are not yet fully explained; however, various studies have shown differences in the types of proteins in *Symbiodinium*. Proteins tend towards β structures under stresses such as increasing temperature [97], [118]. It is impossible to determine which of the specific side-chains are contributing to the bands in the spectra for clades A and F, given the complexity of the cells being analysed here. Further investigation using techniques such as NMR spectroscopy or chromatography might shed more light on which individual amino acids are present and the implications of changing environmental conditions [55], [61], [78], [119]. However the purpose of this study was to assess macromolecular state of *Symbiodinium* as a whole and so the fine-scale differences in a single side chain, for example, was outside of the scope of this experiment.

Other reports have shown an increase in Heat Shock Protein (Hsp) expression [24] in response to elevated temperature. Specifically, two types of Hsp; Hsp70 and Hsp90, both with different conformational structures [120], [121]. However this type of protein only contributes approximately 1% of the total protein present in *Symbiodinium* [120], so it is unlikely to be the sole cause of the differences observed in the FTIR spectra.

The more likely sources of protein signal observed in the FTIR spectra are complexes found in the thylakoid membrane, which are vital for the photosynthetic processes within the cells [21]. Photosystem II (PSII) and the Light Harvesting Complexes (LHC) of various photosynthetic organisms have been widely analysed previously and their secondary structures have been characterised by techniques such as FTIR spectroscopy,

X-Ray Diffraction (XRD), Circular Dichroism (CD) and protein crystallography [35], [36], [122]–[125]. Both complexes were found to contain predominantly α-helix protein structure [126], [127]. The only source of β-sheet structure within the PSII complexes and thylakoid membranes appears to be from extrinsic protein sub-units responsible for stabilising the water-splitting manganese complexes [21], [35].

Peridinin-chlorophyll-protein (PCP) complexes are another source of protein found within the thylakoid membrane environments of *Symbiodinium* [80]. The secondary structural characteristics of these complexes contain a high α helix content [128]. The results of this study could also indicate a much lower PCP content in clade F cells than clade A.

3.5 Conclusions

As a result of the findings in this chapter, it is proposed that there is a significant difference in the structure of proteins and lipids between the two clades analysed in this study. It is speculated that subjecting the various clades to different environmental conditions and assessing the changes in the structure, and possibly content, could determine whether these differences in their conformation have an effect on their physiological tolerance to environmental changes, as has been shown to be the case in membrane lipid structure [55]. This will be examined in subsequent chapters.

Understanding the macromolecular content when exposed to variable environmental conditions is a vital component of developing energy budgets of micro-organisms [12]. Here, the use of FTIR spectroscopy for semi-quantitative content calculations, as well as a classification technique was shown to be an effective method for assessing macromolecular changes between genetic clades of *Symbiodinium*. Further statistical analysis and development of classification models also revealed a difference in protein

and lipid structure which could have an effect on the way the genetic clades respond to environmental stress.

Chapter 4. Macromolecular composition of symbiotic dinoflagellates; variation in response to elevated irradiance and temperature

4.1 Introduction

While effort has been made to understand the fine detail of *Symbiodinium* clades' response to environmental stress, there is currently little understanding of the changes as a whole. This is largely due to the types of macromolecular analysis techniques used to monitor components such as individual fatty acid chains or proteins. While this type of information is vital to the overall understanding of mechanisms within the cells, it is difficult to relate these processes together into one big picture.

The results from the previous chapter demonstrated that there was a significant difference in macromolecular content between clades A and F; specifically in lipid and protein structure. It is unknown as to whether these structural differences have an effect on tolerance to stress and the purpose of this chapter is to analyse the response of two different clades of *Symbiodinium* to increased light and temperature.

Temperature was kept to the lower thermal stress limit to simulate a more likely ecological scenario, as well as prolong the metabolic response so it could be monitored over a realistic period.

4.2 Results

4.2.1 Photosynthetic function

Figure 4.1 shows the maximum quantum yield of PSII over time for clades A and F. Both show statistically significant decreases in F_v/F_m as compared with the control samples, for all treatments (mixed model ANOVA, $p<0.05$). Maximum quantum yield measurements show the largest decrease across all treatments for clade A cells (Table A2.1). rmANOVA results indicate that clade A cells underwent significant changes in maximum quantum yield of PSII for all treatments. The cells exposed to elevated light and temperature underwent the largest decrease in function, while elevated temperature alone appeared to have the least effect. Clade F cells exhibited a similar effect, but to a lesser degree. The rmANOVA results indicate that there was no statistically significant changes occurring for cells exposed to elevated temperature alone, whereas both elevated light and the combination of elevated light and temperature treatment gave significant changes over time. This indicates that the combination of high light and high temperature increases the degree of stress experienced by the cells and that clade A is less tolerant to this stress as indicated by pilot studies described in Chapter 3.

It should be noted here that growth rate calculations were inconclusive. Significant aggregation of the cells was observed, which increased as the number of days exposed to stress increased. This resulted in overly large error in cell density estimation.

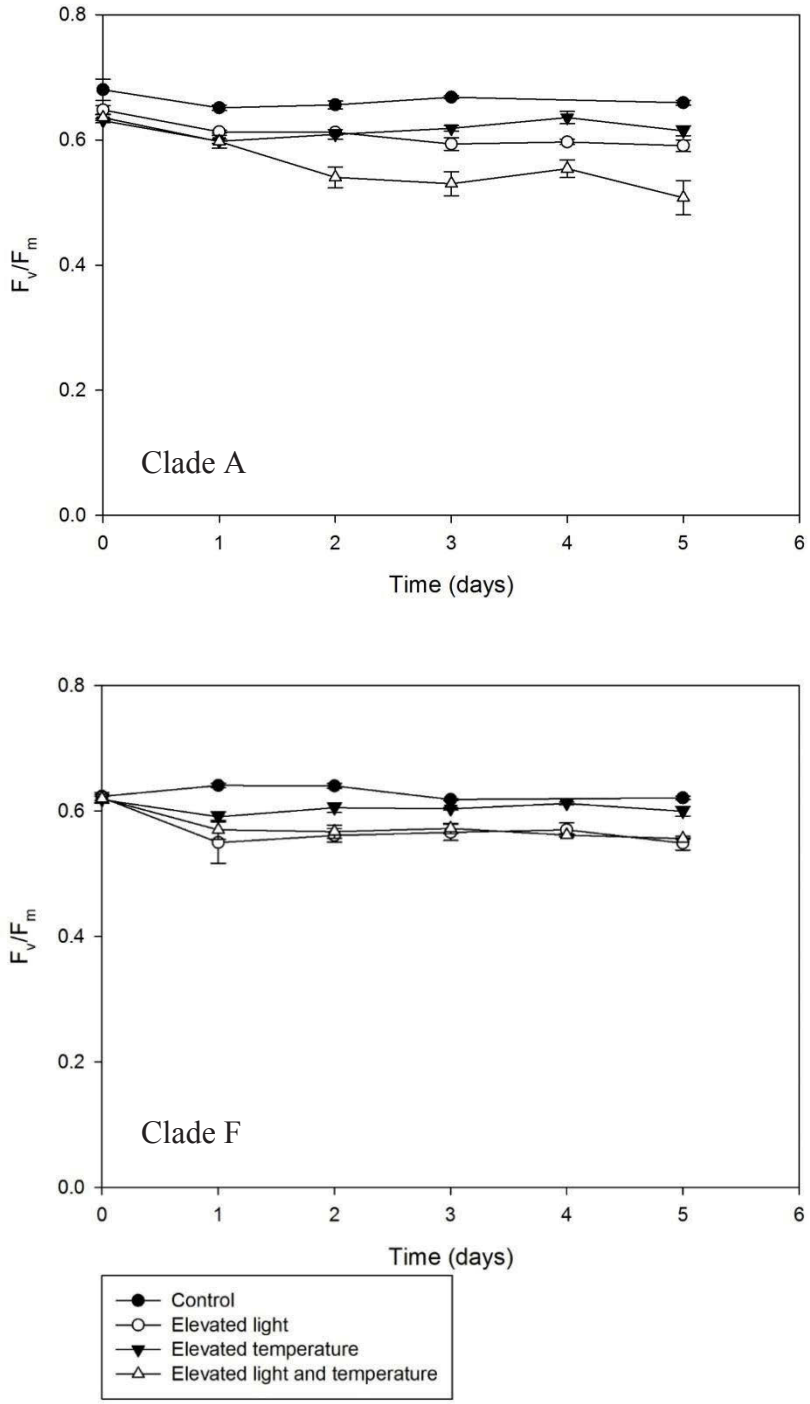

Figure 4.1: Photosynthetic efficiency of clades A and F exposed to environmental treatments. Elevated light = 100 μmol photons.s^{-1} and elevated temperature = 31°C. Data points are mean (n=4) and error bars are ± SEM. rmANOVA results are summarised in Tables A2.1-A2.2.

4.2.1 Macromolecular content changes

In the following sections, the protein, carbohydrate, lipid and phosphorylated compound contents were measured as a percentage of the whole area under the curve as described in section 2.4. Change over time was then analysed as a percentage differing from T0 in order to normalise the relative differences that may be occurring.

4.2.1.1 Protein

Figure 4.2 shows the change in percentage composition for total protein content from both clades over time. Clade A showed the most change; mixed model ANOVA showed that cells exposed to elevated temperature treatment were significantly different to the control cells. Elevated light stress appears to have the opposite effect, resulting in an increase in protein content (Table A2.3); however, the mixed model ANOVA results did not show any significant differences between these cells and the control. Clade F, however, did not exhibit any significant changes in total protein content (Table A2.4). Mixed model ANOVA also showed that the response to environmental stress in terms of protein content, was significantly different between clades of *Symbiodinium* for cells exposed to elevated light and a combination of elevated light and temperature.

4.2.1.2 Carbohydrates

Clade A cells exposed to elevated temperature (including the high light and high temperature treatment) significantly increased their carbohydrate content after five days of exposure to the changed environmental conditions (Figure 4.3, Table A2.5). Clade A exposed to elevated light alone, however, appeared to have the opposite effect with content decreasing significantly after two days of exposure. All of these treatments

deviated from the behaviour of the control cells and mixed model ANOVA showed that the response of these cells to the treatments was significantly different.

Clade F cells exposed to high temperature and a combination of elevated light and temperature, exhibited a similar trend in response to clade A cells; however, clade A cells increased in carbohydrate content to a much higher degree. Once again, cells exposed to high light alone exhibited the opposite response and carbohydrate content decreased steadily over time relative to the control samples. Mixed model ANOVA showed that the response of both clades to elevated light, was similar.

4.2.1.3 Phosphorylated compounds

The change in phosphorylated compounds shown in Figure 4.4 appeared to be similar for both clades of *Symbiodinium*. Clade A cells showed a slightly greater degree of change and all treatments for this clade deviated significantly from the response of the control cells. A positive change in composition was found for the cells exposed to high light (refer to Table A2.9 for rmANOVA results). The opposite response was found for cells exposed to high temperature and a combination of high light and temperature. Mixed models ANOVA revealed that there was no difference in response for cells exposed to elevated temperature stress alone. It should also be noted that the clade A samples showed a sharp decrease in content under high temperature conditions between four and five days of exposure.

Mixed models ANOVA also revealed that both clades responded in a similar way to elevated temperature stress. Statistical analysis of the response to elevated light suggested that, while both clades appeared to have similar trends, the degree of change was significantly different.

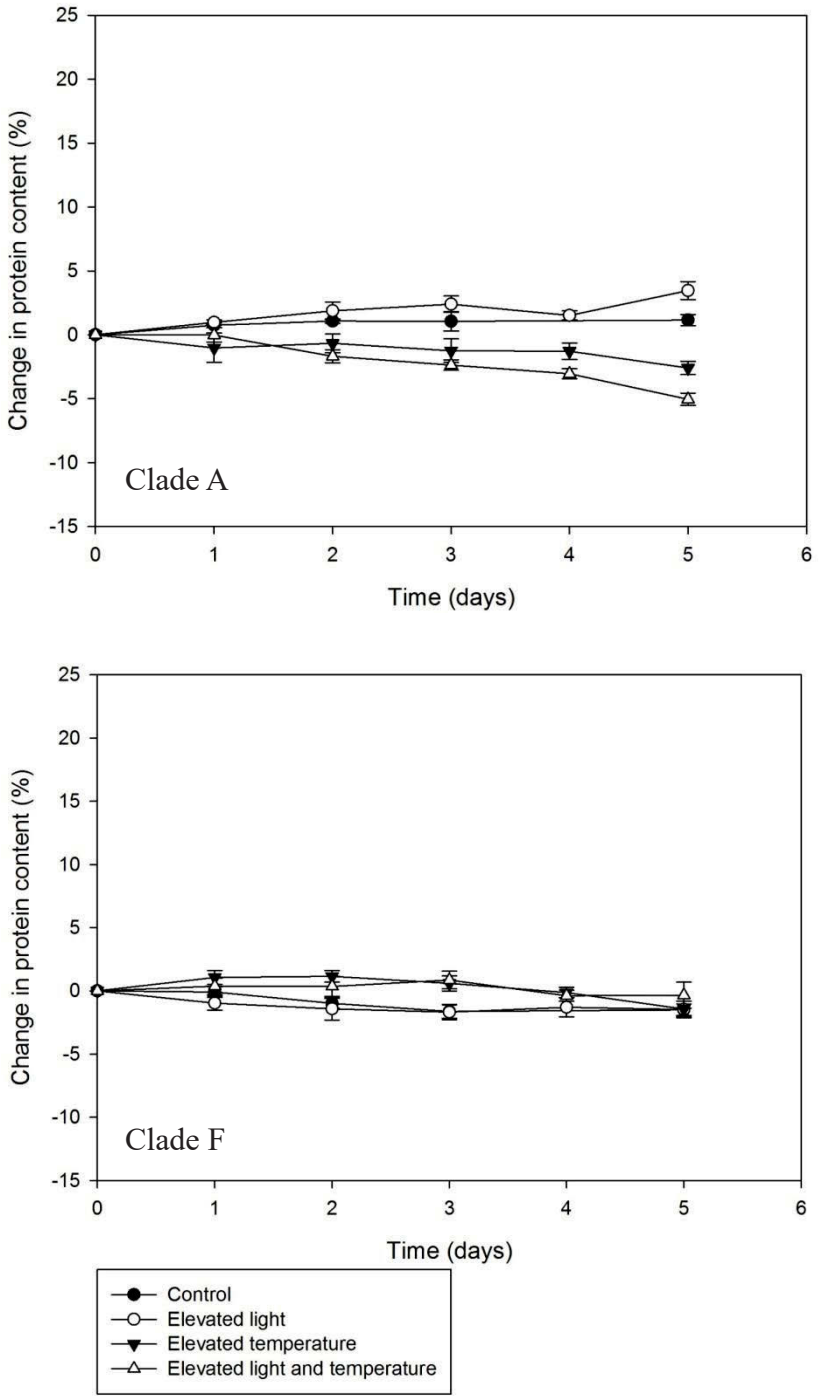

Figure 4.2: Change in protein content (%) over time for clade A and F. Elevated light = 100 µmol photons.s^{-1} and elevated temperature = 31ºC. Data points are mean (n=4) and error bars are ± SEM. rmANOVA results are summarised in Tables A2.3-A2.4.

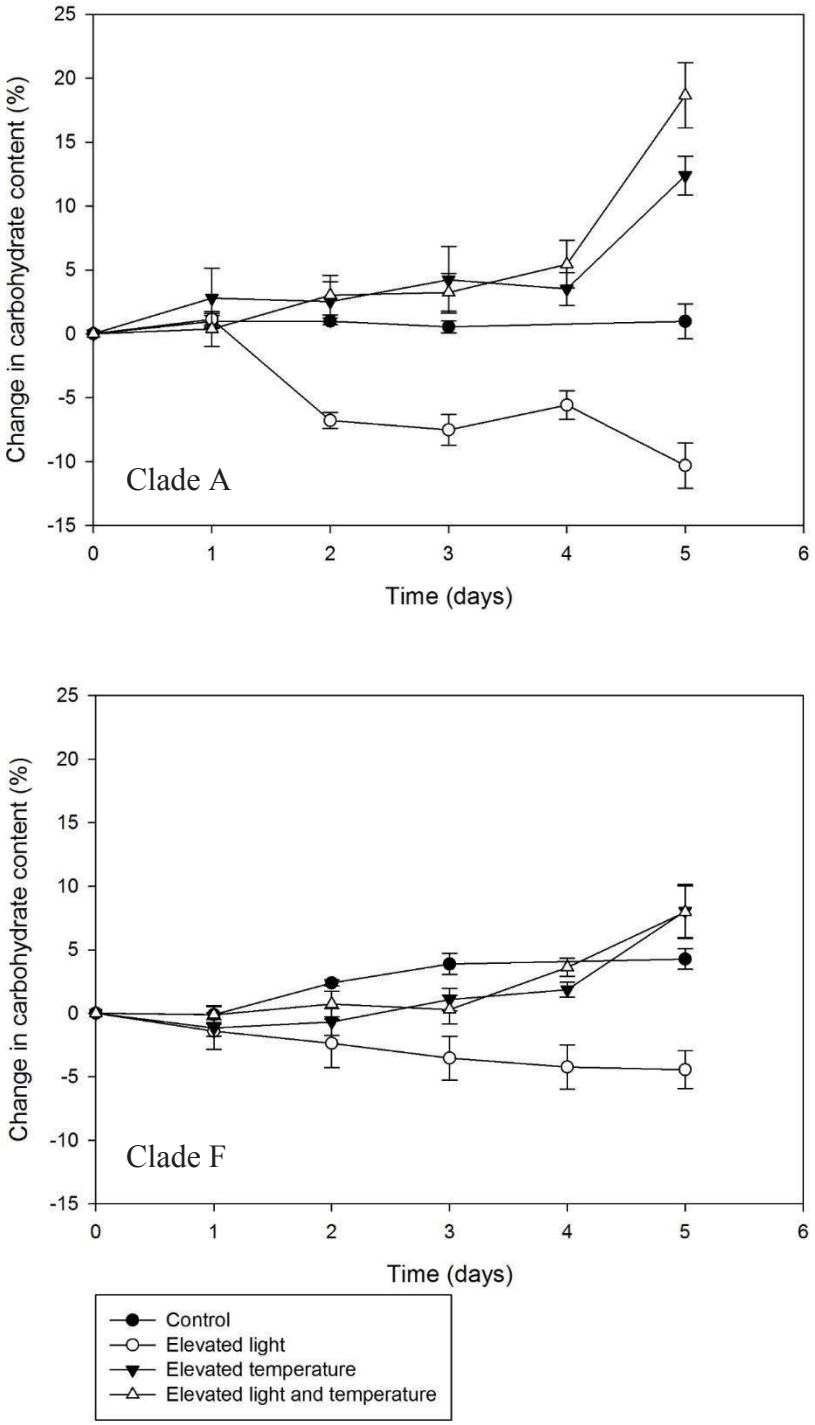

Figure 4.3: Change in carbohydrate content (%) for clade A and F. Elevated light = 100 µmol photons.s^{-1} and elevated temperature = 31ºC. Data points are mean (n=4) and error bars are ± SEM. rmANOVA results are summarised in Tables A2.5-A2.6.

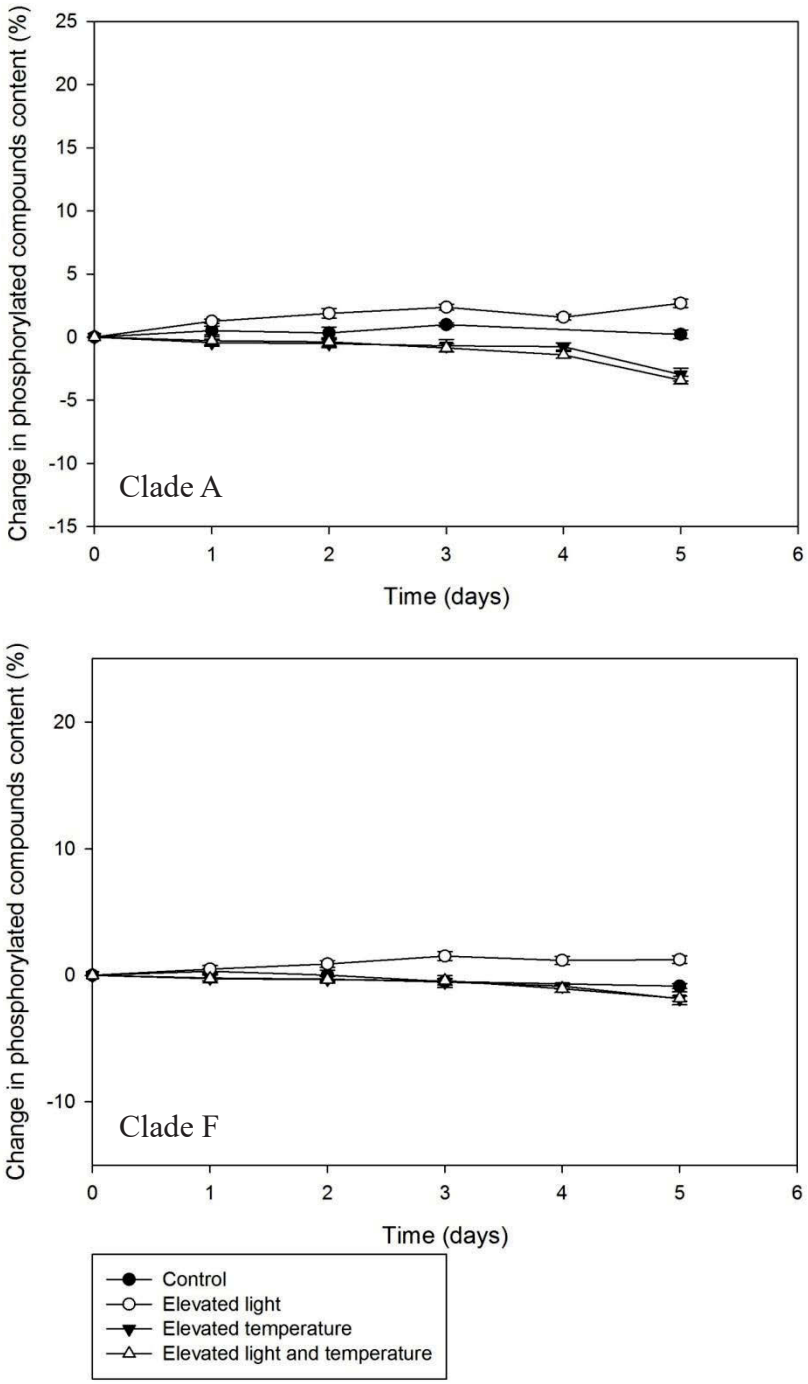

Figure 4.4: Change in phosphorylated compounds content (%) over time for clade A and F. Elevated light = 100 μmol photons.s^{-1} and elevated temperature = 31ºC. Data points are mean (n=4) and error bars are ± SEM. rmANOVA results are summarised in Tables A2.9-A2.10.

4.2.1.4 Lipids

Total lipid content was monitored by the lipid carbonyl band at 1730 cm^{-1} (refer to Appendix 1 for full spectra). Figure 4.5 shows the change in total lipid content for both clades (the y-axis is set to a common range for comparison with Figures 4.2-4.4). Clade A cells exposed to all treatments, exhibited no overall significant change in content at any time (Table A2.7). Clade F cells appeared to change their lipid content significantly in response to elevated temperature stress more than the less thermally tolerant clade A cells. Temperature treatments produced a decrease in overall content from zero to five days of exposure compared to the control samples. Elevated light appeared to have the opposite effect with an increase in content observed, but rmANOVA showed that this was not statistically significant over time. It is interesting to note that the clade F cells exposed to a combination of high light and temperature showed a decrease in lipid content, however, this decrease was not as marked as for the cells exposed to solely elevated temperature alone. Both of these treatments were significantly different from the control cells. The responses of both clades to all treatments were significantly different to each other.

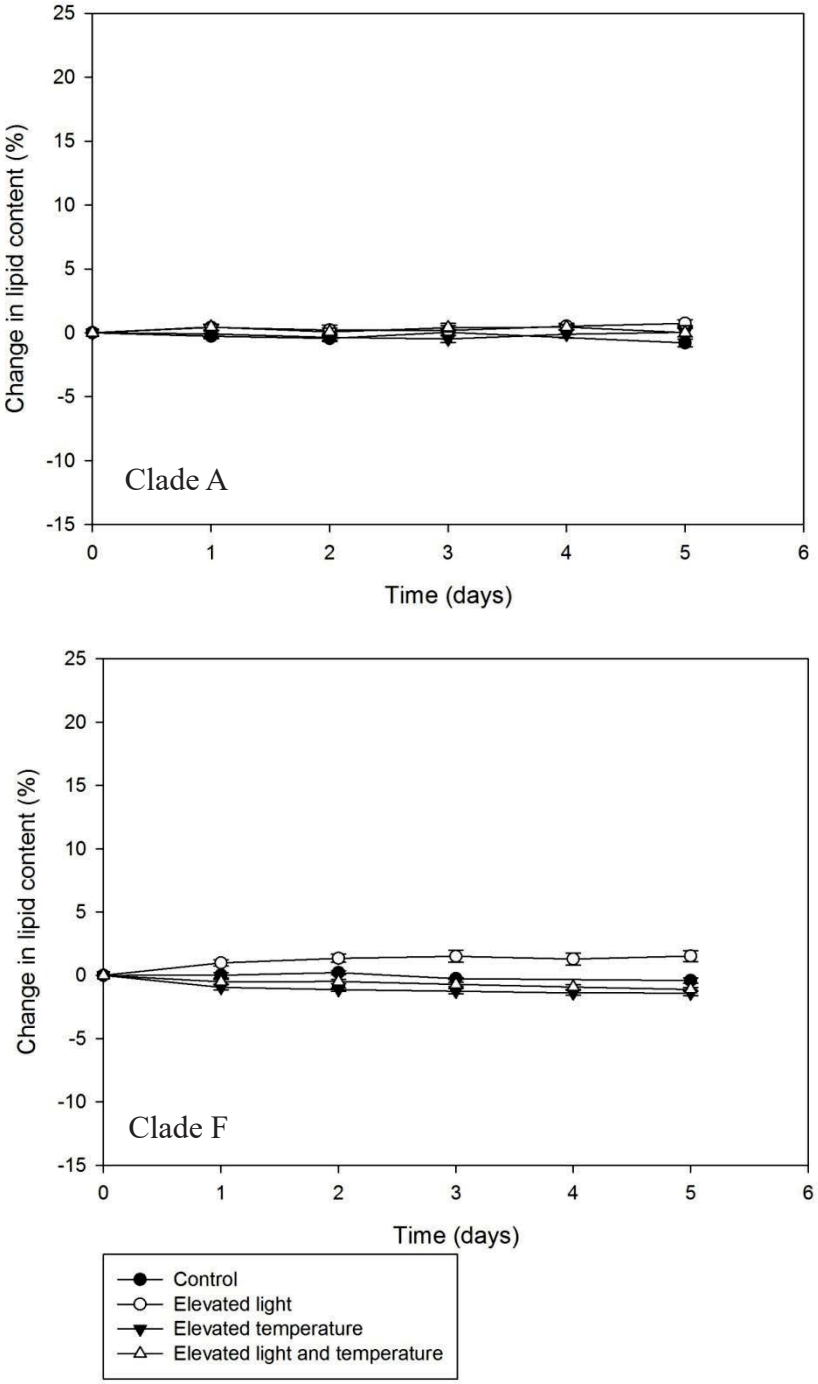

Figure 4.5: Change in total lipid content (%) over time for clade A and F. Elevated light = 100 μmol photons.s^{-1} and elevated temperature = 31°C. Data points are mean (n=4) and error bars are ± SEM. rmANOVA results are summarised in Tables A2.7-A2.8.

4.2.2 Structural analysis

4.2.2.1 Lipids

The infrared region between 3020 and 2800 cm^{-1} can reveal some useful information about the structure of the total lipid content within the sample. Intensities of the bands outlined in section 2.4 were identified and different ratios calculated using Equations 2.1-2.3. Figure 4.6 shows the calculated ratios of unsaturated: saturated lipids for both clades. It should be noted that, once again, the y-axes are set to a common scale for comparison with Figures 4.7 and 4.8. As was the case with the total lipid content, clade F appear to be affected more than the less thermally tolerant clade A cells and this was confirmed by rmANOVA. The clade A cells exposed to elevated light showed the most change with an increase in saturation, and overall were significantly different to the other treatments and control. Clade F cells showed a consistently higher ratio than the control cells. The samples exposed to elevated light showed a greater increase in lipid saturation ratio than those cells exposed to elevated temperature and were shown to be significantly different by mixed models ANOVA.

Figure 4.7 shows the degree of lipid branching within both the clade A and F cells. Clade A did not show any significant changes, whereas clade F showed a similar trend to the unsaturation ratios; cells exposed to elevated light experienced a greater change in lipid structure than those exposed to elevated temperature alone.

The final lipid structural value calculated was the degree of disorder (Figure 4.8). Lipid disorder showed no overall significant change for clade A cells. Clade F however, appeared to be affected by environmental change with significant differences observed between the control cells and those exposed to all treatments. Elevated light and

elevated temperature alone seemed to have the same effect and were not significantly different to each other.

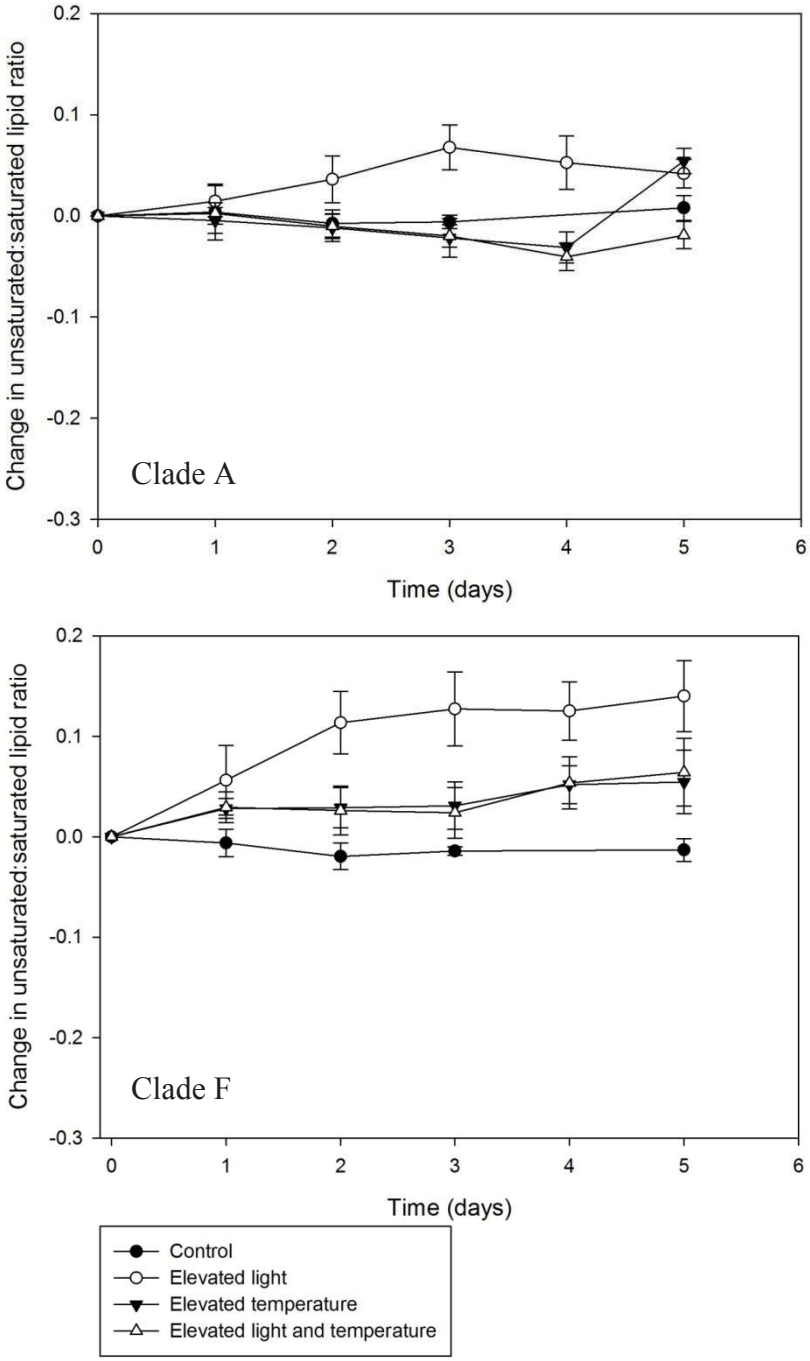

Figure 4.6: Change in lipid saturation over time for clade A and F. Elevated light = 100 μmol photons.s^{-1} and elevated temperature = 31ºC. Data points are mean (n=4) and error bars are ± SEM. rmANOVA results are summarised in Tables A2.11-A2.12.

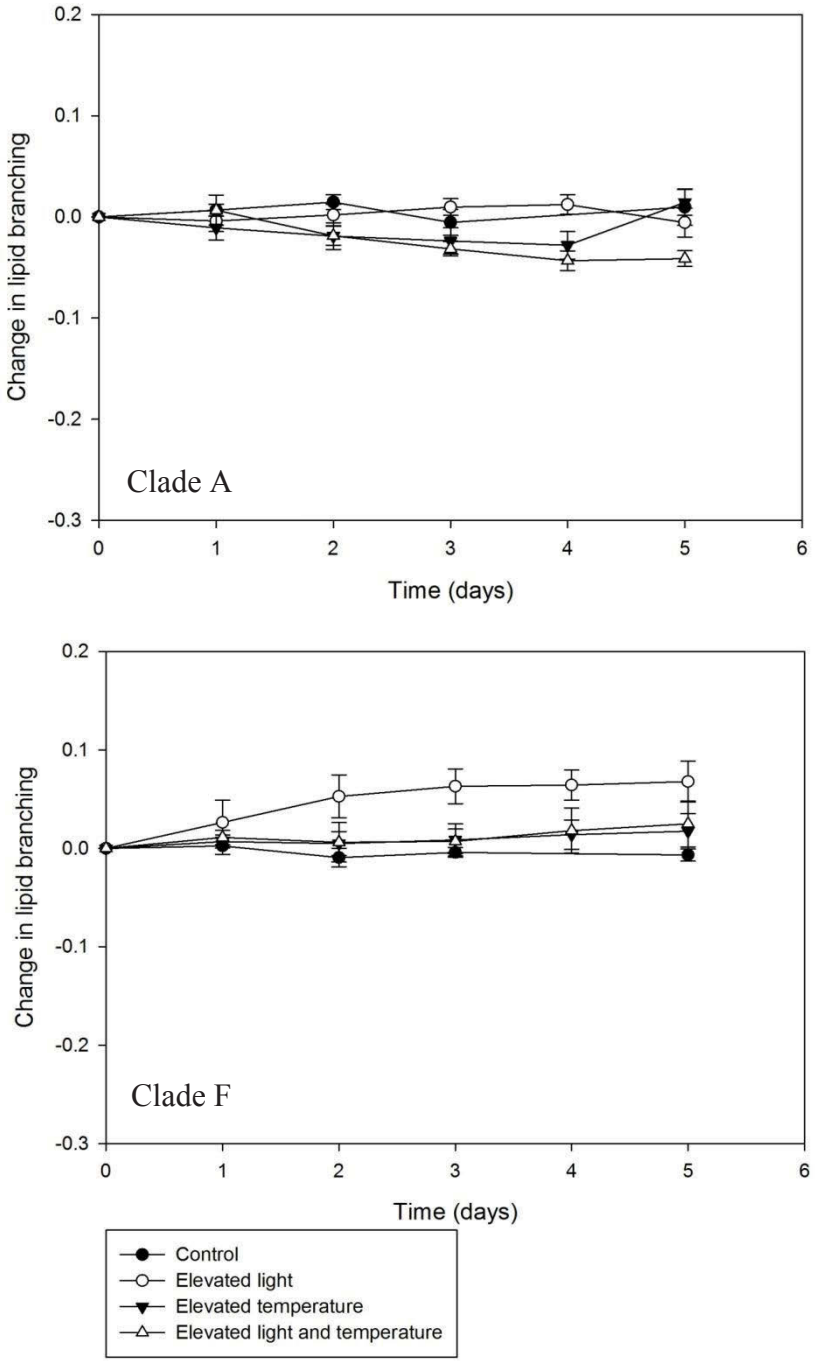

Figure 4.7: Change in lipid branching over time for clades A and F. Elevated light = 100 μmol photons.s^{-1} and elevated temperature = 31°C. Data points are mean (n=4) and error bars are ± SEM. rmANOVA results are summarised in Tables A2.13-A2.14.

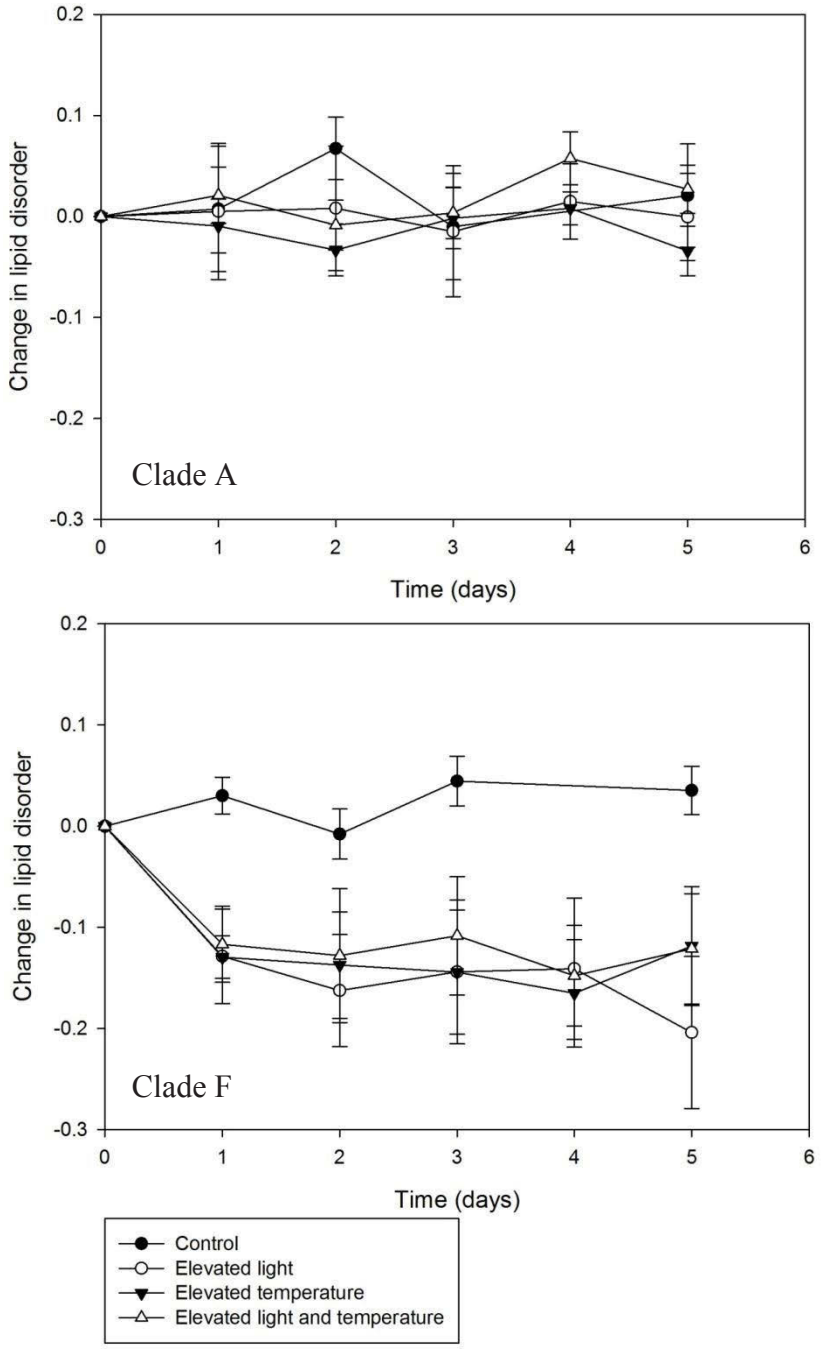

Figure 4.8: Change in lipid disorder over time for clade A and F. Elevated light = 100 μmol photons.s^{-1} and elevated temperature = 31ºC. Data points are mean (n=4) and error bars are ± SEM. rmANOVA results are summarised in Tables A2.15-A2.16.

4.2.2.2 Protein

Comparisons of the amide I regions of derivatised spectra (Appendix 1, Figures A1.7 – A1.12) revealed a number of trends. Firstly, there did not appear to be any changes in protein structure for clade A cells exposed to elevated irradiance – neither of the troughs at 1650 or 1620 cm^{-1} changed. Clade F showed a greater degree of change under high light conditions. The α-helix content remains about the same (1655 cm^{-1}); however, a distinct increase in β-pleated sheet structure occurs over the time in which the cells are exposed to elevated light levels (1620 cm^{-1}). The trough appearing at 1690 cm^{-1} has previously been attributed to β-sheet structure [97], and clearly increases in intensity from T0 to T5 exposed to elevated light.

The protein structure for clade A cells exposed to elevated temperature did not appear to change over time. The Clade F cells underwent a higher degree of change than clade A under high temperature conditions, as was the case for cells exposed to elevated light. Protein content changed significantly once exposed to elevated temperature (between T0 and T1). Alpha helix structure (1655 cm^{-1}) decreased steadily over the five days of exposure, shifting to a β-pleated sheet structure (1690 and 1620 cm^{-1}).

The cells exposed to elevated light and temperature exhibited a large change in protein secondary structure over time for both clades. Clade A cells showed protein structure that appeared to change over time with an increase in intensities of both the bands in the region 1690 – 1620 cm^{-1}. The α-helix content (1655 cm^{-1}) appears to remain unchanged. This varies from the cells' response to elevated light, where the ratio of β-sheet to α-helix appeared to remain unchanged.

Clade F cells show similar trends in response to elevated temperature, with a number of key spectral differences. The intensity of the band at 1690 cm^{-1} increases sharply

between zero and one day of exposure. This band is commonly attributed to β-sheet [71], [110]. This is accompanied by an increase in intensity of the band at 1620 cm^{-1}. The α-helix content of these cells also appears to decrease in intensity.

4.2.3 Statistical analysis

In order to pick the samples that gave the most change in macromolecular state, PLSDA was used to classify the data. PCA was used to split the data into two sets. Models 1 and 2 split the data into three groups, day 0, days 1-3 and days 4-5, and day 0, days 1-4 and day 5, respectively. Validity of these models was calculated based on sensitivity and selectivity parameters as described by Sackett et al., (2013).

Once the optimal difference between the initial and final macromolecular states had been determined, PLSDA was used again to assess the overall effect of treatment on the cells. Four groups were established. The "initial" group consisted of the control cells and the T0 groups for the three treatments. The other three groups were the "final" groups of the treatments as determined in the previous PLSDA models. Sensitivity and selectivity parameters were once again used to assess the validity of the models generated using these four groups, for each clade. The more successful the classification, the greater the effect of the treatment on the cells.

Table 4.1 is a summary of chemometric model parameters for clades A and F exposed to elevated light. It shows the samples assigned to one of three classes, the r-squared values, RMSEP (root-mean-square error of prediction), sensitivity and specificity. The higher the r^2 value, sensitivity and specificity, and the lower the RMSEP, the better the fit.

Table 4.1: PLSDA model parameters for clade A and F cells exposed to high light.

Clade	Group (days)	r^2	RMSEP	Sensitivity (%)	Specificity (%)
A	0	0.873	0.136	100	100
	1-4	0.738	0.245	100	95.8
	5	0.473	0.277	91.7	100
F	0	0.872	0.299	75.0	100
	1-4	0.845	0.447	100	79.1
	5	0.742	0.290	75.0	100

Based on these parameters, the samples are correctly classified as one of three groups. The initial samples (day 0) were significantly different (with 100% correct classification) than the rest of the days indicating that elevated light induced a significant short-term metabolic response. The cells after five days of exposure were significantly different to the other groups (with 91.7 and 100% sensitivity and specificity, respectively).

Figure 4.9 is a comparison of the scores and loadings plots for clade A. The majority of the variation between the initial and final groups is explained by factor 1 consisting mostly of a carbohydrate band at 995 cm^{-1}. Since these chemometric models were built using 2nd derivatives, the interpretation of the loadings must be reversed. This means that the cells have more carbohydrate at day 5 than at day 0.

The intermediate group (days 1-4) is largely explained by changes in protein structure and lipids according to factor 2. There is more β-sheet in the intermediate stage, as well as more lipid. The phosphate band at 1080 cm^{-1} also contributes a large amount to the variation in factor 2. Since this is a positive band in the loadings, the intermediate group has less phosphate than the initial and final. Clade A cells are affected by exposure to high light.

Table 4.1 is a summary of the PLSDA model parameters for clade F cells exposed to elevated light. It is immediately obvious, looking at both these values and the groupings in Figure 4.10, that the model for clade F are not as good a fit as for clade A (Table 4.1).

Inspection of the groupings shown in Figure 4.10, and the loadings plots associated, demonstrates that, although there is not as clear a separation between the three groups, there is a clear difference between initial and final. This indicates that there was a metabolic change occurring under high light with clade F, but probably not to the same extent as clade A.

The loadings indicate that the majority of difference between the initial and final groups for clade F cells is explained by factor 1. The most intense band for this model is the β-pleated sheet at 1690 cm^{-1} followed by the β-pleated sheet band at 1620 cm^{-1}. These are both negative bands in the loadings and so the cells at five days of exposure to high light had a greater β-pleated sheet secondary structure content than those at the beginning of the treatment. This correlates with visual analysis of the 2^{nd} derivatives (see section 4.2.2.2). Lipid content at 1730 cm^{-1} is a positive band in the loadings and so there is less lipid at five days than at the beginning of the experiment.

Comparing the chemometric models for both clades reveals a difference in the degree of separation of the groups, and the model parameters. Overall, clade A cells gave a better classification than clade F, indicating a greater degree of metabolic change within the cells. Therefore, clade A cells were more affected by high light conditions than clade F.

Table 4.2 is a summary of model fit parameters for clade A cells exposed to high temperature. This is also an indication of how much the cells were affected by the specific treatments.

Table 4.2: PLSDA model parameters for clade A cells exposed to high temperature.

Clade	Group (days)	r^2	RMSEP	Sensitivity (%)	Specificity (%)
A	0	0.718	0.377	60	100
	1-3	0.687	0.393	97.1	77.8
	4-5	0.768	0.207	100	97.8
F	0	0.909	0.230	100	100
	1-3	0.785	0.274	100	91.7
	4-5	0.820	0.314	95.8	100

Overall, clade A cells gave poor prediction scores for all model groupings as compared with the cells exposed to elevated light conditions. Scores and loadings for this model is shown in Figure 4.11 and confirm the poor fit. The scores plots in Figure 4.11 show no clear differentiation between groups. The loadings plots in Figure 4.11 show that the variation explained by factors 1 and 2 are generally noise from the spectra, rather than due to biological bands. This is a clear indication that the clade A cells exposed to high temperature were generally not affected.

Clade F cells exposed to elevated temperature; however, showed a significantly improved fit for both models, confirming that these cells were adversely affected by this treatment. Table 4.2 is a summary of the prediction parameters for both models and show that prediction rates were high.

Figure 4.12 show the scores plot and clearly indicates a separation between the three groups in the model. The loadings plots (Figure 4.12) show that, as opposed to clade A cells exposed to elevated temperature, the variation explained by PC-1 and PC-2 is largely due to biological bands in the spectra. The majority of the variation is due to the secondary structure of the protein (1700 – 1600 cm^{-1}). Beta-pleated sheet (1690 and 1620 cm^{-1}) and α-helix (1655 cm^{-1}) structures are oppositely correlated for both PC-1 and PC-2. This shows that between the initial and intermediate groups, there was a higher β-pleated sheet content for the intermediate group. There was another increase in

β-pleated sheet content between the intermediate and final group in this model. The loadings for both models also indicate that phosphate content increased from 0 to 5.

From an examination of the fit of these models for *Symbiodinium* exposed to elevated temperatures, it can be concluded that clade F exhibited a higher degree of metabolic change under these conditions.

Table 4.3 is a summary of model fit parameters for clade A cells exposed to high light and temperature.

Table 4.3: PLSDA model parameters for clade A cells exposed to high light and temperature.

Clade	Group (days)	r^2	RMSEP	Sensitivity (%)	Specificity (%)
A	0	0.574	0.270	0	100
	1-3	0.457	0.468	84.8	66.7
	4-5	0.678	0.306	79.2	100
F	0	0.902	0.230	100	100
	1-3	0.821	0.420	97.1	91.7
	4-5	0.758	0.373	87.5	97.9

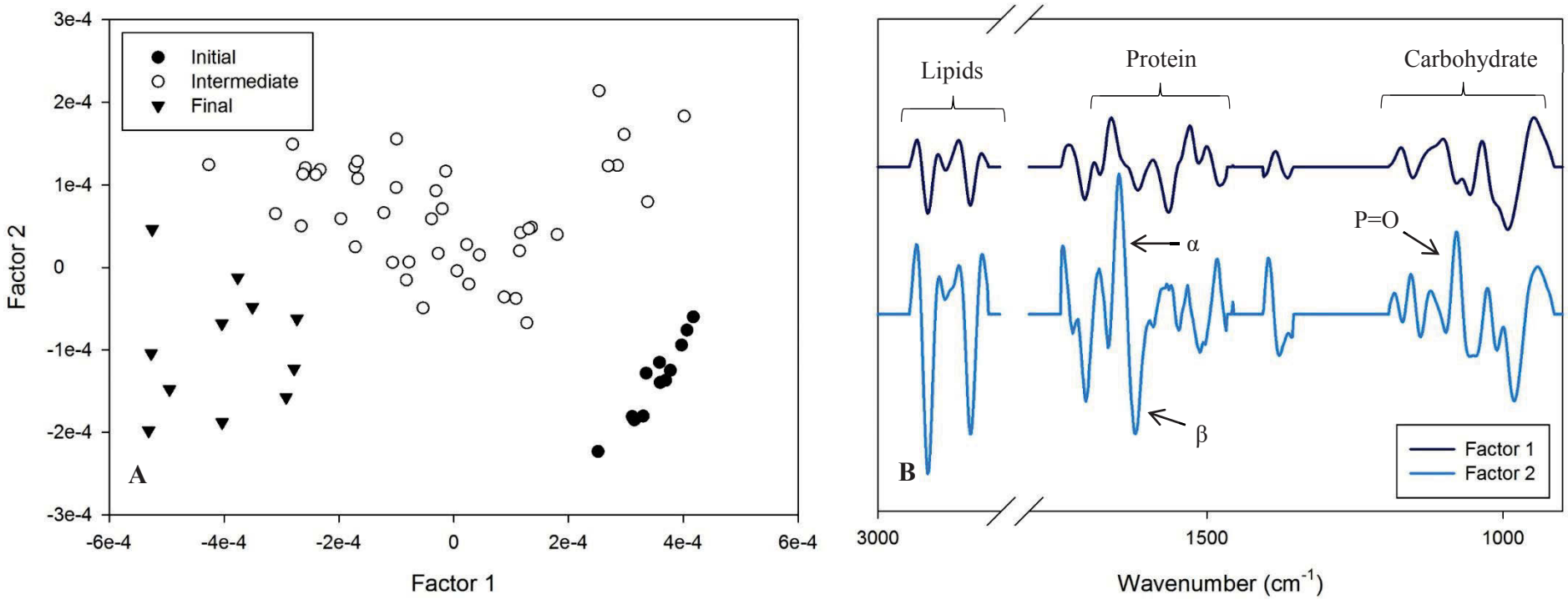

Figure 4.9: PLSDA scores (A) and loadings (B) for clade A cells exposed to elevated light.

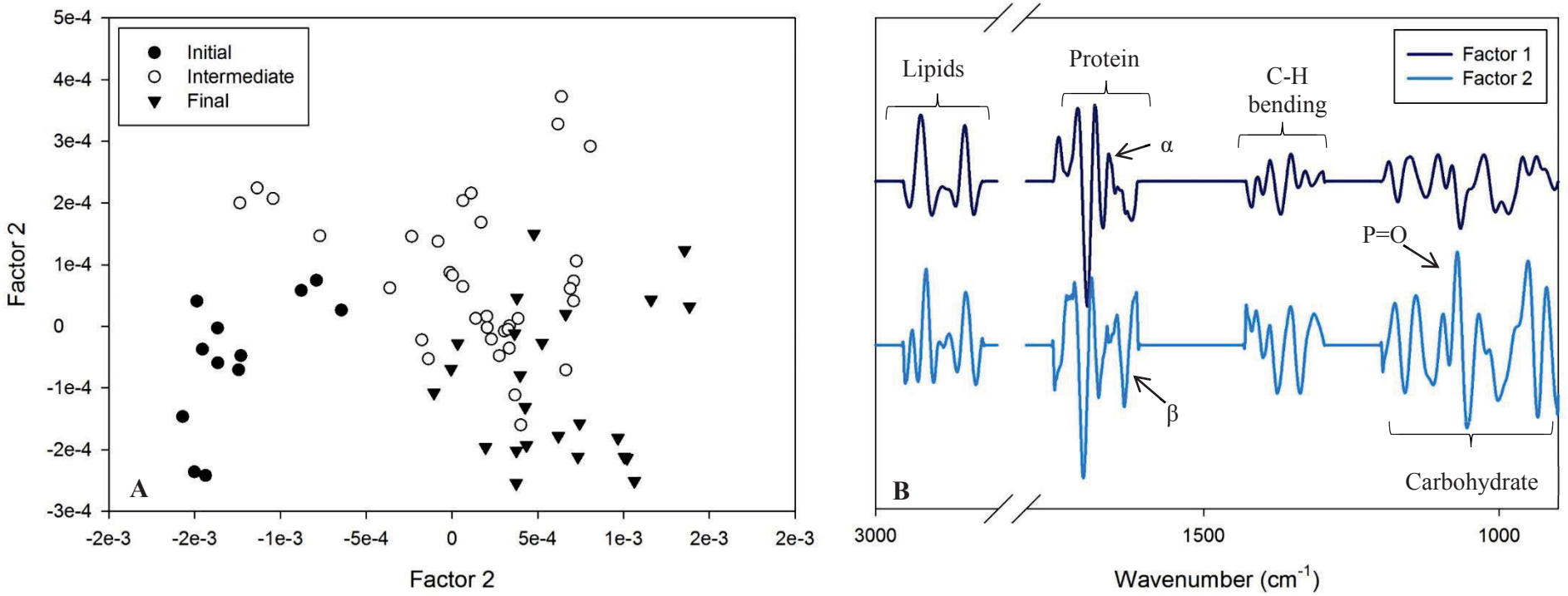

Figure 4.10: PLSDA model scores (A) and loadings (B) for clade F exposed to elevated light.

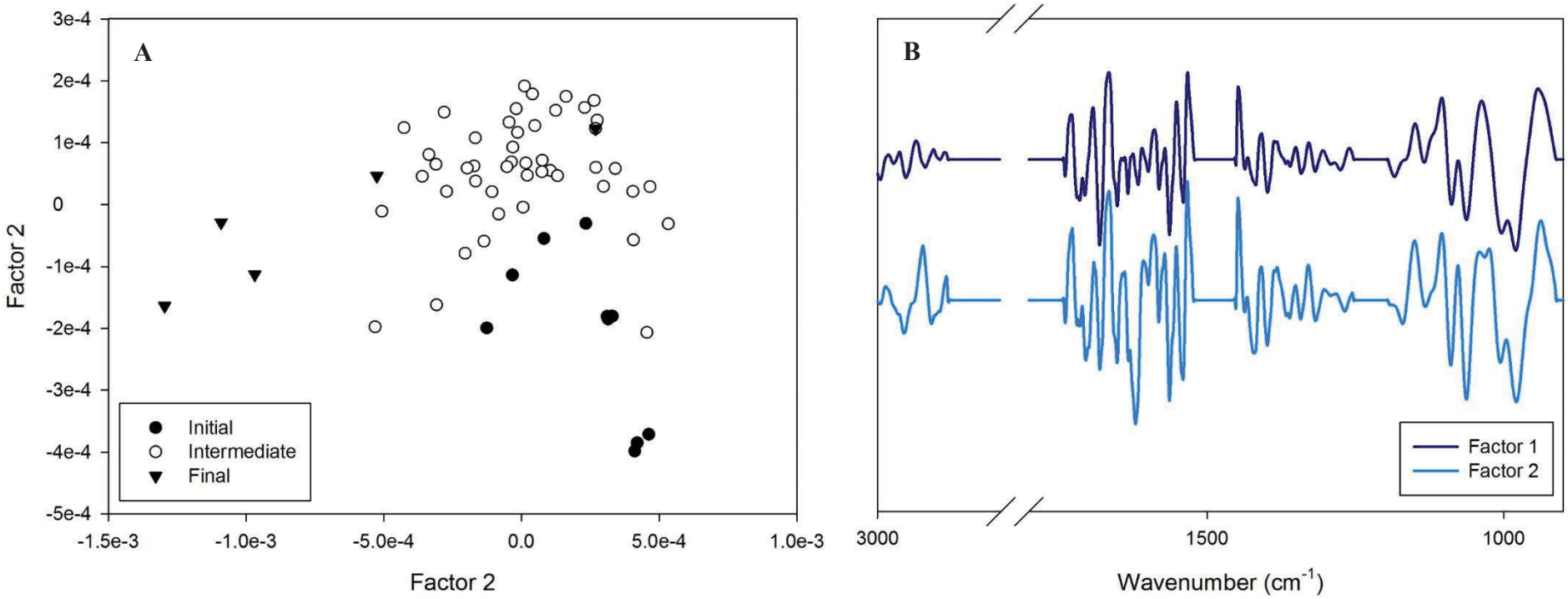

Figure 4.11: PLSDA model scores (A) and loadings (B) for clade A exposed to elevated temperature.

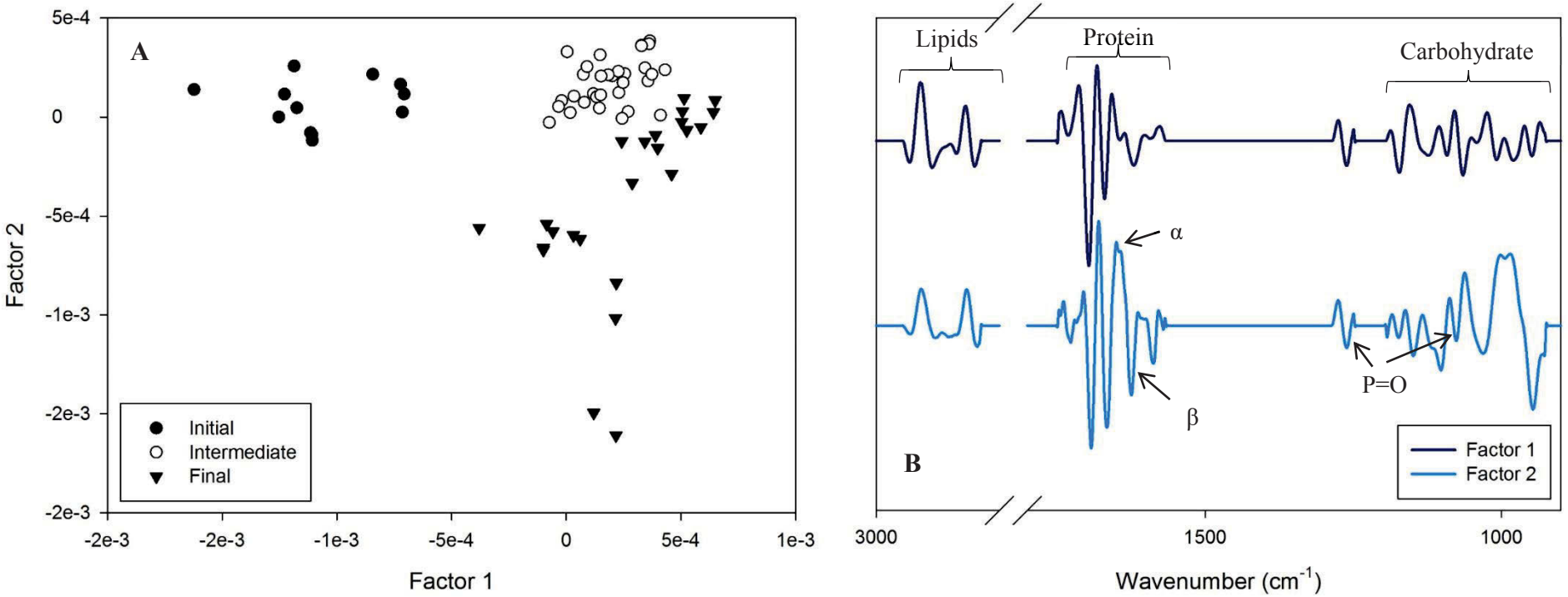

Figure 4.12: PLSDA model scores (A) and loadings (B) for clade F exposed to elevated temperature.

The model generated for clade A cells was a much better fit than the cells exposed to elevated temperature alone. The sensitivity of the model with respect to day 0 was extremely low indicating that none of the validation samples were correctly classified. This is an indication that the separation between day 0 and the intermediate group of samples was not significant. The loadings plot for the model shows that the lipid content increased over time (Figure 4.13). Both the protein α-helix and β-sheet content were positively correlated in the loadings which indicates a decrease over time since the models were built using 2nd derivative spectra. Carbohydrate content also contributed to the separation of the groups with glucose (1020 cm^{-1}) and ribose (995 cm^{-1}) having the most effect on the loadings.

Clade F exhibited a markedly better separation with significant improvements in model parameters (Table 4.3). Correct classification did not stray below ~80% and r^2 and RMSEP values were good. The loadings plots (Figure 4.14) indicate that the majority of the variation between these three groups was due to carbohydrates (~995 cm^{-1}), lipid content and protein secondary structure. Once more, the β-sheet content increased over time.

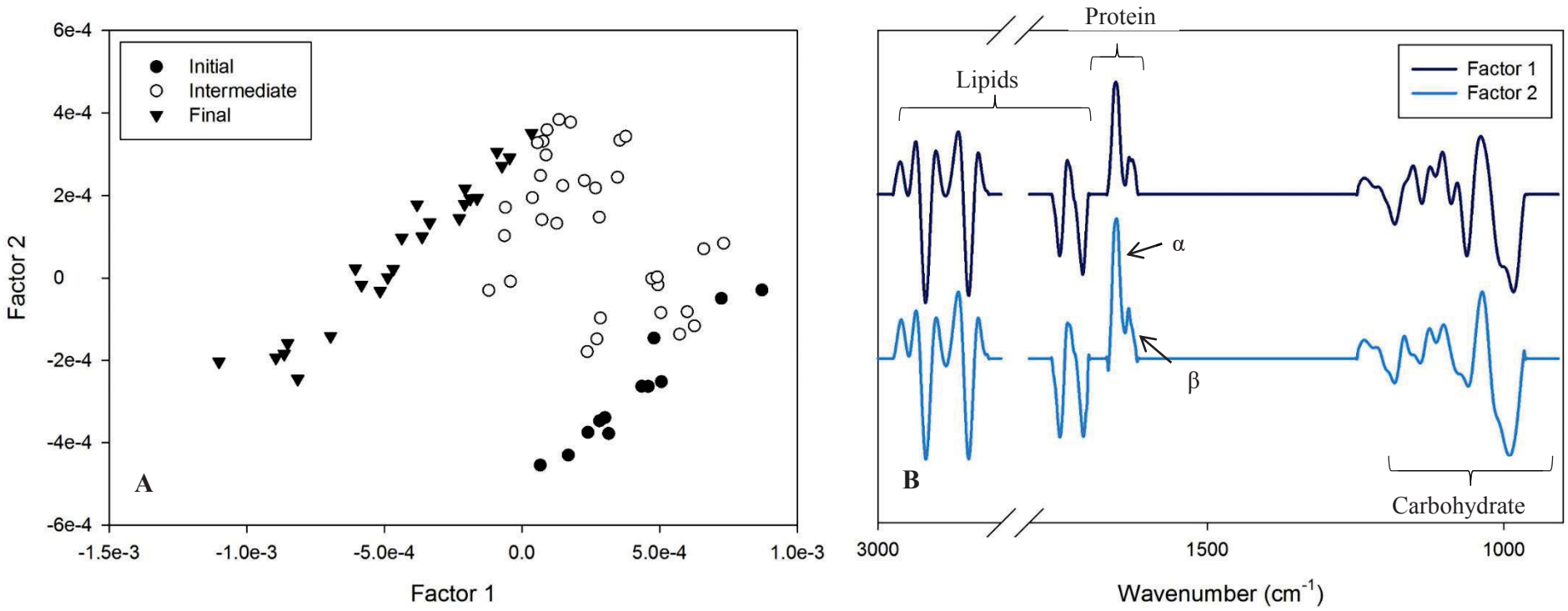

Figure 4.13: PLSDA model scores (A) and loadings (B) for clade A cells exposed to elevated light and temperature.

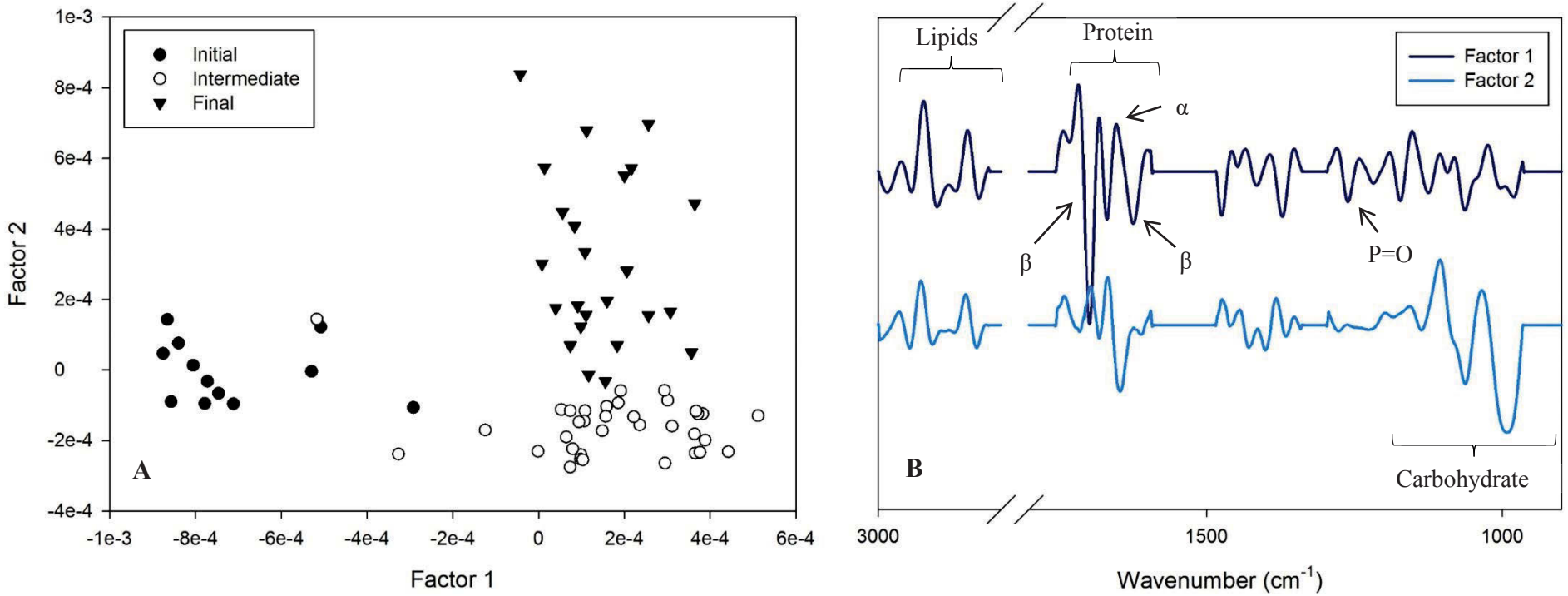

Figure 4.14: PLSDA model scores (A) and loadings (B) for clade F cells exposed to elevated light and temperature.

Using these groupings, the effect of treatment on macromolecular content was tested using PLSDA. Two chemometric models were developed; one comparing the initial and final groups of clade A cells exposed to all of the treatments, and the other containing the same, but for clade F. Scores and loadings of models with respect to clade A cells are shown in Figure 4.15, and Tables 4.4-4.6 outline the models' parameters.

Table 4.4: Parameters for PLSDA model for clade A split into two groups.

Group	r^2	RMSEP	Sensitivity (%)	Specificity (%)
Initial	0.823	0.207	100	100
Final	0.823	0.207	100	100

Table 4.5: Parameters for PLSDA model for clade A split into three groups.

Group	r^2	RMSEP	Sensitivity (%)	Specificity (%)
Initial	0.817	0.211	100	100
Elevated light + Elevated temperature	0.618	0.263	85.7	100
Elevated light and temperature	0.913	0.113	100	100

Table 4.6: Parameters for PLSDA model for clade A split into four groups.

Group	r^2	RMSEP	Sensitivity (%)	Specificity (%)
Initial	0.821	0.208	100	100
Elevated light	0.637	0.215	100	99.1
Elevated temperature	0.228	0.250	41.7	100
Elevated light and temperature	0.824	0.160	100	100

Three model groups were developed and tested for clade A cells. Model one (Table 4.4) showed that there were significant differences in macromolecular content between cells grown in normal conditions, and cells exposed to stress. Once the spectra were further divided into groups based on treatments, it was found that cells exposed to elevated light and elevated temperature alone gave an unclear separation. Model two revealed that the best classification was achieved when the spectra were divided into three

groups. This is an indication that clade A cells exposed to a combination of elevated light and temperature underwent a significantly different macromolecular response.

From an inspection of the groupings generated in model 3 (Figure 4.15), it appears that the two main factors explaining the model, separated different treatments in the following way; Factor 1 explained the difference between the initial samples and elevated temperature and the combination of elevated light and temperature; Factor 2 explained the difference between the elevated light samples and the other groups.

Factor 1 separated the elevated temperature samples and further separated the elevated light and temperature samples. This indicated that the samples exposed to the latter treatment were significantly more affected than the former. Lipid content appeared to be the greatest contributor to this factor. Methylene chain vibrations underwent a great amount of change over the course of the treatment. It should be noted that all of the bands used to calculate Equations 2.1 to 2.3 are all positively correlated in the loadings plots, which could explain why the calculated structural parameters did not show significant changes. The α-helix content is the next greatest contributor to the separation along Factor 1 with a decrease in this band between the initial and final samples for both temperature treatments. The addition of elevated light to temperature resulted in a larger change in this band. Finally, carbohydrate content, particularly the band attributed to ribose, increased over the course of the temperature treatments. The contribution of carbohydrates to this factor was less than that of the protein and lipid macromolecules.

Factor 2 separated the temperature treatments from the elevated light treatment. This Factor contained some noise in the protein region; however, it is proposed that a large proportion of the separation is explained by the carbohydrates. Cellulose at 1150 cm^{-1}

and ribose at 995 cm^{-1} are negative bands. This is an indication that there was an increase in these macromolecules over the cells' exposure to elevated light.

Tables 4.7 and 4.8 are summaries of the parameters for models generated for clade F cells. Unlike clade A models, there were no clear groups forming between treatments. As a result, only two models were developed and tested.

Table 4.7: Parameters for PLSDA model for clade F split into two groups.

Group	r^2	RMSEP	Sensitivity (%)	Specificity (%)
Initial	0.829	0.204	100	100
Final	0.829	0.204	100	100

Table 4.8: Parameters for PLSDA model for clade F split into four groups.

Group	r^2	RMSEP	Sensitivity (%)	Specificity (%)
Initial	0.497	0.350	100	98.6
Elevated light	0.379	0.273	70.8	95.6
Elevated temperature	0.329	0.284	16.7	98.6
Elevated light and temperature	0.224	0.117	33.3	96.6

The model based on two groups; those exposed to stress and those grown in normal conditions, gave the best separation. No spectra were classified incorrectly. When these spectra were further classified into treatment groups, the model parameters returned a relatively bad fit. This can be seen especially in the spectra of those cells exposed to elevated temperature; the percentage of correctly classified cells (sensitivity) was very low. However, the loadings for these models were very different to those generated for clade A cells, which confirms that the clades experienced a very different response to environmental stress.

Using these models, it is clear that clade F cells were able to be classified based on time, however, there appeared to be no difference in macromolecular response to different treatments. Loadings plots for the model split into two groups revealed that the majority

of the spectra were classified based on protein secondary structure, as well as lipid structure (Figure 4.16). The β-pleated sheet bands at 1690 and 1620 cm^{-1} were both negative peaks in the loadings. This indicated that the cells contained more of this type of structure after the elevated light and temperature treatments The α-helix content did not appear to have any effect on the loadings with the band at 1655 cm^{-1} very close to zero. The lipid peak at 1730 cm^{-1} also indicated that the treatments increased the lipid content over time. Structurally, there was a clear difference between initial and final groups with most methylene chain vibrations increasing. The asymmetric CH_3 band was the only vibration to show less initially, but this is such a small band in the loadings that it is unlikely to be significant. Carbohydrates also contributed, but significantly less so than proteins and lipids. This correlates with the carbohydrate content calculated in Section 4.2.1.2. As shown in Figure 4.3, there is little change as compared to the controls.

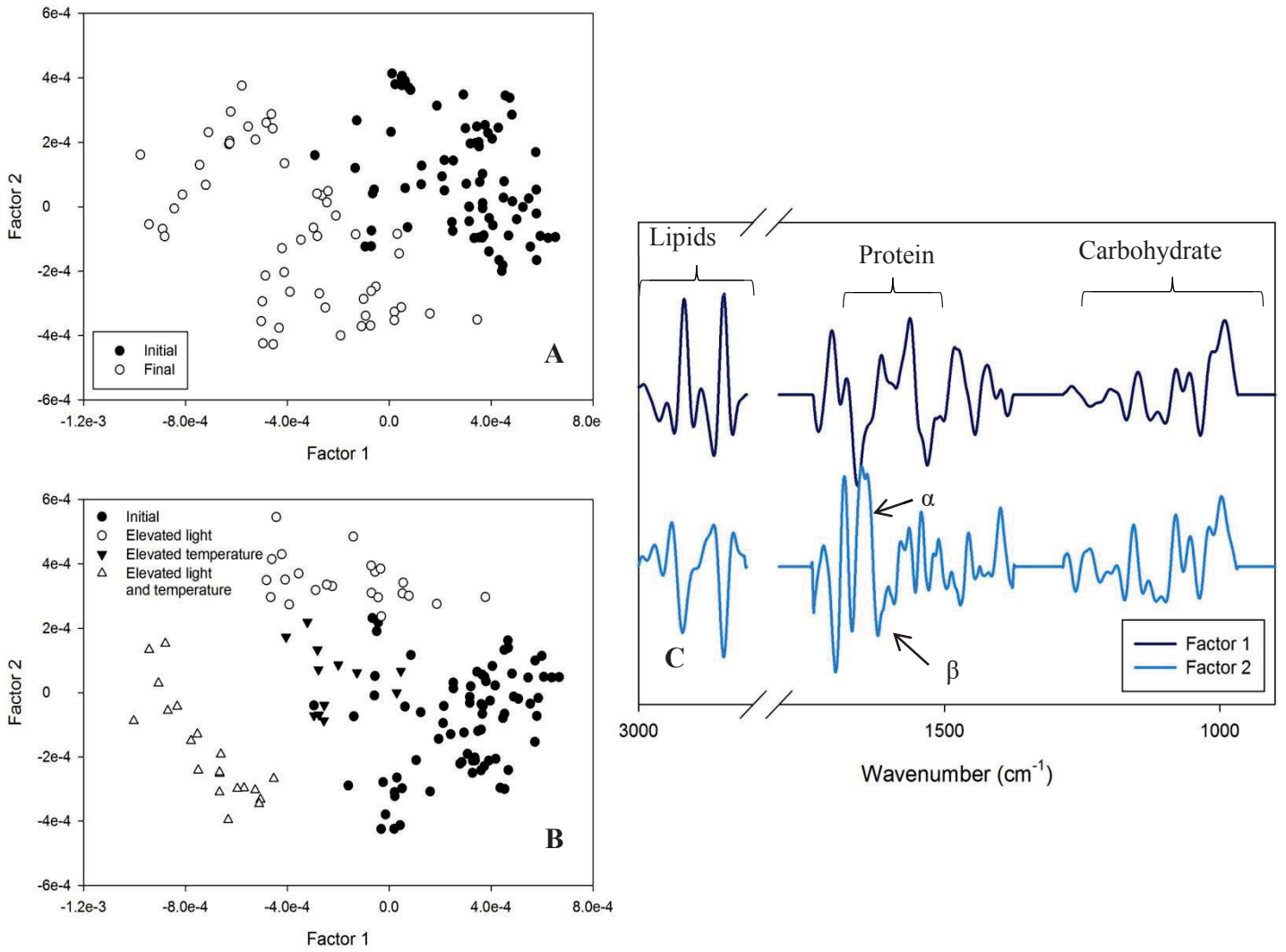

Figure 4.15: PLSDA model scores (A and B) and loadings (C) for clade A cells exposed to all treatments.

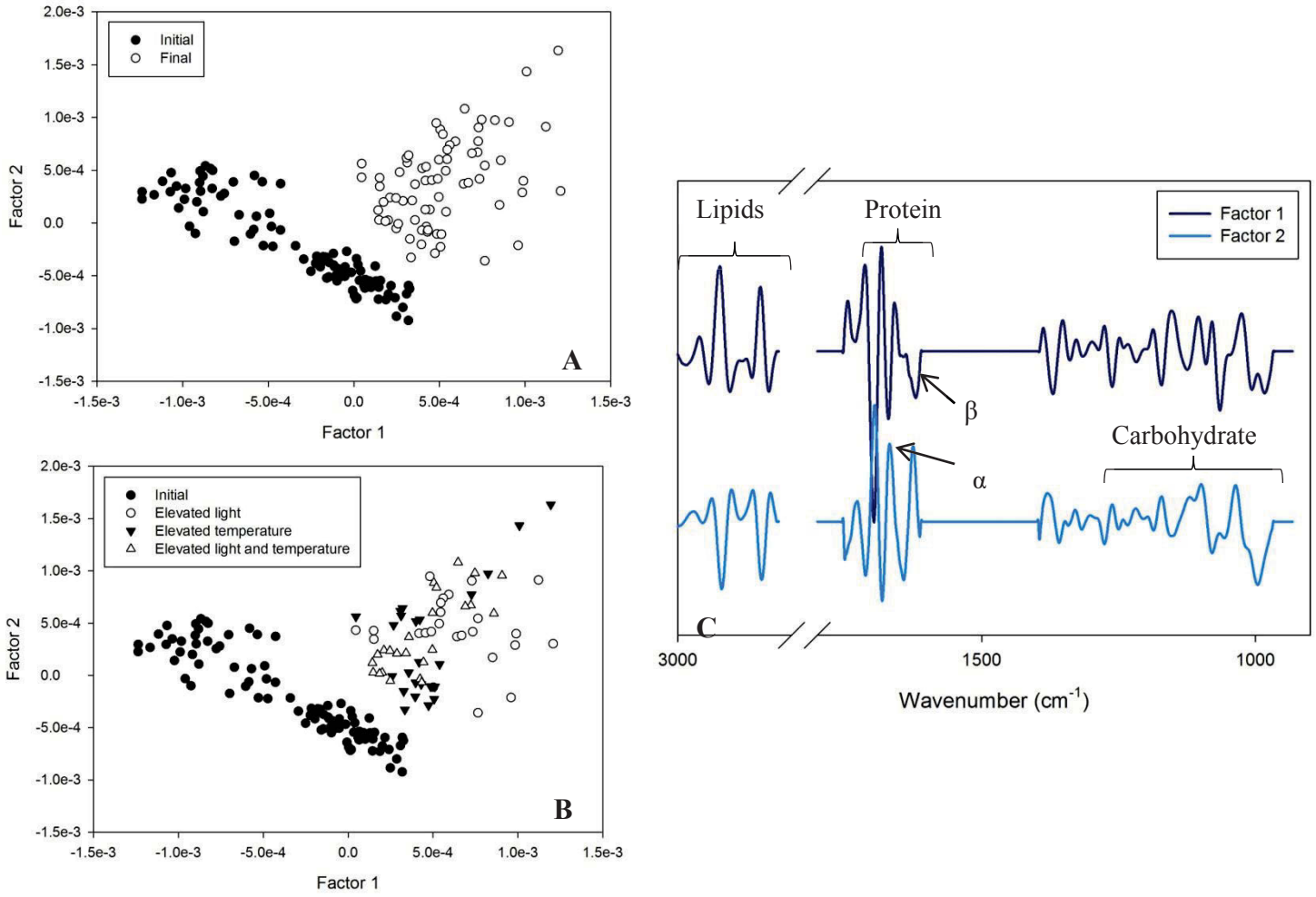

Figure 4.16: PLSDA model scores (A and B) and loadings (C) for clade F cells exposed to all treatments.

4.3 Discussion

This study compared the macromolecular response of two different clades of *Symbiodinium* to mild environmental stress. Analysis of FTIR spectra revealed interesting macromolecular information that will add to the overall understanding of these cells' response to changes in environment. In a recent paper by Suggett *et al* (2015), researchers compared photobiological parameters of CS-73 (clade A) and CS-156 (Clade F) under various environmental conditions. It was found that these clades expressed significantly different photosynthetic responses that were correlated with cell size. Cell size has been shown to be a factor in light harvesting and nutrient uptake [129]. The results in photosynthetic efficiency indicated impairment in function. As described by Iglesias-Prieto *et al* (1992), *Symbiodinium* experience this impairment in function over 30 ^{o}C. This photobiological response has been shown to differ between clades [46], [52], [80] and this correlates with the results observed in Figure 4.1. This study also reveals that these differences in photosynthetic function are accompanied by a change in macromolecular content and structure.

It should be noted that the literature on elevated light stress suggests that the light levels used in this study were very low [52], [53], [80]**.** However, the cultures were grown at relatively low light conditions, and so in order to introduce stress, the light was only increased by from 25 to 100 μmol photons m^{-2} s^{-1} . This level of increased light has been performed previously, and the *Symbiodinium* cells were found to experience stress [24].

This study also highlights the benefits of using a suite of common data analyses used in spectroscopy. Analysis of ratios of bands in spectra, in combination with multivariate

statistical modelling, results in a comprehensive investigation of the data. In the case of statistical modelling, if there is a component of the spectra that is changing significantly, it can overwhelm the loadings plots (e.g. lipids in Figure 4.13) while changes in other sections of the spectra can be missed. Likewise, structural changes can be overlooked when calculating total content. For example, clade F protein content was shown to undergo no changes (Figure 4.2), however, when analysed by PLSDA models, it was clear that there were significant shifts in structure occurring that were missed by employing the analysis of ratios alone. A combination of these two approaches ensures no important information is overlooked.

An examination of the data analysis reveals a number of significant patterns occurring. First of all, the FTIR spectra showed that, for some of the treatments, there were changes in lipid and protein structure over time. It is well-documented that surplus carbon acquisition in higher plants and algae is stored as lipid [56]. Saturation of these storage lipids (triacylglycerides and wax esters) has recently been a topic of interest [53], [55], [56]. Many studies have investigated the fatty acid content of various clades of *Symbiodinium* with varying results [53], [55]. Our results indicate that, with elevated light, there was a corresponding increase in lipid content (1730 cm^{-1}). Addition of elevated temperature appeared to negate this storage of excess energy with decreases in content observed for both clades. This could be an indication that both these clades of *Symbiodinium* will utilise stored energy in the form of lipid in order to adjust to elevated temperature.

Our results indicated a difference between changes in carbohydrate content based on treatment for both clades. The same occurred for lipid content. It is possible that under elevated temperature, *Symbiodinium* clades increase their carbohydrate content in order to store energy. This was shown in the PLSDA models and overall content calculations.

Interestingly, lipid content was shown to decrease under these conditions, but under elevated light it appeared as though the cells were increasing their lipid content. Lipid content has been shown to increase under elevated light conditions as the cells increase their stored energy reserves [51].

Clades of *Symbiodinium* also displayed differences in their lipid structure upon exposure to elevated light and temperature treatments. Clade F appears to have been the most affected in terms of all three lipid structural parameters; however, the clade A cells did exhibit an increase in saturation ratio when exposed to elevated light. A number of possibilities can explain these differences. Temperature has previously been shown to have an effect on both membrane fluidity and the degree of saturation of the lipids both in culture [53] and *in hospite* [55]. Melting temperatures of thylakoid membranes, located within the chloroplast and vital for photosynthesis, are also known to be clade-specific [53]. Detailed analysis of the thylakoid membranes have also revealed important changes in galactolipid saturation [130]. The differences observed in lipid structure, specifically lipid saturation and disorder, could be related to these changes in thylakoid membrane lipids; however, analysis of the whole cell in this case renders certainty of the location of these changes impossible. Further isolation of thylakoid membranes and analysis by FTIR spectroscopy, or use of chemical imaging techniques, could isolate these changes in lipid structure of *Symbiodinium* sp.

As noted by Trench [43] in his initial studies into these cells, the trends observed in carbohydrate and lipid content are similar for both clades; however, the degree to which this occurs is quite different. Clade A cells appeared to experience the greatest change in carbohydrate content under elevated temperature with loadings for PLSDA models consistently being explained by carbohydrate vibrations. This was also confirmed by the much greater increase in carbohydrate content as a percentage.

Conversely, clade F cells appeared to undergo the greatest increase in lipid content under elevated light conditions. It is possible that this difference in response to treatment is related to a difference in energy storage strategies. In a recent paper by Wang *et al*. [59] it was proposed that clades of cultured *Symbiodinium* displayed varying energy storage strategies. Clade B seemed to store energy in the form of starch, whereas C and D had higher concentrations of lipid. Although the authors of this study did not analyse the clades A or F, the results presented in this thesis could be an indication that these storage strategy differences are occurring.

Phosphorylated compounds include macromolecules such as phospholipids and phosphorylated proteins. Changes in both of these compounds can result in structural changes in areas such as protein folding and lipid branching or disorder. An increase in light intensity has been previously shown to have a direct effect on phospholipid content in isolated zooxanthellae [59], [131]. This correlates with the results found using FTIR spectroscopy. Under elevated light, the phosphorylated compounds increased over time. Clade F *Symbiodinium* cells underwent changes in structure as denoted by Equations 2.1-2.3.

This study also revealed a number of differences in protein secondary structure that play a role in metabolic protection from environmental stress. First of all, the analysis of the total protein content and change in structure combined seemed to indicate that clade A underwent a loss or gain of protein rather than change in secondary structure. The opposite was found to be the case for clade F. Clade F *Symbiodinium* consistently changed the ratio of α-helix to β-sheet structure in the face of both elevated temperature and elevated light. Whereas clade A only seemed to shift secondary structure in the face of a combination of light and temperature; a treatment that both photosynthetic efficiency and PLSDA models revealed had the most effect on these cells. While the

degree to which the cultures underwent shifts in secondary structure differed, the effect was similar; the β-pleated sheet structure increased in intensity (1690 and 1620 cm^{-1}). It is therefore possible that this type of secondary structure is involved in protecting cells from adverse conditions and is possibly an acclimation response.

As mentioned previously, at temperatures above 30 ^{o}C, photosynthetic function in *Symbiodinium* cells is known to be adversely affected [80]. These cells are constantly undergoing a repair cycle in which damaged photosystem II proteins are replaced [21]. Photoinhibition is a state in which this repair cycle is unable to keep up with the rate of damage [23]. Cells in this study did not exhibit any signs of photoinhibition; however, F_v/F_m measurements of cells exposed to environmental stress, particularly a combination of elevated light and temperature, did experience a drop in photosynthetic function. PSII is known to be the site of damage to these cells experiencing a decline in function [37], [132]. This is a protein complex found in the thylakoid membranes. It is therefore logical to assume that some portion of the protein secondary structural changes observed within the FTIR spectra are due to changes in PSII function and repair.

Protein crystallographic analyses of the secondary structure of photosystems within plant and algal cells show a predominantly α-helical structure with large protein sub-units that consist of β-sheet and random turn structures [35], [36]. These extrinsic proteins (specifically PsbO) have also been shown to stabilise vital components of PSII called the calcium manganese cluster [32]. This cluster has been implicated as the initial site of photodamage and so it is possible that an increase in β-sheet could indicate an increase in extrinsic protein function [21]. Isolation of the thylakoid membranes or analysis using chemical imaging would further confirm the location of these changes in secondary structure.

This study revealed a number of important observations that significantly add to the metabolic understanding of the *Symbiodinium* cells and their response to environmental stress and it also highlighted a number of key areas for future work.

FTIR spectroscopy, as stated previously, has a significant advantage over other analytical techniques in that it allows samples to be analysed with very little preparation. This results in a metabolic snapshot unspoiled by extraction methods or other destructive preparation techniques. This does, however, lead to complex spectral data that can obscure important information. Chemometric methods do take advantage of this complexity by reducing the spectra to a unique point in multi-dimensional space resulting in easy visualisation. The disadvantage here depends on the research questions being asked. In this study, patterns in overall metabolic response to environmental stress were being analysed and so this lack of specificity was not a significant problem, in fact it added to the information used to build the chemometric models. Now that these initial models have been built, it is hoped that they will lend insight to studies into the changes occurring within individual macromolecular classes.

It could be possible to take advantage of this technique's sensitivity to structural changes, and couple it with Focal Plane Array (FPA) technology, to obtain a picture of where these particular structural changes are occurring across a cell. However, due to the size of the cells and the limits of resolution, a powerful synchrotron radiation source would be required.

This study looked at cells grown under laboratory conditions at a specific stage of growth. *In hospite Symbiodinium* shown to have significantly different responses to environmental stress than those in culture [133]. A significant advantage for macromolecular studies using laboratory culture is that the growth media can be closely

controlled and, hence, no external nutrients can interfere with the cells' responses to stress factors. This control is lost when analysing cells *in hospite*; however, in order to obtain an accurate picture of their behaviour, isolated zooxanthellae must be analysed. Using the methods developed in this and the previous chapter, it would be possible to analyse *Symbiodinium* isolated from a host organism. It would also be worth taking advantage of the control offered by using laboratory cultures, and analysing the response of *Symbiodinium* in different stages of growth. This way, a comprehensive map of the cells could be established. This would heavily rely on establishing a reliable method of calculating growth rates. Measuring the chl *a* fluorescence by proxy using a fluorimeter is only effective under non-stressed conditions. Once exposed to the stressful treatments, the amount of chlorophyll emitted by the cells differs [80]. A method for preventing the cells' aggregating together is also needed for further analysis. Correlating growth rates with spectra using a chemometric method such as Partial Least Squares regression, could relate carbohydrate and lipid content with cell growth.

4.4 Conclusions

As a result of the findings in this chapter, it is clear that there is a difference in macromolecular response to non-lethal environmental stress response for clades of *Symbiodinium*. Clades A and F appear to display differences in energy storage under different conditions. It was also found that the clades exhibited different protein secondary structures, which are proposed to be a result of chloroplast protein folding. However, isolation of thylakoid membranes is needed to confirm this is the case. Subjecting clades to extremes in temperature to induce photoinhibition would also shed

more light on photosystem breakdown and the effect on macromolecular content. This will be investigated further in Chapter 5.

Chapter 5. Macromolecular composition of symbiotic dinoflagellates; variation in response to extreme temperature

5.1 Introduction

It is a well-established observation that the majority of the coral species live in environments that are very close to their upper thermal limits [9], [12], [30]. In fact, an increase in temperature of just 1-2 ^{o}C can induce coral bleaching [23]. The previous chapter described the macromolecular response of two clades of *Symbiodinium* sp. to environmental stress designed to approach this upper limit, and results showed that these cells shifted to an entirely different macromolecular state. However, it is impossible to determine if this new state is related to some sort of protective mechanism as neither clade was subjected to temperatures considered to induce bleaching in the most susceptible corals [9], [80].

In this chapter, clades A and F are once again subjected to environmental stress. This time, however, the conditions are gradually ramped to simulate a bleaching event. Maximum quantum yield of PSII is used as a measure of health of the clades and the macromolecular content is monitored over time, by FTIR spectroscopy. Under these conditions, it is hoped that the macromolecular shifts observed in chapter 4, will become clearer and offer greater insight into the process or trigger of bleaching.

5.2 Results

The maximum quantum yield of PSII measurements showed that the clade A culture was less thermally tolerant than the clade F cells. rmANOVA results showed that clade A cells were grouped from beginning to day 3 and then exhibited a significant drop in F_v/F_m at day 4. Clade F cells exhibited no significant change in maximum quantum yield until day 5 (34 ºC). Both clades showed significantly different responses to the control cells, and mixed model ANOVA showed this response was different between each clade.

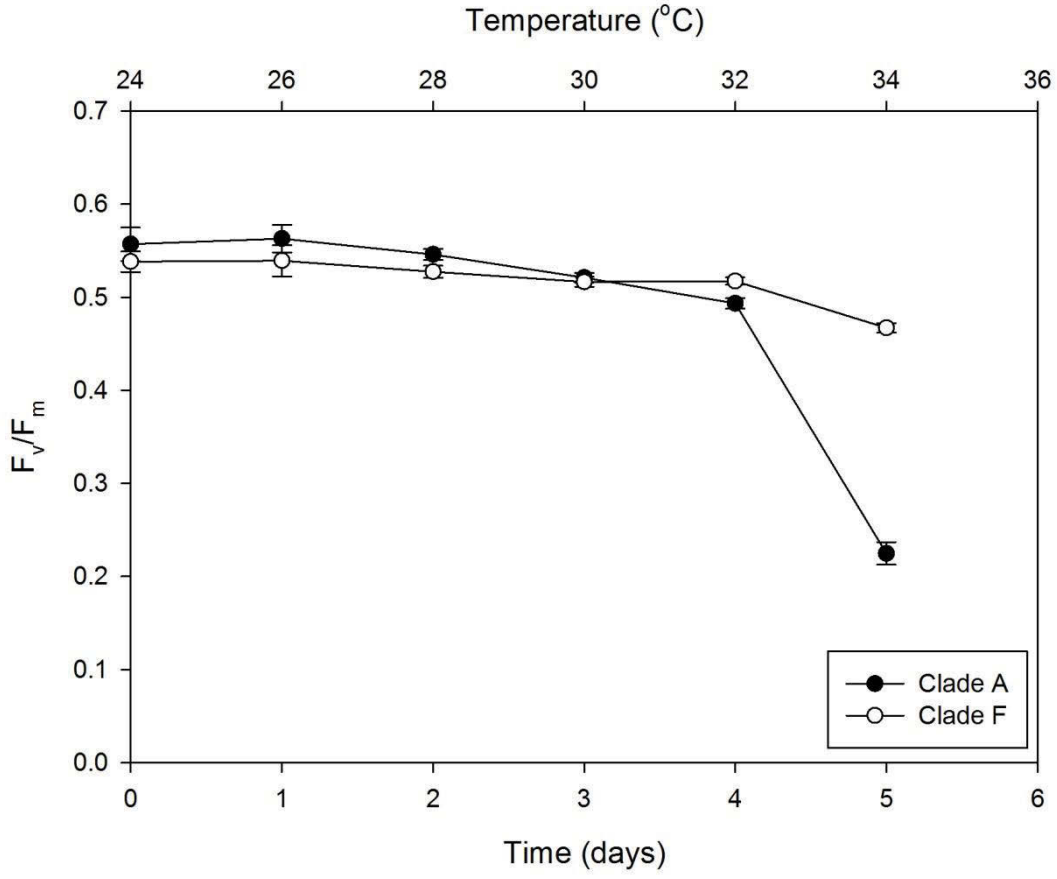

Figure 5.1: Maximum quantum yield of PSII of cells exposed to 2 ºC/day increase in temperature. All error bars are ± SEM (n=5). Refer to Tables A4.1 and A4.2 for rmANOVA results.

5.2.1 Macromolecular content for micro-FTIR spectroscopy

Calculated protein content (Figure 5.2) displayed a high standard error of the mean. This meant that there was no difference in observable changes in protein content over time as temperature increased (refer to Appendix 4 for rmANOVA results). Carbohydrate content as a percentage (Figure 5.3) did not appear to change over the course of the experiments for both clades and rmANOVA showed that there were no significant differences occurring. For both macromolecular components, a higher SEM than control samples was observed.

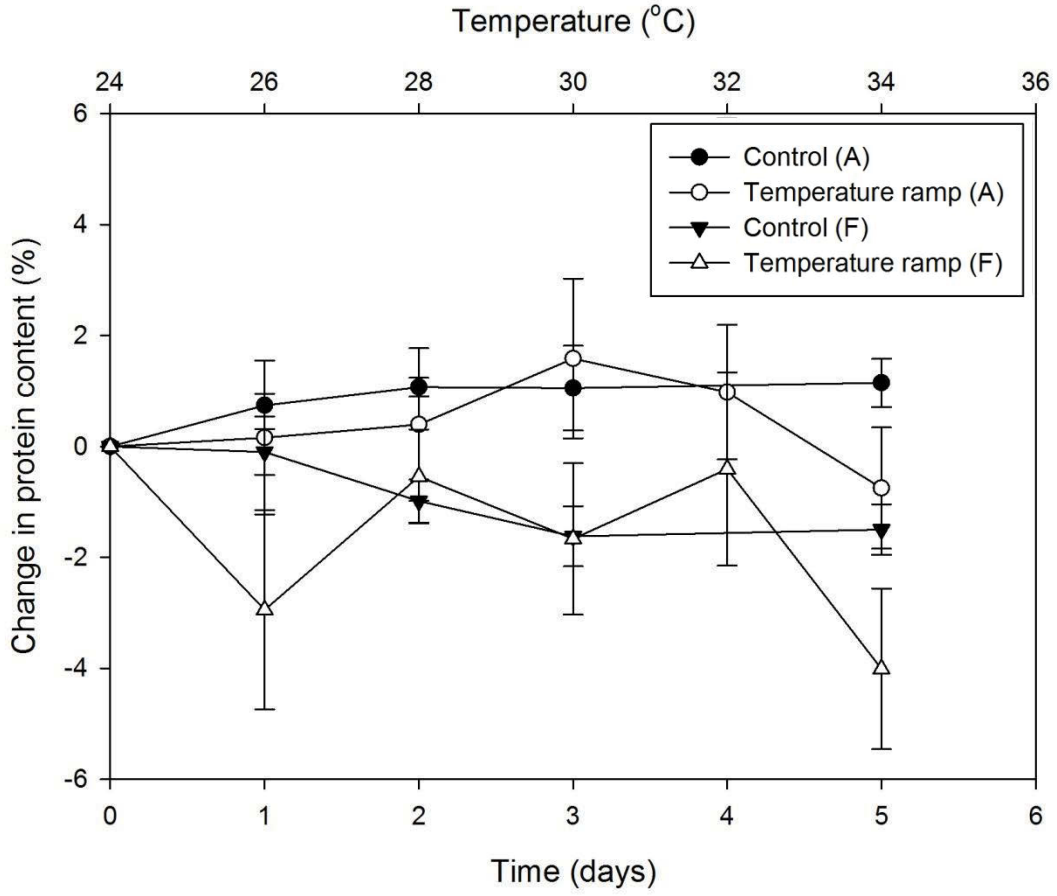

Figure 5.2: Change in protein content over time as a percentage for cells exposed to a 2 °C/day increase in temperature. Data points are mean (n=5) and error bars are ± SEM. Refer to Tables A4.1 and A4.2 for rmANOVA results.

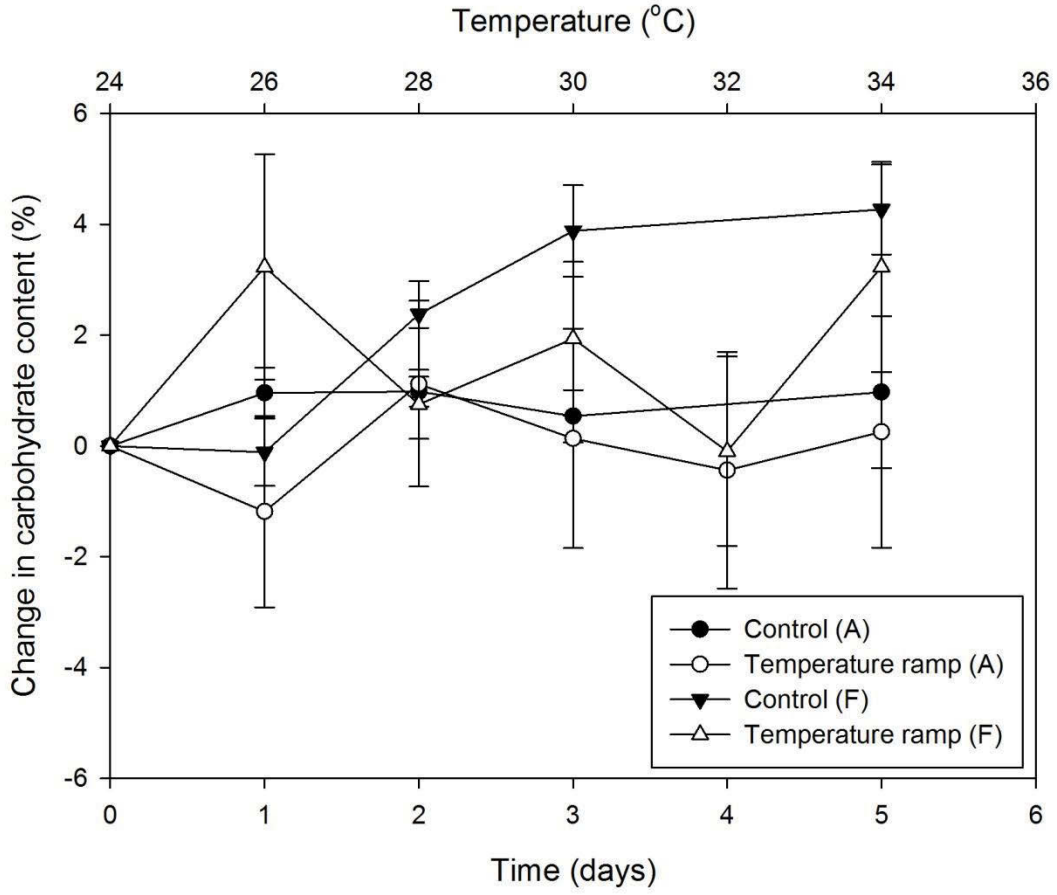

Figure 5.3: Change in carbohydrate over time as a percentage for cells exposed to a 2 °C/day increase in temperature. Data points are mean (n=5) and error bars are ± SEM. Refer to Tables A4.1 and A4.2 for rmANOVA results.

Phosphorylated content (Figure 5.4) did not exhibit any change in percentage until five days of exposure for both clades (refer to Appendix 4 for rmANOVA). This correlated to a temperature of 34 ^{o}C. It is interesting to note that the thermally tolerant clade F exhibited a greater change in this macromolecular component as compared with the control; however, mixed model ANOVA showed that the response for both clades was similar. Total lipid content (Figure 5.5) did not appear to change significantly until both clades were exposed to 34 ^{o}C. Clade F cells exhibited the greatest percent of change with an overall decrease of 1.5% after 5 days of exposure to a temperature ramp (Table A4.2). Clade A cells increased their lipid content until 34 ^{o}C where a significant decrease was observed (Table A4.1). The degree of change here was also shown to be significantly different between clades.

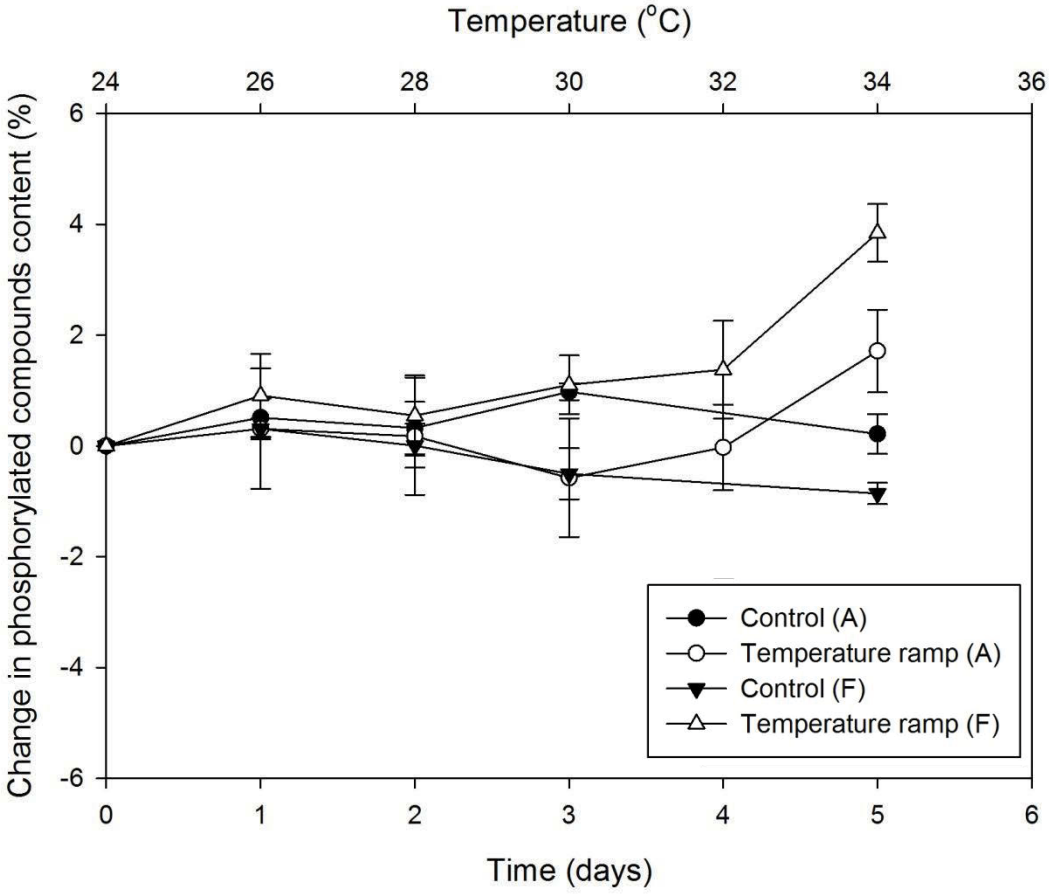

Figure 5.4: Change in phosphorylated compounds over time as a percentage for cells exposed to a 2 ºC/day increase in temperature. Data points are mean (n=5) and error bars are ± SEM. Refer to Tables A4.1 and A4.2 for rmANOVA results.

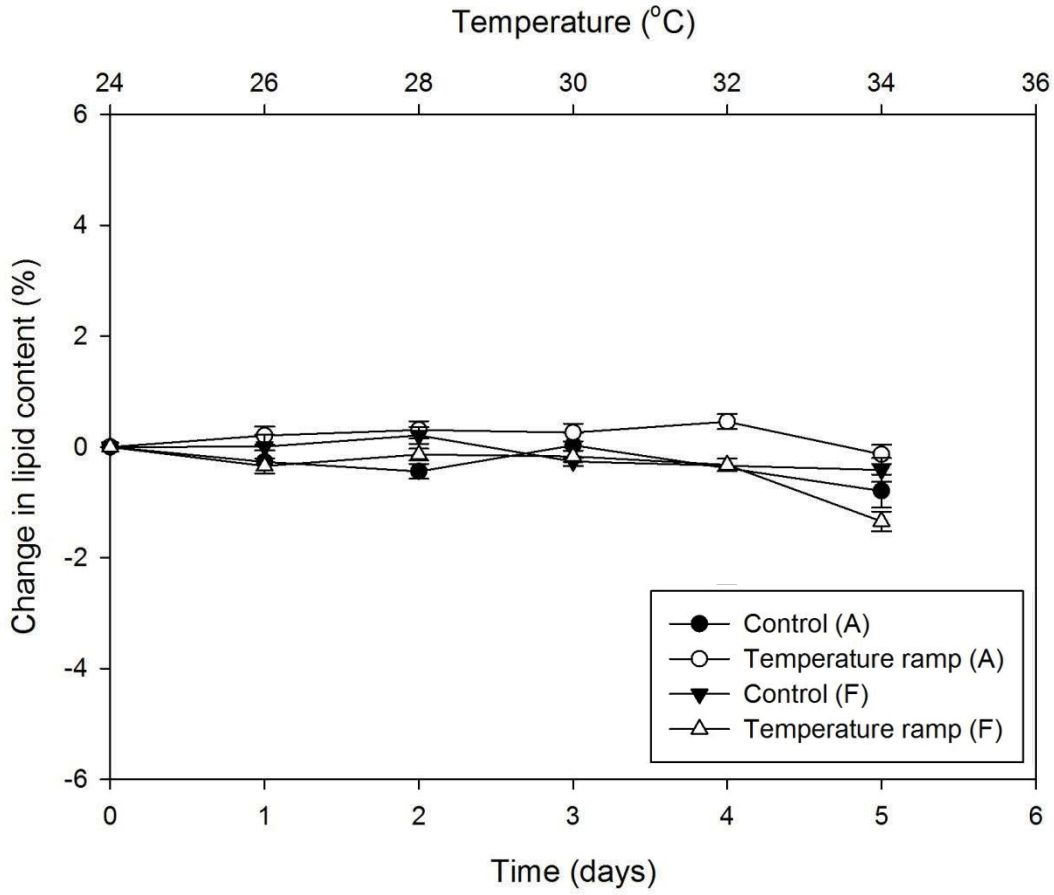

Figure 5.5: Change in lipid content over time as a percentage for cells exposed to a 2 °C/day increase in temperature. Data points are mean (n=5) and error bars are ± SEM. Refer to Tables A4.1 and A4.2 for rmANOVA results.

5.2.2 Structural analysis using micro-FTIR spectroscopy

FTIR spectroscopy can reveal important information about the structure of certain macromolecules. Detailed comparison of the amide I region (1700 – 1600 cm^{-1}) and the C-H stretching regions (3050 – 2800 cm^{-1}) can provide insight into protein and lipid structure, respectively. Figure 5.6 is a comparison of the 2nd derivatives and reveals a number of differences. First of all, the ratio of random turns (1670 cm^{-1}) to α-helix changes as temperature increases. The α-helix decreases between the beginning and day 4 before increasing once more at day 5. β-sheet content also appears to increase in intensity between day 2 and 4 indicating an overall shift in structure as the temperature increases.

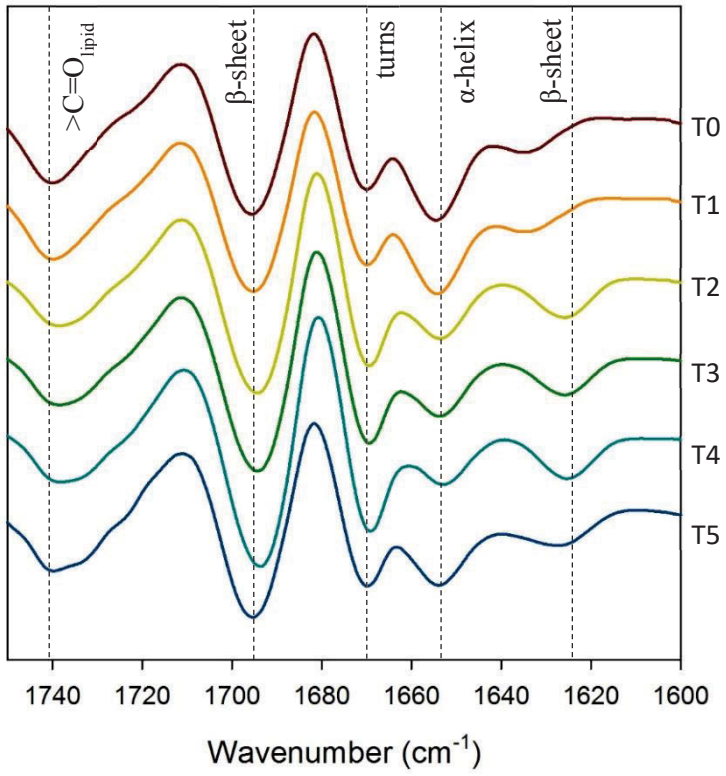

Figure 5.6: Comparison of derivatised spectra from Amide I region for clade A cells exposed to a 2 °C/day increase in temperature. Spectra are averages (n=16) and different colour represents different day (T0-5).

A similar trend to the clade A cells can be seen in Figure 5.7 with the Amide I region for clade F. There is a decrease in α-helix content and a corresponding increase in β-sheet structure. As shown in Figure 5.6, there was a change between day 4 and 5. This change was not seen in the clade F cells.

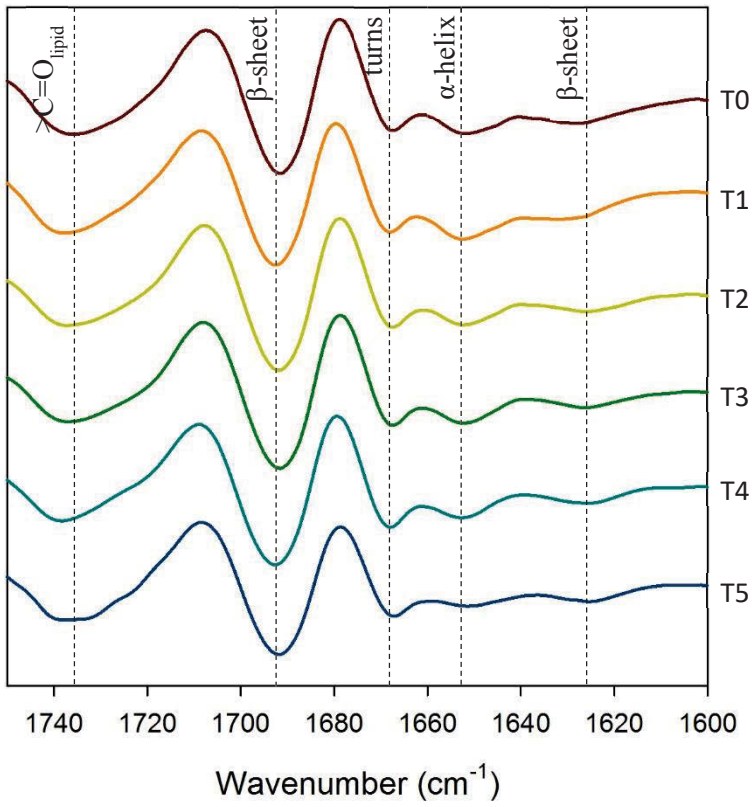

Figure 5.7: Comparison of derivatised spectra from Amide I region for clade F cells exposed to a 2 °C/day increase in temperature. Spectra are averages (n=16) and different colour represents different day (T0-5).

Figure 5.8 is a comparison of the C-H stretching region for lipids. This comparison reveals a number of changes occurring within the lipid content for clade A; however, it is difficult to see these changes by a visual inspection alone. Figures 5.9 to 5.11 show the results of applying Equations 2.1-2.3 for clade A control samples and those exposed to a gradual increase in temperature. rmANOVA results (Table A4.1) indicate that, in general, the three structural lipid parameters can be split into three groups; T0-T1, T2-T4 and T5. Mixed model ANOVA also reveals that overall, the clade A cells subjected to a gradual increase in temperature were significantly different to the control results. Mixed model ANOVA also revealed that the responses of clades A and F were significantly different from each other.

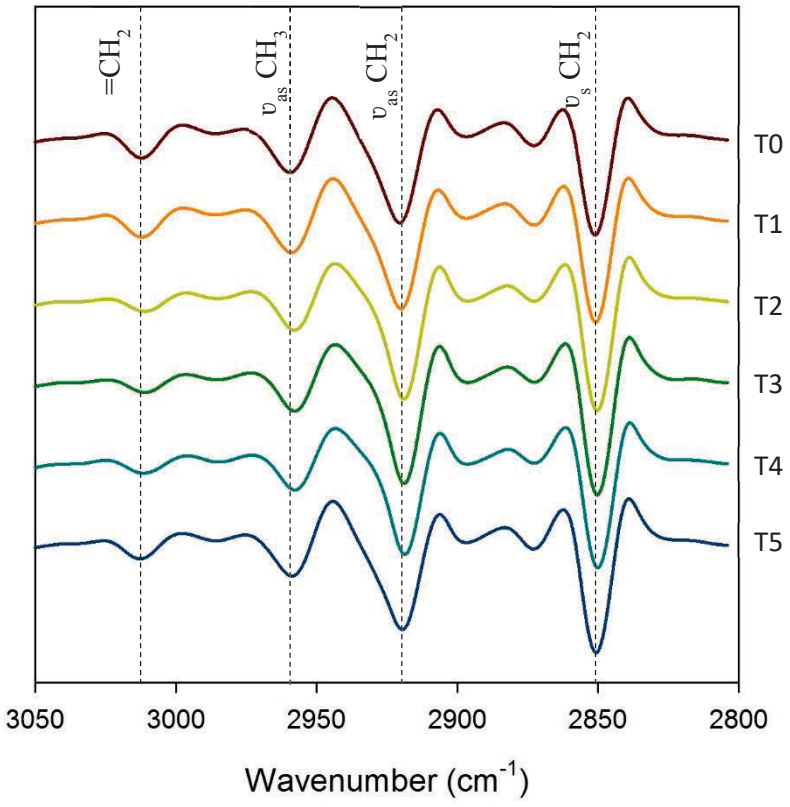

Figure 5.8: Comparison of derivatised spectra for C-H stretching region for clade A cells exposed to a 2 ºC/day increase in temperature. Spectra are averages (n=16) and different colour represents different day (T0-5).

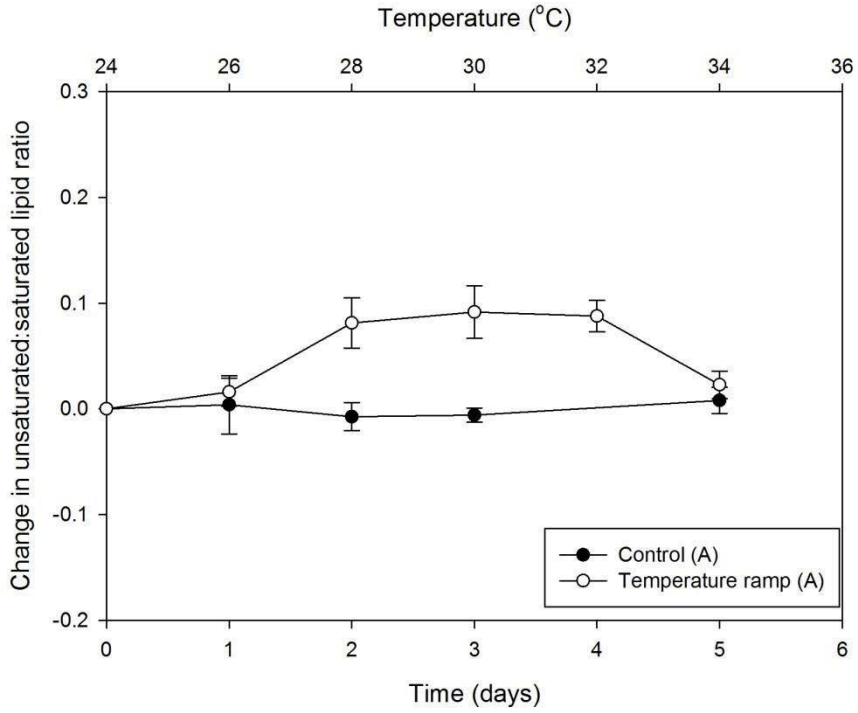

Figure 5.9: Change in lipid saturation for clade A cells exposed to a 2 °C/day increase in temperature. Data points are mean (n=5) and error bars are ± SEM.

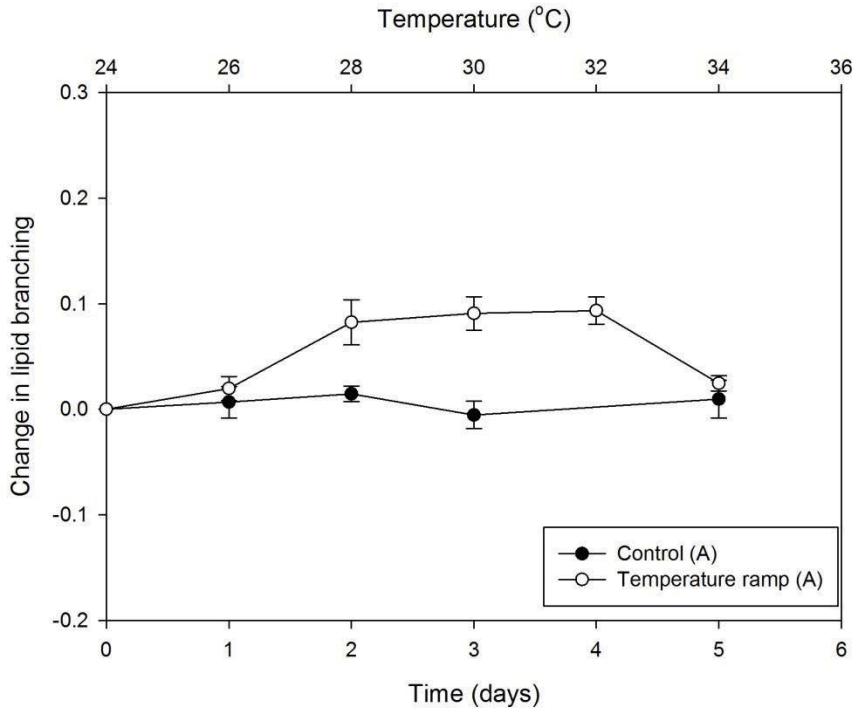

Figure 5.10: Change in lipid branching for clade A cells exposed to a 2 °C/day increase in temperature. Data points are mean (n=5) and error bars are ± SEM.

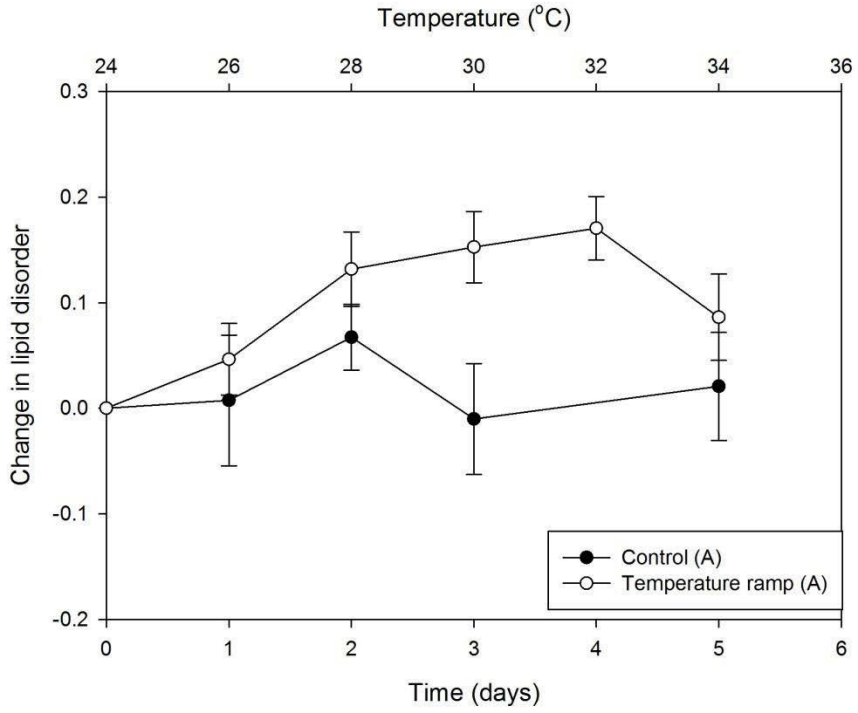

Figure 5.11: Change in lipid disorder for clade A cells exposed to a 2 °C/day increase in temperature. Data points are mean (n=5) and error bars are ± SEM.

Figure 5.12 is a comparison of the C-H stretching region for clade F exposed to a gradual increase in temperature. It is difficult to see if there are any changes occurring in this region for this clade, as the overall lipid content appears to be lower than that of clade A (refer to Appendix 3 for full spectra). Figures 5.13-5.15 are a comparison of the parameters calculated by Equations 2.1-2.3. rmANOVA results for these three parameters and indicate that there are no significant changes occurring for either saturation ratios or lipid disorder. Lipid branching reveals an increase in the ratio between the CH_3: CH_2 bands between days 2 and 3, before a decrease is observed from days 4 to 5. This is an indication that the lipid chain length is increasing.

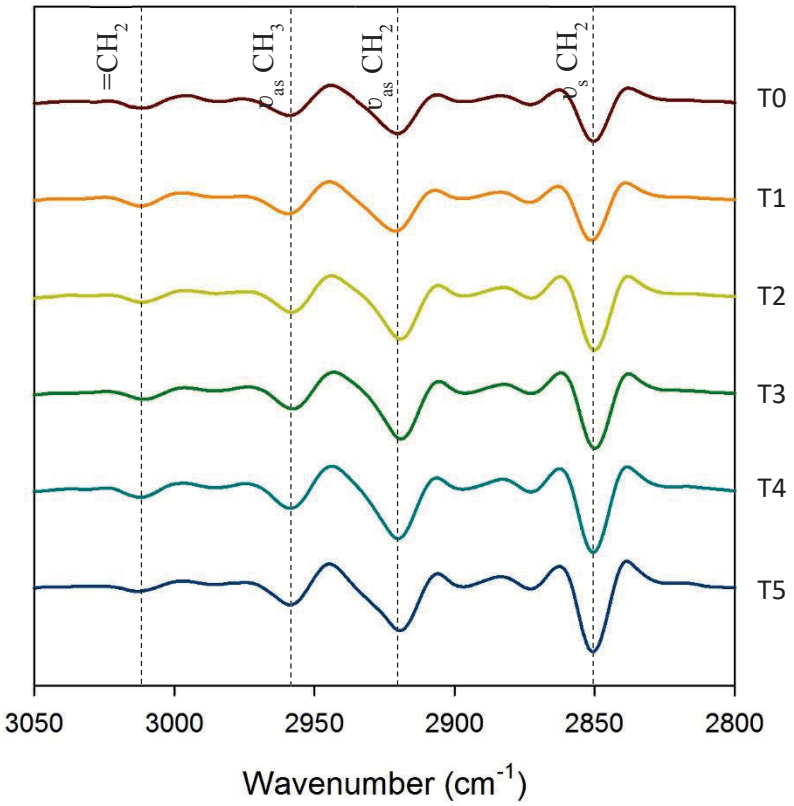

Figure 5.12: Comparison of derivatised spectra for C-H stretching region for clade F cells exposed to a 2 ºC/day increase in temperature. Spectra are averages (n=16) and different colour represents different day (T0-5).

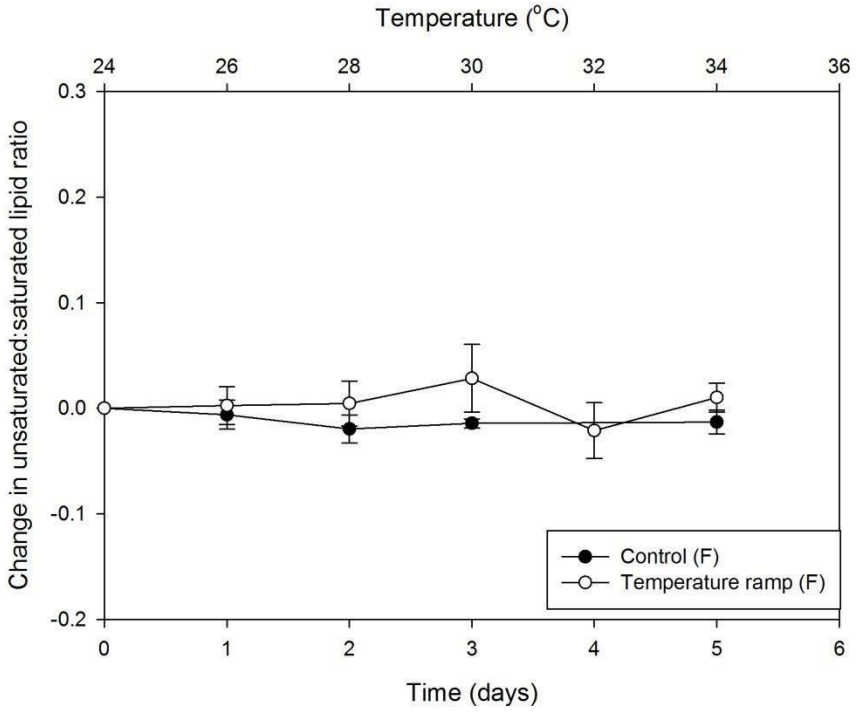

Figure 5.13: Change in lipid saturation for clade F cells exposed a2 ºC/day increase in temperature. Data points are mean (n=5) and error bars are ± SEM.

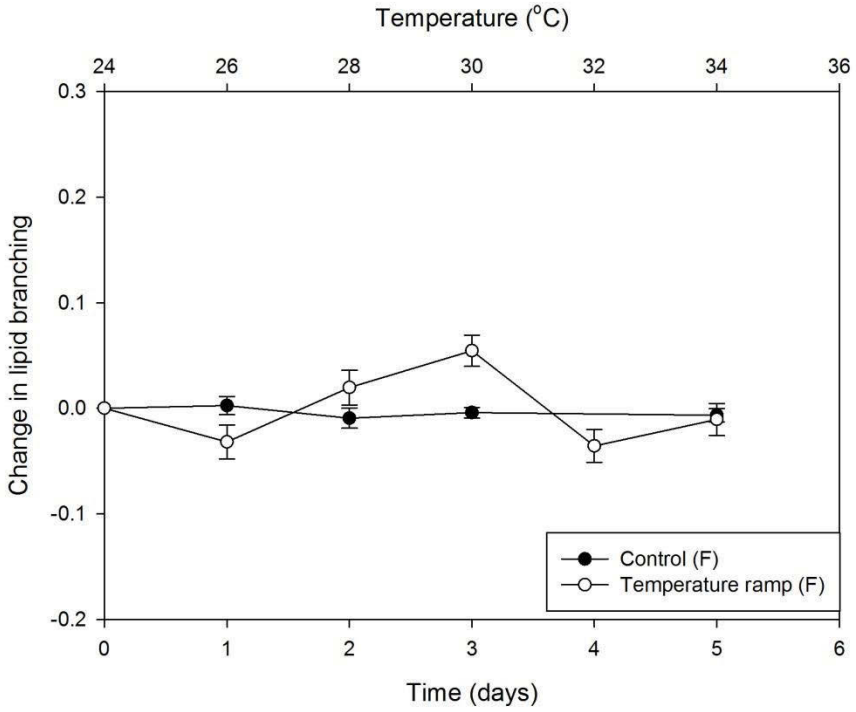

Figure 5.14: Change in lipid branching for clade F cells exposed to a 2 ºC/day increase in temperature. Data points are mean (n=5) and error bars are ± SEM.

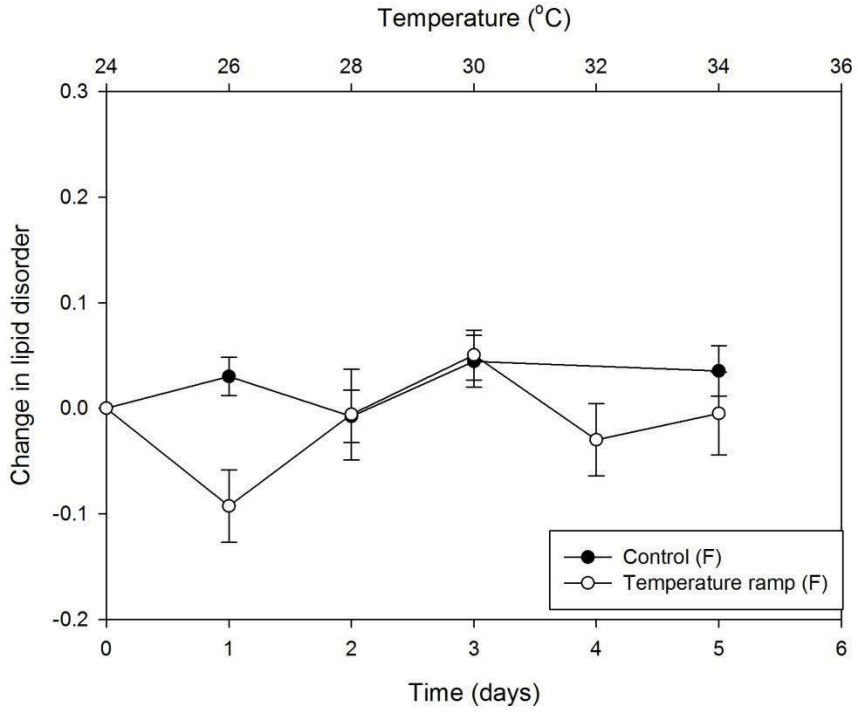

Figure 5.15: Change in lipid disorder for clade F cells exposed to a 2 °C/day increase in temperature. Data points are mean (n=5) and error bars are ± SEM.

5.2.3 Statistical analysis of micro-FTIR spectroscopy samples

In order to assess the groupings and differences between spectra, PCA was performed using the whole dataset. As with previous chapters, clades A and F showed significant macromolecular differences. Once this was established, the data was split into two groups based on clade, and then further into training and test sets (refer to statistical modelling for Chapters 3 and 4).

Initial PCA models of the two clades revealed groupings based on time. For clade A, days 0 and 1, days 2 to 4 and day 5 were grouped together. For clade F, days 0 and 1, days 2 and 3, and days 4 and 5 appeared to be most similar. PLSDA was then used to classify the spectra into these groups. Sensitivity, specificity, r^2 and RMSEP parameters of these models were calculated in order to evaluate the fit of the PLSDA models (Table 5.1).

Further analysis of the spectra data was performed by Partial Least Squares (PLS) regression. This was done to explore any relationship between photosynthetic function and macromolecular content. The same training and test sets were used to build models for both clades. F_v/F_m values were predicted for the test set spectra and plotted against the reference F_v/F_m for these samples. r^2 values were used to evaluate the fit of the PLS models.

Table 5.1 is a summary of the PLSDA model parameters for clade A cells split into three groups. Sensitivity and specificity percentages indicate that this model was able to correctly predict the identity of the test set spectra with a success rate of 100%. Figure 5.16 shows scores and loadings plots for the model summarised in Table 5.1. Using these plots, it is clear that the majority of the variation between time groups is explained by factor 1. Loadings for this factor show the sources of this variation; the lipid C-H stretching region (3050 – 2800 cm^{-1}) and the amide I region (1700 – 1600 cm^{-1}). Both of these regions contain important information about the secondary structure of lipids and proteins, respectively. It is interesting to note that, unlike models developed for cells exposed to sub-lethal stress (see Chapter 4), carbohydrates and phosphorylated compounds contributed very little to the loadings of the PLSDA models for clade A.

Table 5.1: Parameters for PLSDA model split into three groups.

Group	r^2	RMSEP	Sensitivity (%)	Specificity (%)
T0 - T1	0.938	0.121	100	100
T2 - T4	0.958	0.102	100	100
T5	0.887	0.114	100	100

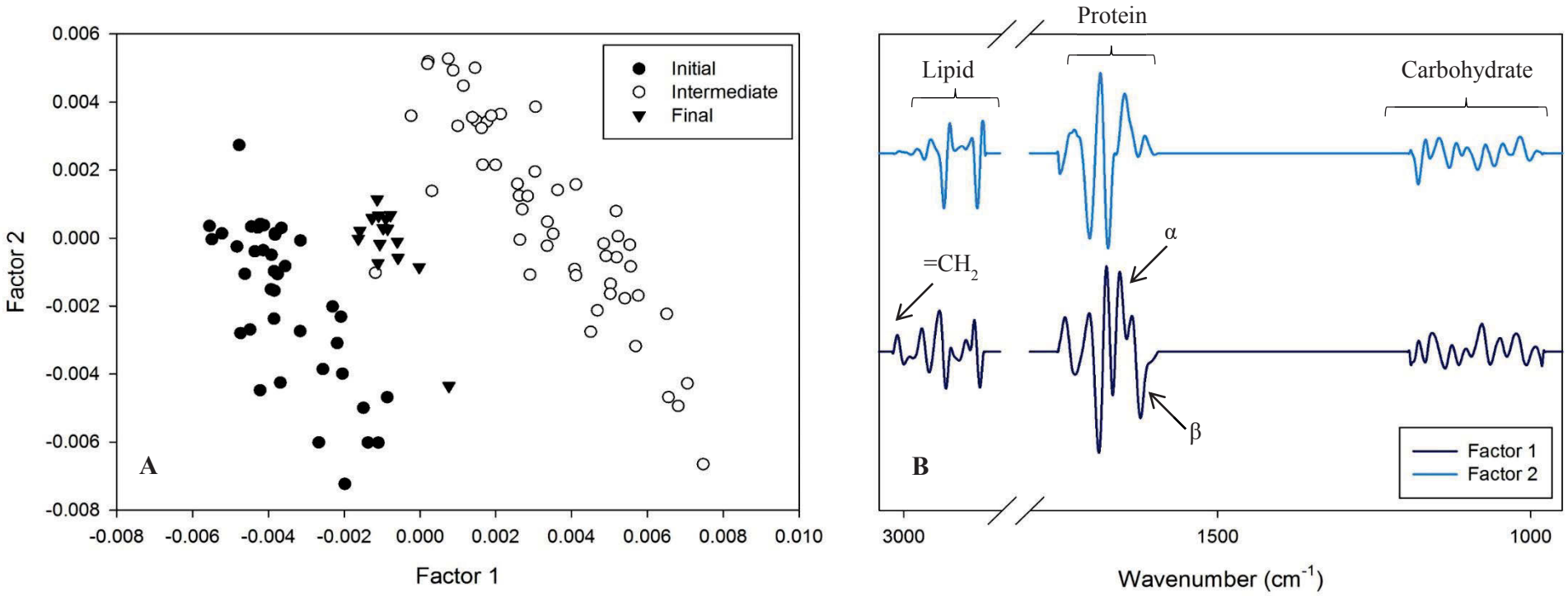

Figure 5.16: PLSDA scores (A) and loadings (B) for clade A cells exposed to a 2 ºC/day increase in temperature.

According to the scores plot (Figure 5.16), the three groups are arranged in order; initial, final and intermediate. This indicates that the cells move to a different macromolecular state under increasing temperature stress, before falling back to a state somewhere in between the initial and intermediate groups at extreme temperatures. The initial and intermediate states are separated mainly by a difference in β-sheet protein secondary structure. This particular secondary structure increases with exposure to elevated temperature. The $=CH_2$ band at ~3012 cm^{-1} appears to be contributing to the loadings. The initial group shows a higher content of this particular band, which then decreases over time. It is interesting to note here, that these groups follow the rmANOVA groupings calculated for lipid structural parameters.

Table 5.2: Parameters for PLSDA model for clade F split into three groups.

Group (days)	r^2	RMSEP	Sensitivity (%)	Specificity (%)
0 - 1	0.763	0.229	96.6	100
2 - 3	0.563	0.327	81.6	92.7
4 - 5	0.683	0.242	84.0	100

Clade F cells were broken into three groups based on preliminary PCA model scores and loadings. These were then used to generate PLSDA models. Table 5.2 shows the parameters for this chemometric model.

Sensitivity and specificity parameters for this model were lower than the model generated for clade A. The scores plots shown in Figure 5.17 indicated that the cells could be better split into two groups. Table 5.3 is a summary of this new PLSDA model's parameters.

Table 5.3: Parameters for PLSDA model for clade F split into two groups.

Group (days)	r^2	RMSEP	Sensitivity (%)	Specificity (%)
0 - 1	0.926	0.129	100	100
2 - 5	0.930	0.129	100	100

It is clear from the PLSDA model parameters outlined in Tables 5.2 and 5.3, that the second model built for clade F cells produced the best fit. The division into two groups instead of three, is an indication that there was less change occurring within the cells for clade F than those of clade A. This is supported in the results presented previously in Sections 5.3.1 and 5.3.2.

As for the PLSDA models for clade A, factor 1 explains the majority of the variation observed for the clade F cells. The loadings for factor 1 show that initially, clade F contained less β-sheet protein secondary structure than those cells exposed to higher temperatures. The lipid carbonyl band (~1730 cm^{-1}) decreased in content over time from initial to final groups. Interestingly, carbohydrate and phosphorylated compound bands contributed more to the loadings for the clade F PLSDA model than clade A. Cellulose (~1150 cm^{-1}) increased from initial to final groups and phosphorylated compounds had the opposite response. Saturated lipid content (~3012 cm^{-1}) did not contribute to the model at all, a trend that is supported by the lack of significant change shown in Figure 5.13.

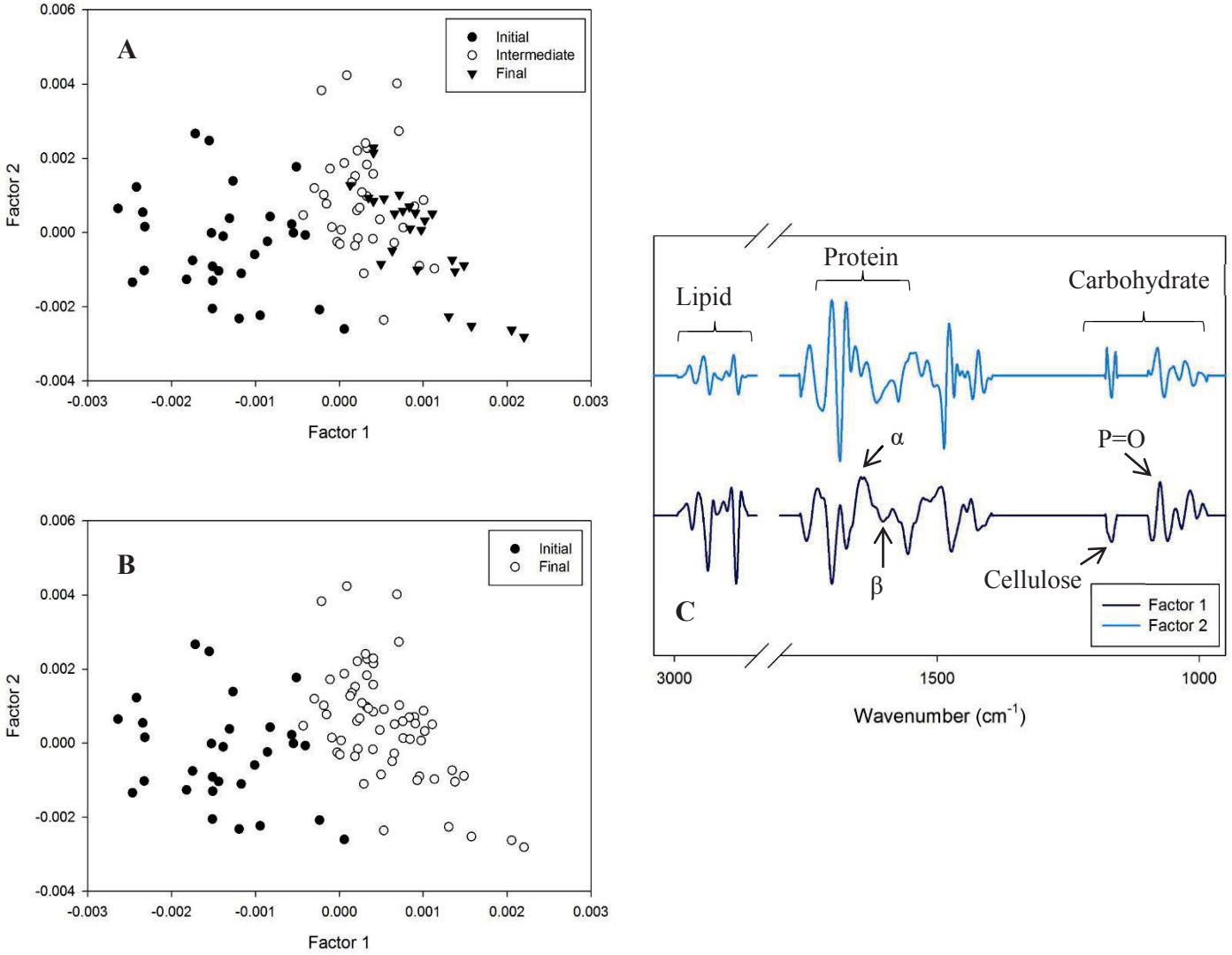

Figure 5.17: PLSDA model scores for three group model (A), two group model (B), and loadings (right) for clade F cells exposed to a 2 ºC/day increase in temperature.

In order to examine the relationship between maximum quantum yield of PSII and macromolecular content, PLS models were built. This was a supervised prediction model where reference F_v/F_m values paired with spectra were used to predict new values. These were plotted against each other and accuracy and fit of the models evaluated by r^2 values of references verses predicted plots.

PLS models for clade A gave the best results. This model was explained best by the first three factors as shown in Figure 5.18. The best separation of the three groups (days 0-1, 2-4 and 5) was along factor 3. Factors 1 and 2 are unable to split the initial and final groups, but show that these two groups are significantly different to the intermediate time group. All three factors are explained largely by the protein secondary and lipid structures with very minor contributions from the lower wavenumber regions (carbohydrates and phosphorylated compounds). In all factors, α-helix and β-sheet bands (~1650 and 1620 cm^{-1}) were oppositely correlated with the intermediate cells containing a higher β-sheet content than the other two groups. The cells classified into the intermediate time point also appeared to contain a higher level of saturated lipid (~3012 cm^{-1}).

Figure 5.19 shows the scores and loadings for a PLS model built for clade F cells using F_v/F_m results. This model is not as good a fit as that observed for the clade A cells. This is likely due to the very small change in maximum quantum yield observed over the course of this temperature ramp experiment for this clade. There is a small separation between the initial + intermediate cells (T0-T3) and the final group (T4-T5); however, there is still some overlap. No significant conclusions could be drawn from this model's scores and loadings.

Figures 5.20-2.21 show plots of predicted F_v/F_m vs reference F_v/F_m for clades A and F respectively. Test set spectra were used to calculate the predicted F_v/F_m values based on the model build using the training set. These values were then compared with known reference data for the spectra. The r^2 value for clade A was calculated to be 0.913 indicating a good linear fit and accurate prediction. As shown in Figure 5.20, the values can be grouped as initial, intermediate and final groups as with the PLSDA models explained in Figure 5.16. This is an indication that there was a good correlation between temperature, maximum quantum yield of PSII and macromolecular content within the sample set. Figure 5.21 further confirms that there was no correlation between maximum quantum yield of PSII and macromolecular content for clade F cells as the r^2 value for the reference vs predicted F_v/F_m calculated using spectra, was extremely low.

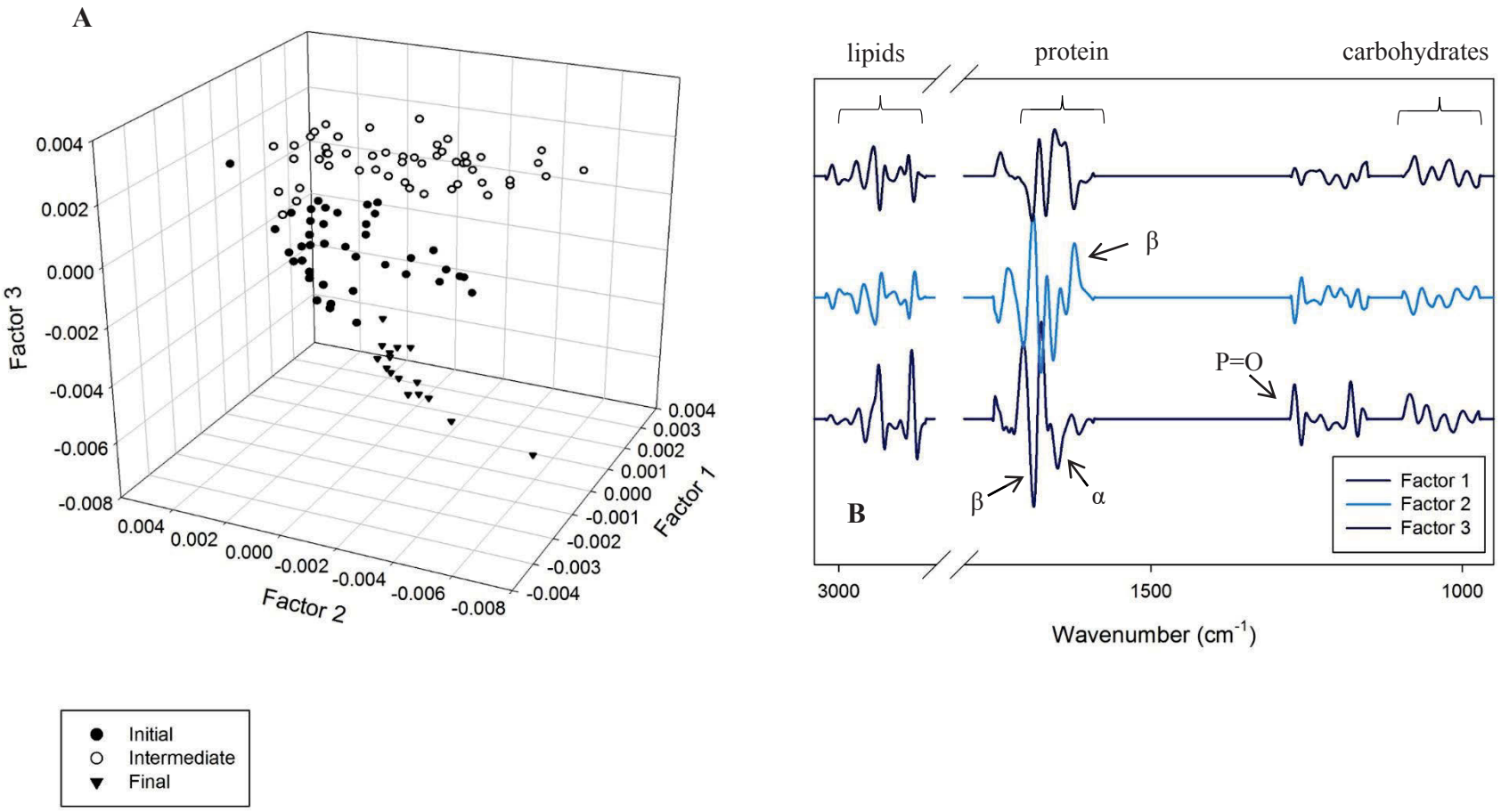

Figure 5.18: Scores (A) and loadings (B) for PLS model for clade A cells exposed to a 2 ºC/day increase in temperature.

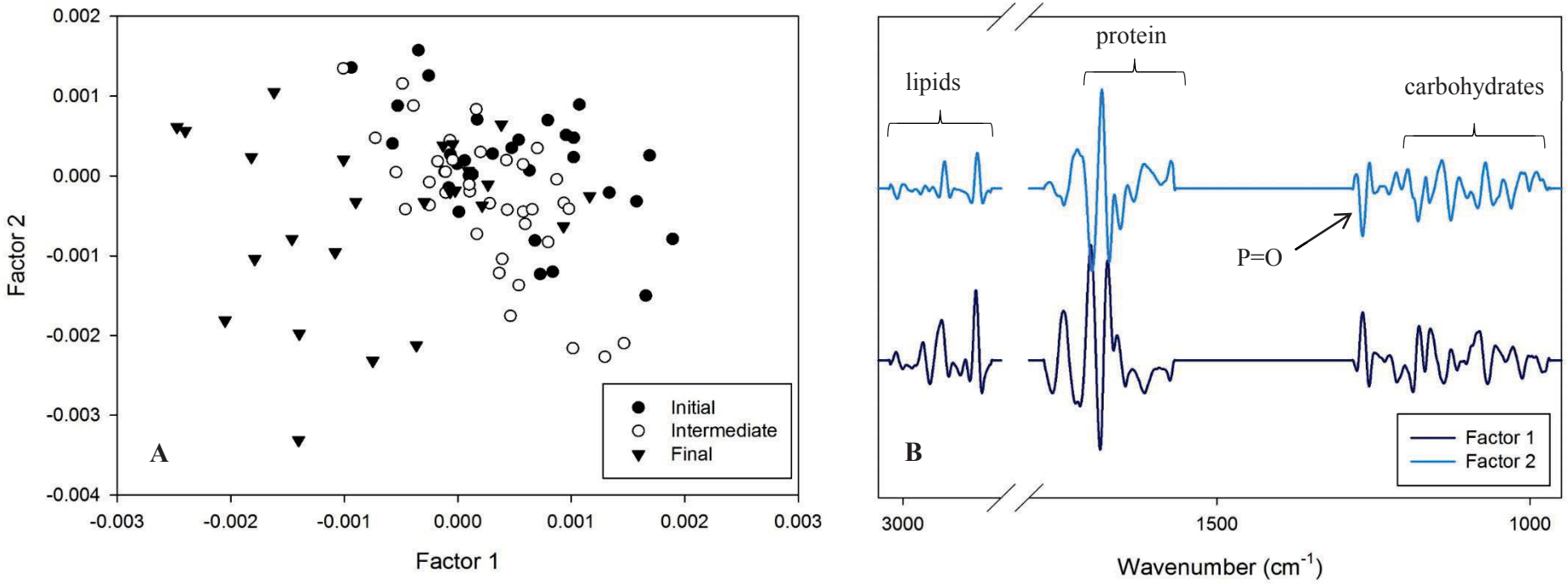

Figure 5.19: Scores (A) and loadings (B) for PLS model for clade F cells exposed to a 2 ºC/day increase in temperature.

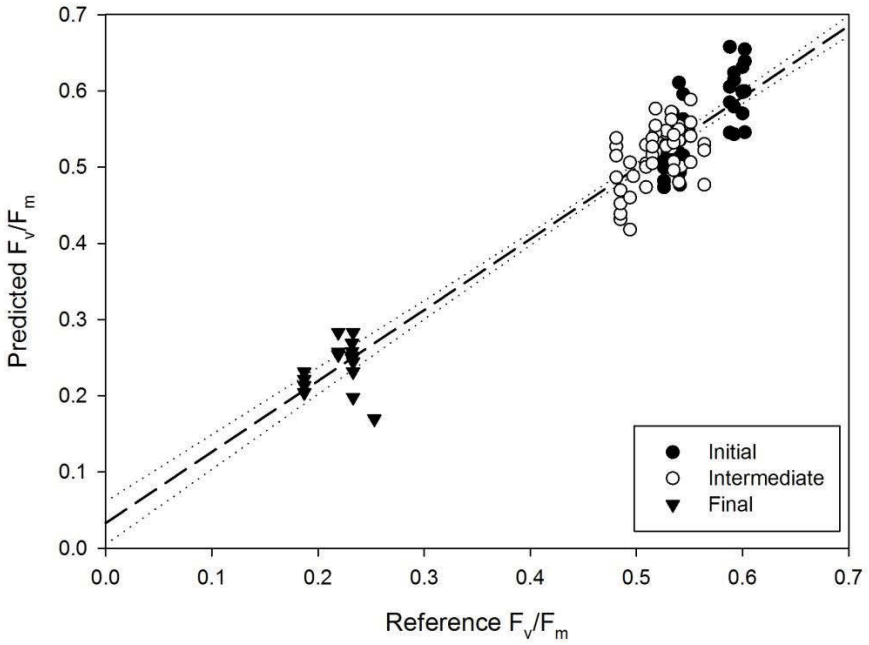

Figure 5.20: Clade A PLS predicted vs reference values for F_v/F_m. Trend line is linear with an r^2 value of 0.913 and confidence intervals are 95%.

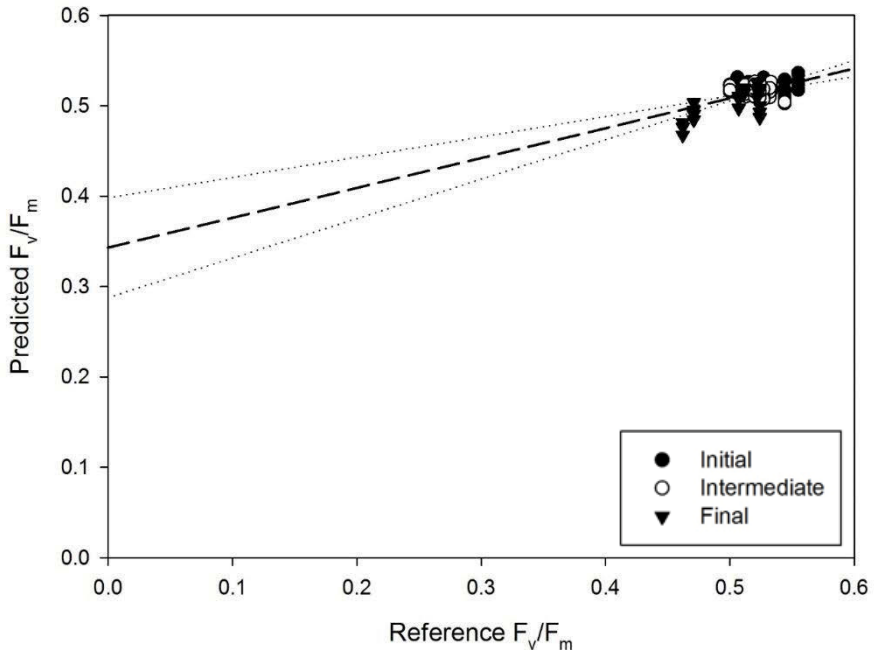

Figure 5.21: Clade F PLS predicted vs reference values for F_v/F_m. Trend line is linear with an r^2 value of 0.295 and confidence intervals are 95%.

5.3 Discussion

The results of this experiment reveal a number of important and interesting trends that were not observed in previous studies. This is likely due to the increase in the degree of the environmental stress. There is a clear difference in the behaviour of the two clades analysed in this chapter; the thermally tolerant clade F and less tolerant clade A. These differences in response could shed some light on how *Symbiodinium* shield themselves from damage *in hospite*.

There were three main macromolecular groups that showed significant changes occurring over the course of this experiment. It is interesting to note here that carbohydrate content did not appear to have any statistically significant contribution to models or overall change in content. Carbohydrate content has previously been shown to be involved in energy storage within *Symbiodinium* sp [59]. It is possible that the extreme conditions the cells were exposed to prevent the organisms from storing energy [59]. This hypothesis is also supported by the trend in lipid content (Figure 5.5). Both clades showed significant loss in overall lipids indicating a need to metabolise energy stores under these extreme conditions. This has implications for nutrient exchange within the coral symbiosis as carbohydrate and lipid has been shown to be exported to the host [8], [20], [30]. Under high temperatures, this energy reserve is therefore unavailable for translocation to the host.

Phosphorylated compounds did not show any overall change until day 5, and the greatest change occurred within cells from clade F. This also correlated with a decrease in photosynthetic function for both clades, however clade F displayed a significantly higher maximum quantum yield of PSII at this point than clade A. Phosphorylated compounds include a number of different compounds such as ATP and phospholipids

[64]. The most likely explanation for this observed increase in phosphorylated compound is an increase in protein phosphorylation. This is a process that is specifically linked with PSII function and repair [32], [34], [134]. Research has shown that phosphorylation of the D1, D2 and CP43 proteins contained within the reaction centre of PSII acts as a signal for this complex to move from the grana to the stroma within the thylakoid membrane [135]. Once in the stroma, the complex is partially disassembled where damaged components can be replaced [31]. Under extreme conditions, the photosynthetic machinery within the cells is damaged. The increase in phosphorylated compounds correlates with an observed decrease in maximum quantum yield of PSII and so it is likely that the number of PSII reaction centres damaged within the chloroplast is increasing [134]; hence there is an increase in protein phosphorylation (Figure 5.4). Mixed model ANOVA showed that clade F cells experienced a significantly higher increase of phosphorylated compounds at T5 than clade A, and a significantly higher maximum quantum yield of PSII. This could be an indication that this repair mechanism is functioning much more efficiently in clade F than A.

In addition to changes in lipid and phosphorylated compounds, clade A cells exhibited a change in protein and lipid structures (Figures 5.6, 5.9 – 5.11). This change was also observed in the groupings found in the PLSDA and PLS models (Figures 5.16 and 5.18), which are influenced by these structural changes. Clade A cells appeared to have three macromolecular states that correlated with maximum quantum yield of PSII. Initially (days 0-1), cells were characterised by a high α-helix content and lesser degree of lipid saturation. Cells classified into the intermediate group also correlated with a slight decrease in PSII function. This macromolecular state showed an increase in β-sheet secondary structure and a higher degree of lipid saturation. The final group

changed macromolecular state once more and this correlated with an extremely low maximum quantum yield of PSII and, hence, a severe drop in photosynthetic function. It is probable that the clade A cells reached their stress threshold and that the intermediate macromolecular state was one where the cells were attempting to counteract the increase in stress by increasing saturation in lipid membranes and shifting protein secondary structure [55]. Once the cells exceeded their thermal maxima, these repair mechanisms ceased resulting in a change in macromolecular content to a state entirely different to the initial and intermediate groups [136]. The results of this experiment, therefore, provide insight into the failure of these repair mechanisms and allow a better picture of the breakdown of function from a macromolecular point of view.

A likely inference from these groupings is that the cells were undergoing some sort of repair process and there are a number of different possibilities. It has long been understood that the PSII repair mechanism involves the D1 protein breakdown and replacement. As reviewed in [21], [31], [32] when PSII is damaged, the reaction centre is partially disassembled and the D1 protein removed and replaced with a new protein in the thylakoid membrane. PSII is then reassembled and the electron transport chain can recommence. It is possible that the increase in β-sheet structure could be a result of this repair process and the D1 protein is replaced with a different structure. This could be tested by extracting the protein using methods of previous studies [23], [126], and using FTIR spectroscopy to analyse the secondary structure.

This hypothesis is, however, unlikely for a number of reasons. Protein crystallographic studies outlining the structure of the PSII complex all depict the D1 proteins as α-helices [35], [36]. Since this turnover of D1 can also occur in chloroplasts not subjected to environmental stress [31], it is unlikely that this protein would be copied and

replaced with a different structure. Recent work has postulated the involvement of other proteins than D1 involved in PSII repair and protection [23]; however, these are yet to be identified. One such candidate also appears to contain the highest β-sheet content of any protein groups within the PSII complex [35], [36]. This protein also contains a high content of random turns and coils within its structure [137]. The extrinsic protein, PsbO, has also been associated with stability of the manganese complex and has been implicated as the likely initial site of photoinhibition within the chloroplast [21], [137]. An increase in the secondary structure of this protein could indicate an increase in the content of PsbO, which in turn could be linked to an increase in the PSII repair mechanism.

Results from a study investigating the PSII subunit content of expelled and *in hospite Symbiodinium* correlate with the results presented here [138]. Total protein content did not change as F_v/F_m values decreased; however, the method used to quantify this gave no indication of protein function. It was proposed that, as maximum quantum yield of PSII decreased, the repair turnover of the inactive D1 protein diminished [138]. It is possible that the increased β-sheet content observed for both clades in this chapter correlates with an increase of inactive PSII protein complexes. However this does not account for the reversion to α-helix for clade A at 34 ^{o}C.

Also linked to this second macromolecular state for clade A, is a distinct shift in lipid structure (Figures 5.9-5.11). Since PLS modelling also correlated this structural shift with maximum quantum yield of PSII, it is likely that these changes in the FTIR spectra are occurring within the thylakoid membranes. Cells appear to undergo an increase in saturation, branching and disorder. Lipid saturation has previously been thought to be a diagnostic indicator of thermal sensitivity and is linked to thylakoid membrane integrity [55]. The results of this experiment also show that lipid disorder

(the ratio of asymmetric to symmetric vibrations) changes in a similar trend to saturation. Research has shown that different clades have different membrane melt-temperatures, which could be what the results of this experiment are indicating here [53].

It is interesting to note that, while clade F exhibited a similar trend to clade A for change in protein structure, lipid structure did not appear to change over the course of this experiment. This may be an indication that different clades have different repair strategies in order to cope with extreme conditions. Total lipid content showed that clade F cells were also consuming a larger lipid content, presumably as a metabolic energy reserve for environmental stress conditions. The shift in lipid structure for clade A might be in indicator of a response to stress that the clade F samples did not need to execute.

Further research is needed here to examine the breakdown of the thermally tolerant clade F samples. Prolonging the exposure of these cells to 34 ^{o}C might clarify some of these hypotheses relating to clade A's repair mechanisms. Isolation of PSII would also help identify these changes in protein and lipid under extreme conditions and eliminate possible interference from the rest of the cells' normal processes. FTIR spectroscopy coupled to a FPA detector could also help resolve where exactly these changes are taking place; however, these cells are so small that use of a synchrotron light source would be essential.

5.4 Conclusions

Exposure to extreme conditions showed, once more, that clades of *Symbiodinium* sp. behave in significantly different ways to environmental stress. Clade A, the less thermally tolerant clade, exhibited a number of distinct macromolecular states that are possibly related to repair mechanisms within the cells. Clade F appeared to differ in terms of the lipid structural response indicating a possible alternative energy storage strategy to that of clade A. This is likely contributing to the difference in thermal tolerance between the clades.

Chapter 6. Assessment of macromolecular variation of symbiotic dinoflagellates by Synchrotron FTIR-imaging spectroscopy

6.1 Introduction

A common limitation of many metabolomics methods, is that the specific changes in macromolecular content cannot conclusively be correlated with cellular mechanisms or processes [51], [139]. Throughout this thesis, a number of hypotheses have been proposed; however, few of these possible mechanisms for altered macromolecular composition have been robustly verified. One of the advantages associated with the use of FTIR spectroscopy is the relatively recent development of FPA detector technology, allowing the collection of chemical images and not only single point measurements. However, the spatial resolution of laboratory instruments is generally too low to allow for the analysis of single algal cells [75]. Synchrotron radiation can be used to increase resolution and allow for the collection of algal cell images.

In this chapter, clade F *Symbiodinium* cells are analysed using FTIR spectroscopy coupled to a FPA detector to generate images with detailed spatial resolution. The data gathered from these images will add important information to the findings presented previously in this thesis.

6.2 Data collection and processing

Samples for this chapter were collected and the results of micro-FTIR spectroscopic analysis were presented Chapter 5. Aliquots of these *Symbiodinium* cultures were taken to the Synchrotron Radiation Center (SRC) in Madison, Wisconsin, USA to be analysed as described in Chapter 2.2.3.

6.3 Results

6.3.1 Chemical imaging

Figures 6.1 – 6.6, are representative images of *Symbiodinium* clade F cells. There are two representative examples shown for each temperature (25ºC, 30 ºC and 34 ºC). Each image is comprised of 4096 individual pixels and the false colour images in each of the figures is measure of the intensity of a given frequency (Figures 6.1-6.6, B-F). It should also be noted that the resolution of the light microscope used to take images for later comparison was too low for the size of these cells (Figures 6.1-6.6, A). It is therefore difficult to match chemical images with specific organelles within the cells. This limits the interpretation of the data; however certain trends are still evident.

First of all, protein secondary structure images generated for α-helix (1655 cm^{-1}) and β-sheet (1620 cm^{-1}) content display a difference in intensity across the cell (Figures 6.1 – 6.6, B and C). This is an indication that these structures are concentrating in different organelles. Lipid also appears to be clustered in concentrated locations within the cells. This mostly appears to be in a different location to the protein clusters (Figures 6.1 – 6.6, C).

Carbohydrate was generally spread across the entire cell for cells collected at 25 ºC with few smaller clusters appearing (Figures 6.1 – 6.2, D). These clusters appeared to decrease in size at days 3 and 5 (Figures 6.3 – 6.6, D) and may indicate a decrease in carbohydrate content with increasing temperature. Phosphorylated compounds were generally gathered in one or two locations within cells (Figures 6.1 – 6.6, E). One of these clusters could often be correlated with the lipid cluster. This could be an indication of a phospholipid cluster.

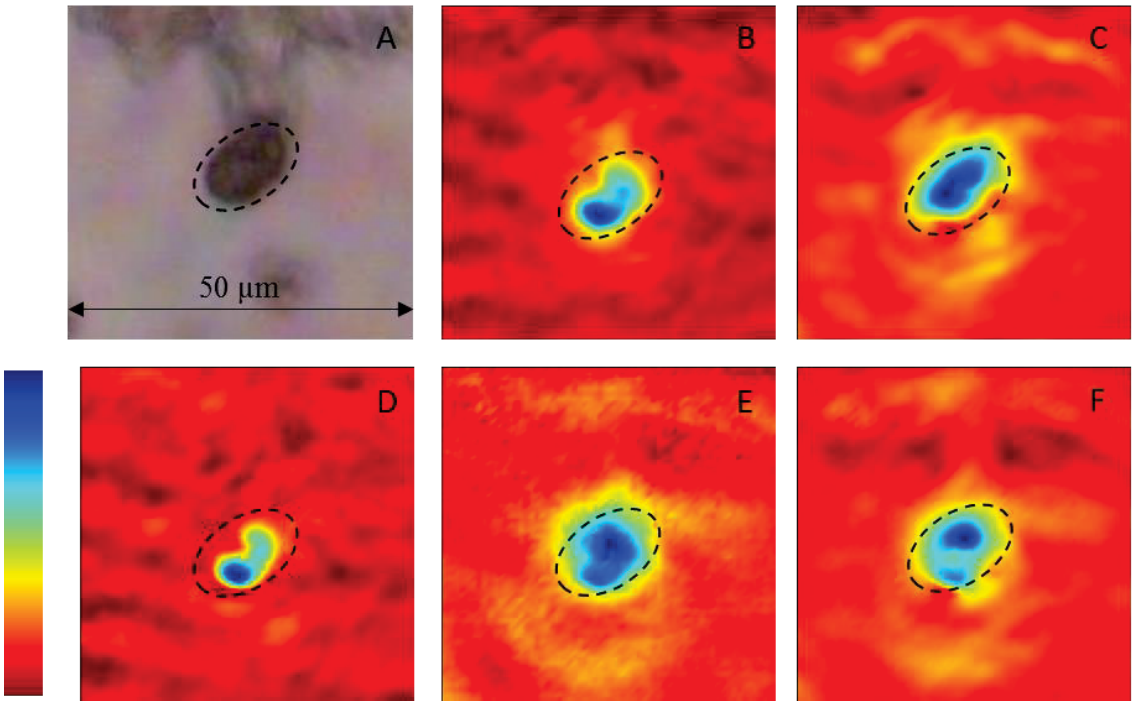

Figure 6.1: Chemical images for Clade F cells collected at 25 ºC (example 1). Images show the following: A = light microscope image, B = α-helix protein, C = β-sheet protein, D = lipid, E = carbohydrates and F = phosphorylated compounds. Colour bar indicates blue is high intensity and red is low.

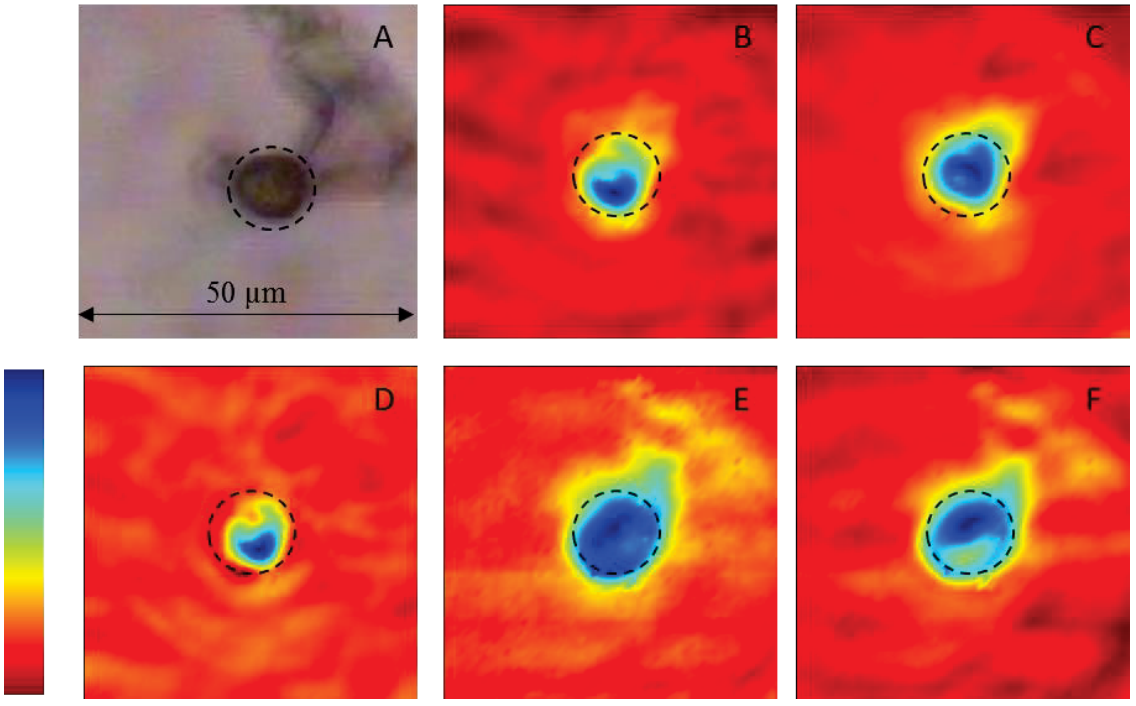

Figure 6.2: Chemical images for Clade F cells collected at 25 ºC (example 2). Images show the following: A = light microscope image, B = α-helix protein, C = β-sheet protein, D = lipid, E = carbohydrates and F = phosphorylated compounds. Colour bar indicates blue is high intensity and red is low.

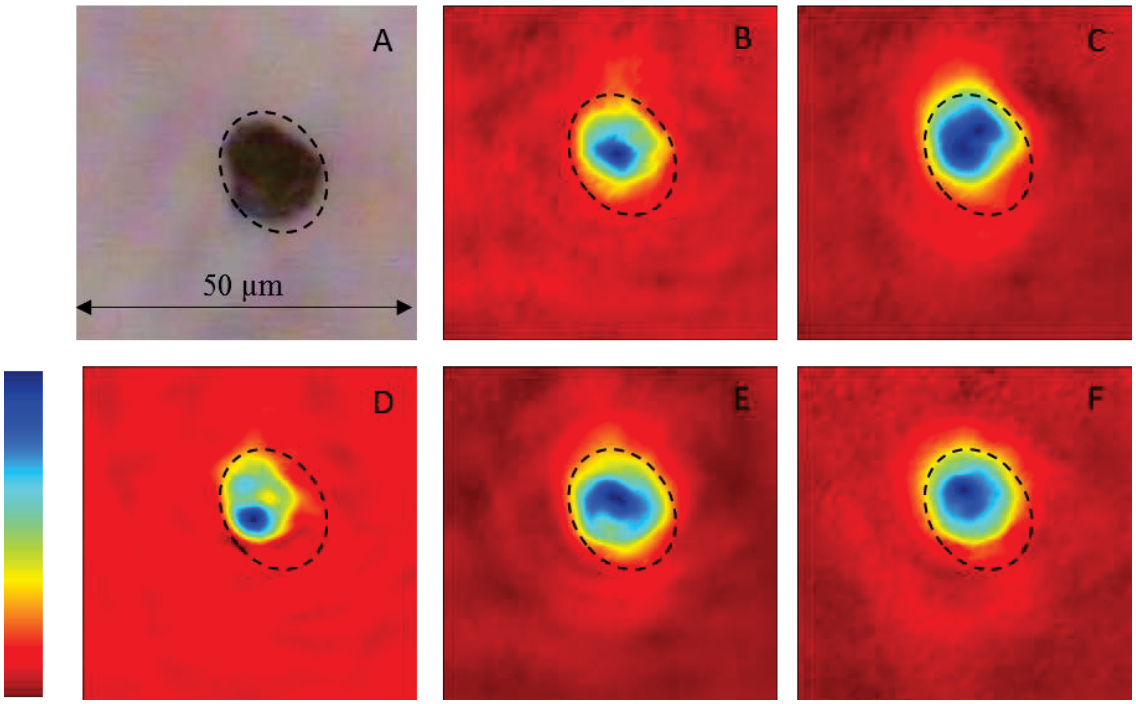

Figure 6.3: Chemical images for Clade F cells collected at 30 ºC (example 1). Images show the following: A = light microscope image, B = α-helix protein, C = β-sheet protein, D = lipid, E = carbohydrates and F = phosphorylated compounds. Colour bar indicates blue is high intensity and red is low.

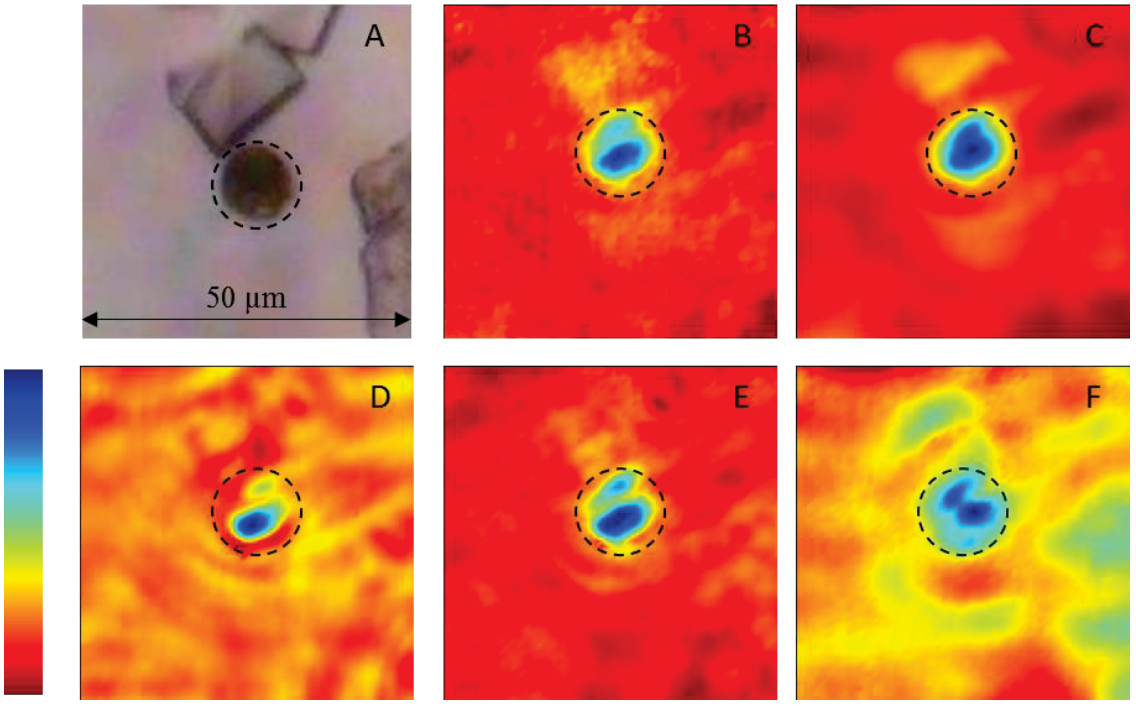

Figure 6.4: Chemical images for Clade F cells collected at 30 ºC (example 2). Images show the following: A = light microscope image, B = α-helix protein, C = β-sheet protein, D = lipid, E = carbohydrates and F = phosphorylated compounds. Colour bar indicates blue is high intensity and red is low.

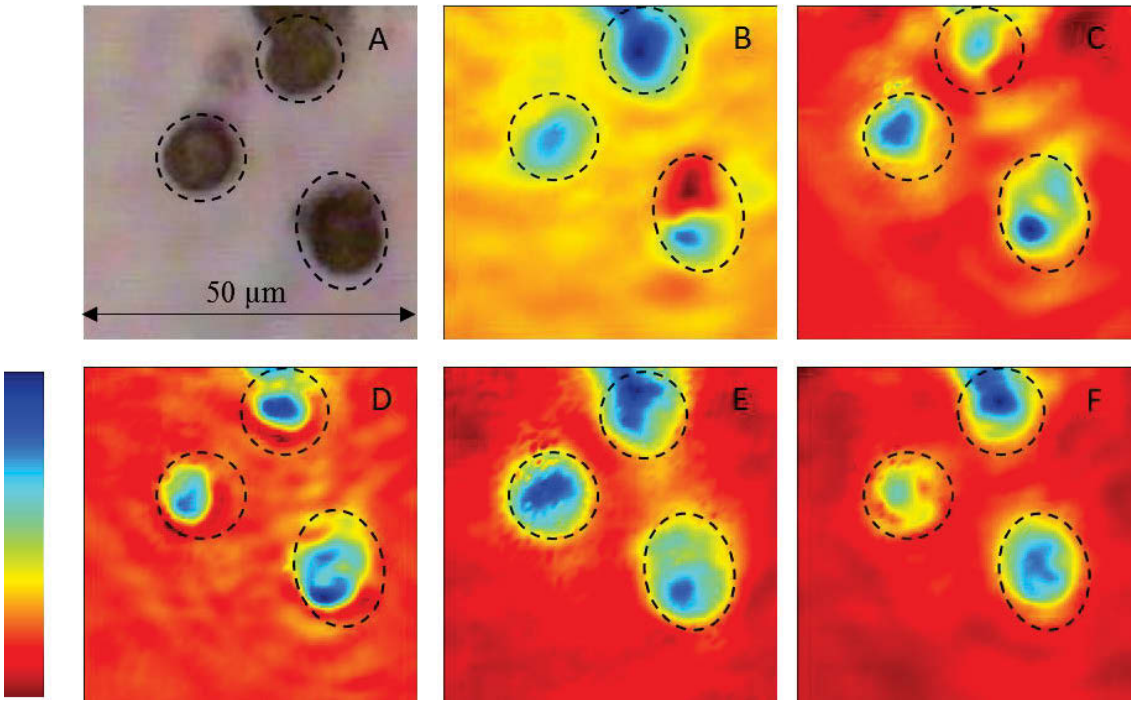

Figure 6.5: Chemical images for Clade F cells collected at 34 ºC (example 1). Images show the following: A = light microscope image, B = α-helix protein, C = β-sheet protein, D = lipid, E = carbohydrates and F = phosphorylated compounds. Colour bar indicates blue is high intensity and red is low.

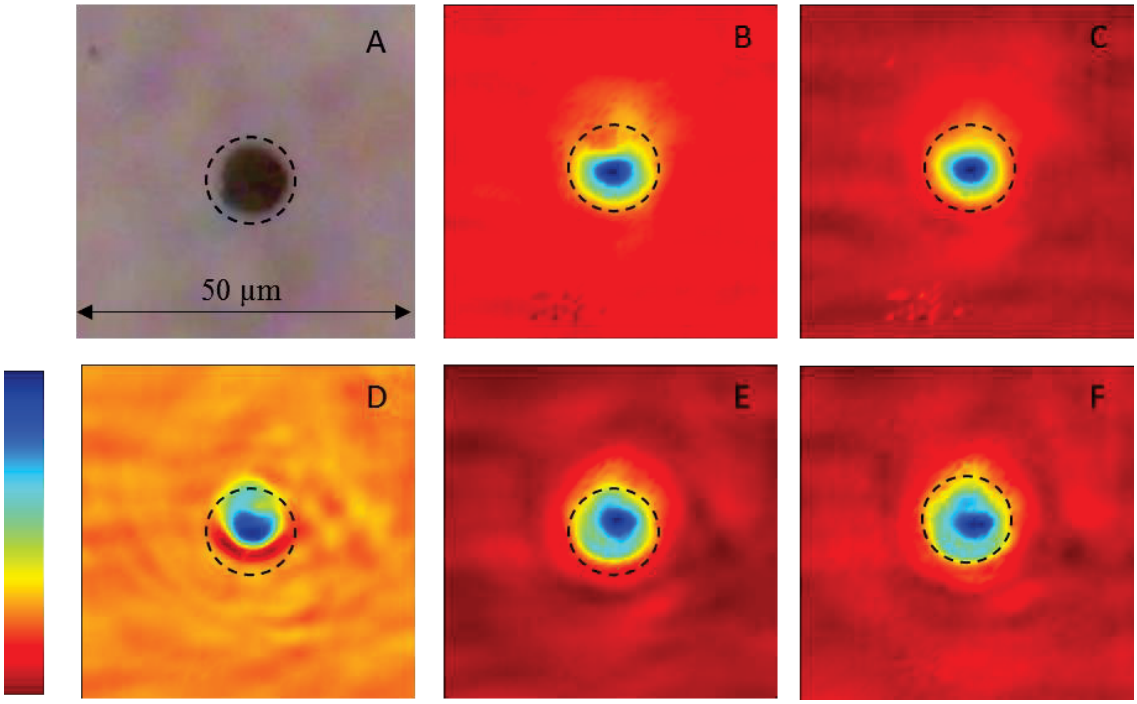

Figure 6.6: Chemical images for Clade F cells collected at 34 ºC (example 2). Images show the following: A = light microscope image, B = α-helix protein, C = β-sheet protein, D = lipid, E = carbohydrates and F = phosphorylated compounds. Colour bar indicates blue is high intensity and red is low.

6.3.2 Statistical imaging

Images were further investigated by statistical imaging, specifically HCA. This technique assesses the spectra contained within each pixel making up the image, and generates clusters based on similarity. Each cluster can therefore be attributed to an average spectrum. This method was used to group spectra within the clade F cells. Representative models are shown in Figures 6.7-6.12. Each of these images corresponds with examples shown in Figures 6.1-6.6 and consist of the light microscopy image for comparison, the false colour images showing clusters of spectra most similar to each other, and the average spectra for each of these clusters.

Across the groups, there are a number of changes that seem to agree with the macromolecular groupings shown in Figures 6.1-6.6. First of all, the cell spectra are clearly separated from the surrounding isotonic saline solution in which the cells were rinsed to remove interference from salt water media. Three specific macromolecular components seem to be contributing the most to the clustering of the spectra; the α-helix and β-sheet protein structures, as well as the lipid content of the cell. Intensities of these components seems to be variable across the cells. Specific protein secondary structures cluster in different areas with different intensity. Looking at the images, it seems that the cells at 25 ^{o}C contain predominantly α-helix structure, while cells collected at 34 ^{o}C appear to contain more β-sheet. However, the overall level of variation across the cells appears to remain the same.

Lipid content does not appear to change structurally between the three temperatures. The ratio of protein to lipid content does change at 34 ^{o}C, the total lipid content appear to be much less than the cells collected at 25 and 30 ^{o}C. The content shown in average

spectra for the clusters indicate that spatially, the amount of lipid changes across the cell.

HCA mapping also revealed that a number of cells showed chemical groups clustering around the outside of the cell walls. These groups were characterised by a lesser concentration of cellular material. This is possibly an indication that the cells burst at some point in the sample preparation, however, inspection of the cells by light microscope consistently revealed that the cells were intact (for example, refer to Figure 6.8 and 6.12).

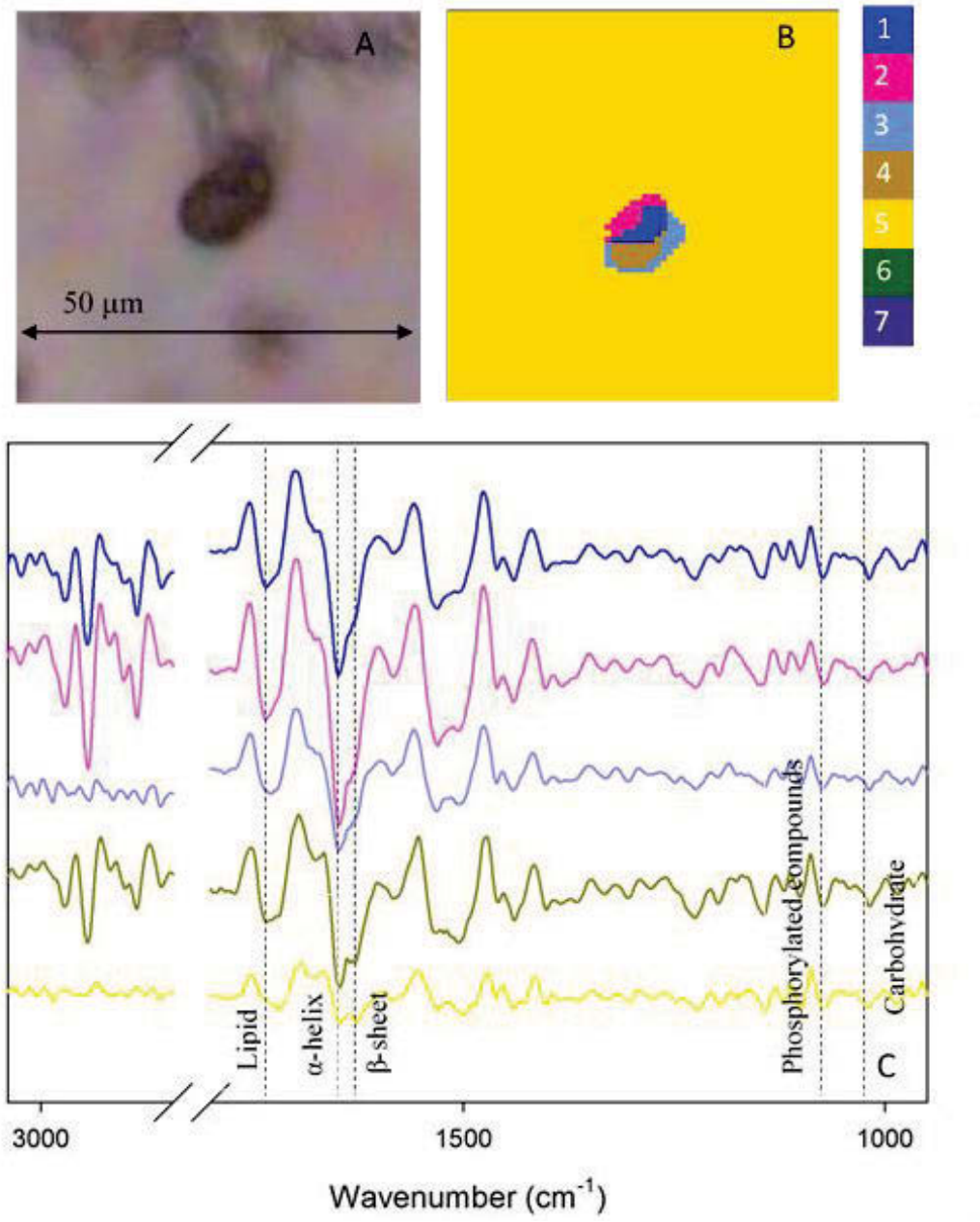

Figure 6.7: HCA mapping for a cell collected at 25 ºC (example 1). Groups are colour coded for both the HCA map (B) and the average spectra (C). Dotted lines indicate band intensities used to build chemical images (Figure 6.1).

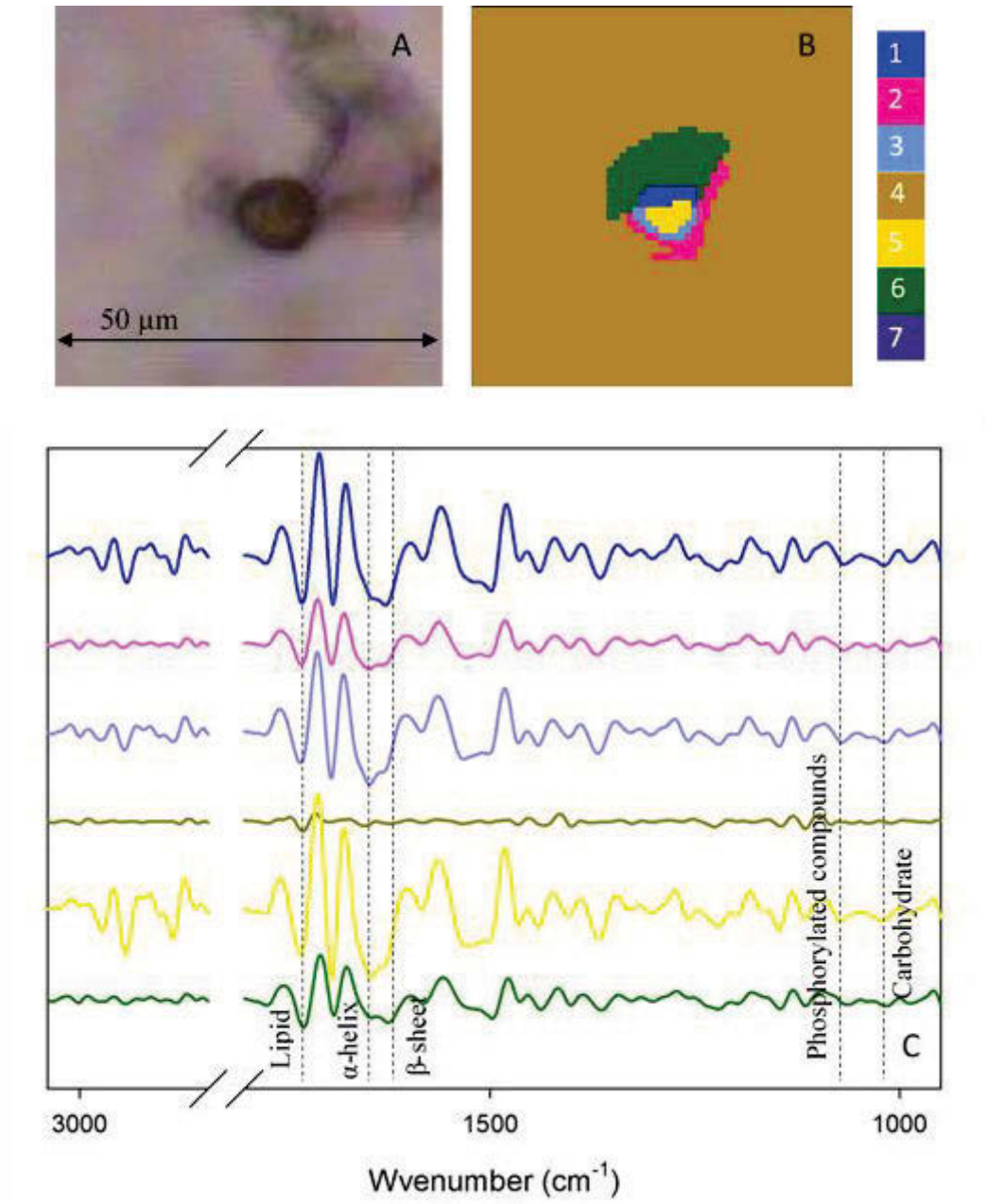

Figure 6.8: HCA mapping for a cell collected at 25 ºC (example 2). Groups are colour coded for the HCA map (B) and the average spectra (C). Dotted lines indicate band intensities used to build chemical images (Figure 6.2).

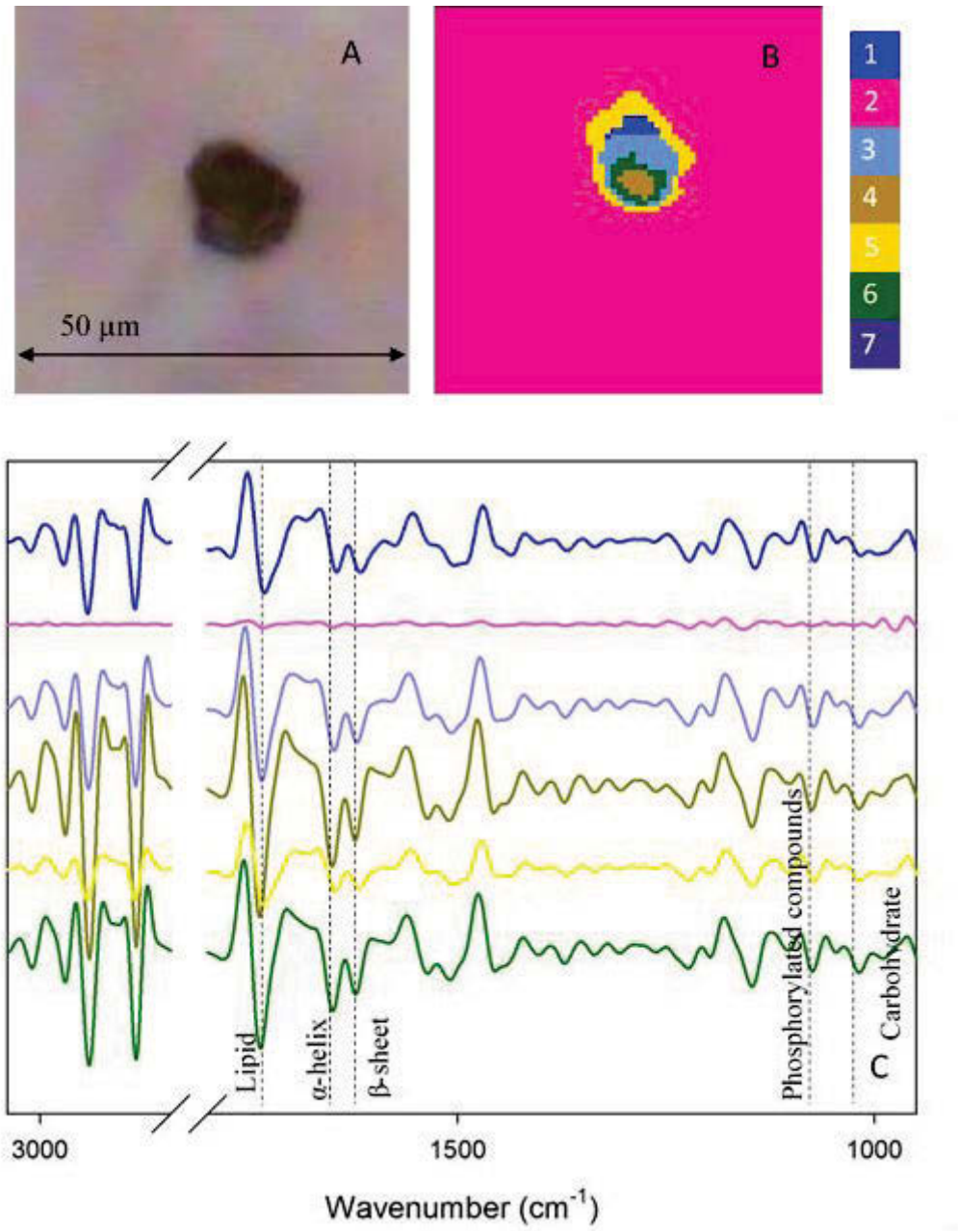

Figure 6.9: HCA mapping for a cell collected at 30 ºC (example 1). Groups are colour coded for the HCA map (B) and the average spectra (C). Dotted lines indicate band intensities used to build chemical images (Figure 6.3).

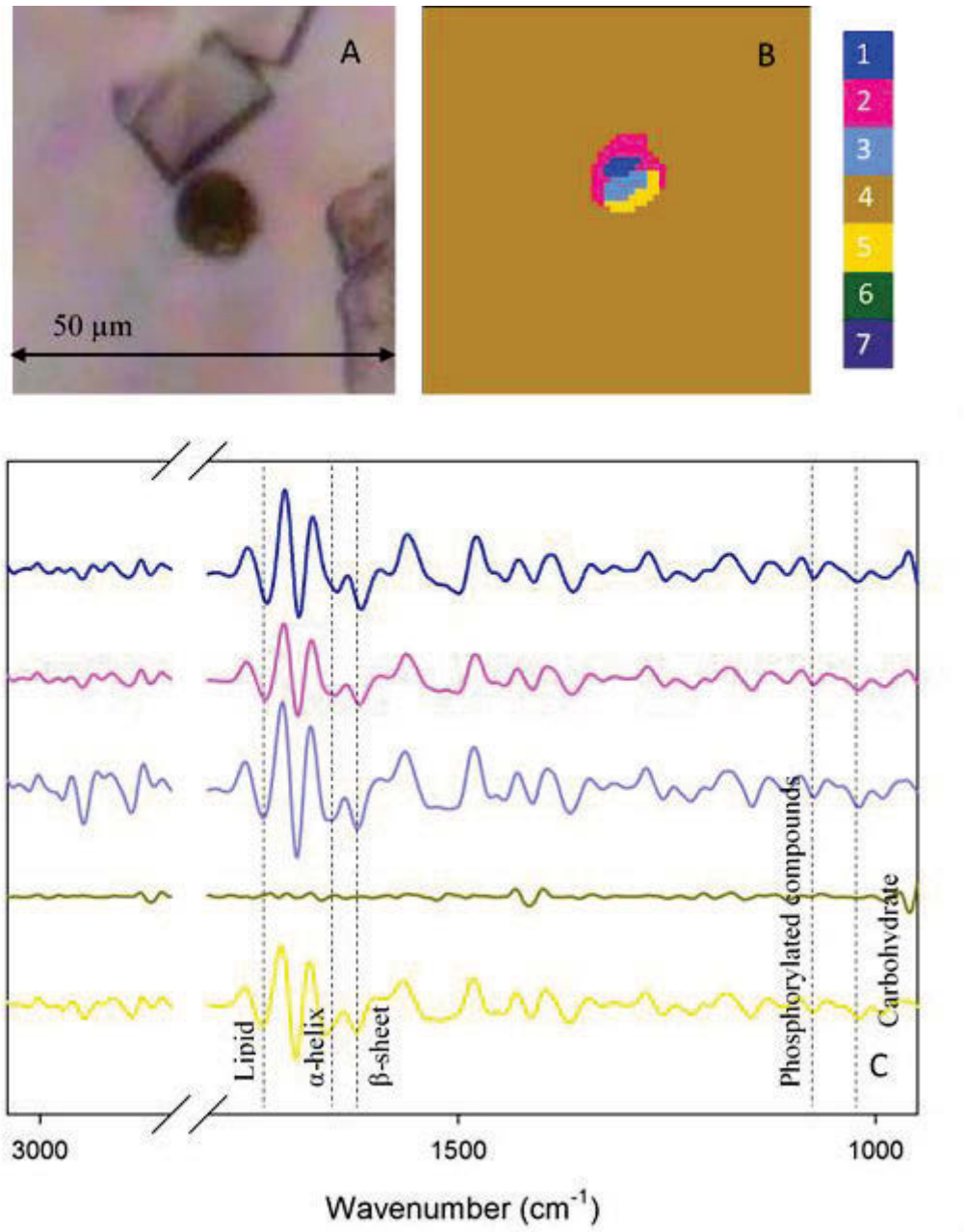

Figure 6.10: HCA mapping for a cell collected at 30 ºC (example 2). Groups are colour coded for the HCA map (B) and the average spectra (C). Dotted lines indicate band intensities used to build chemical images (Figure 6.4).

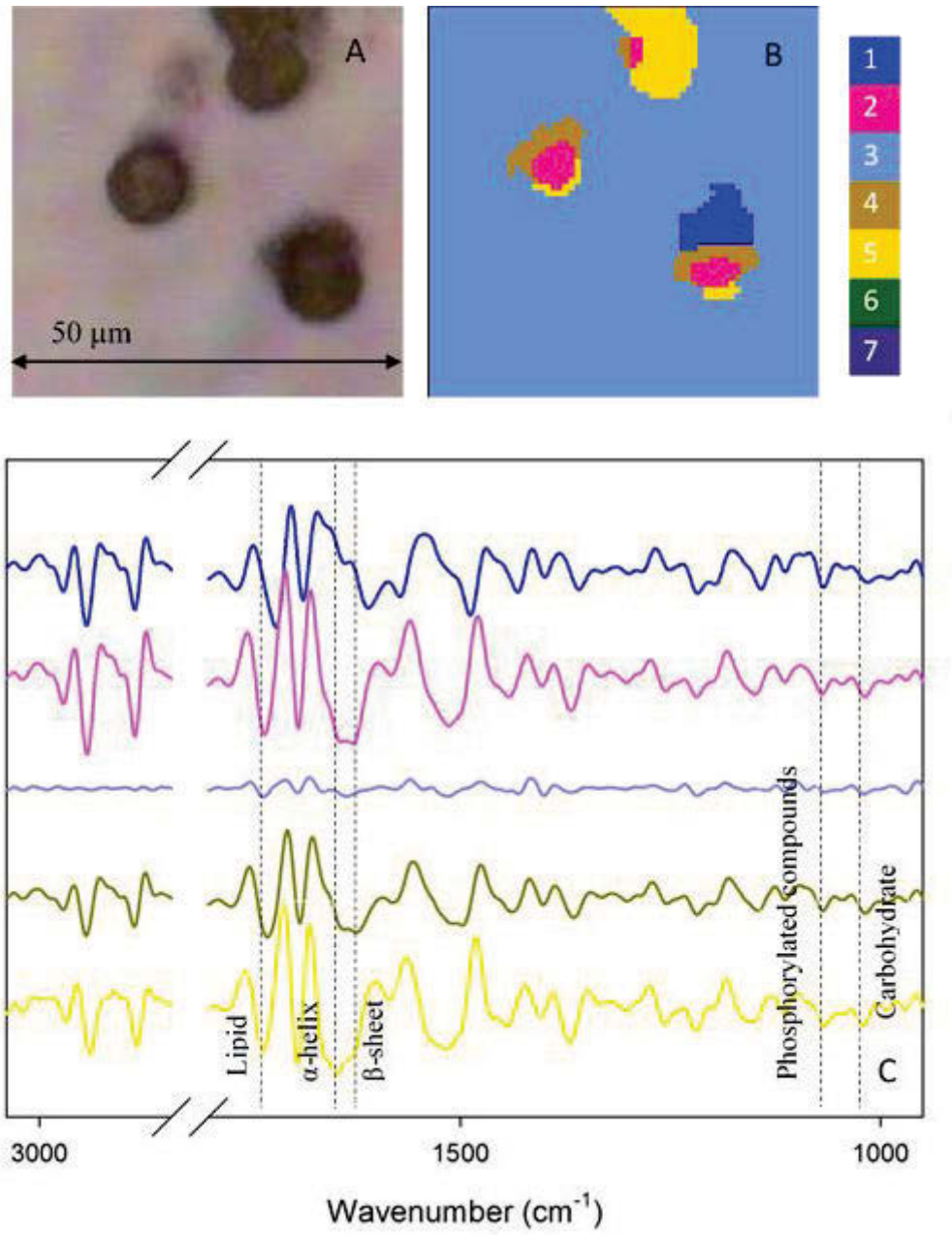

Figure 6.11: HCA mapping for a cell collected at 34 ºC (example 1). Light microscope image is shown in A. Groups are colour coded for the HCA map (B) and the average spectra (C). Dotted lines indicate band intensities used to build chemical images (Figure 6.5).

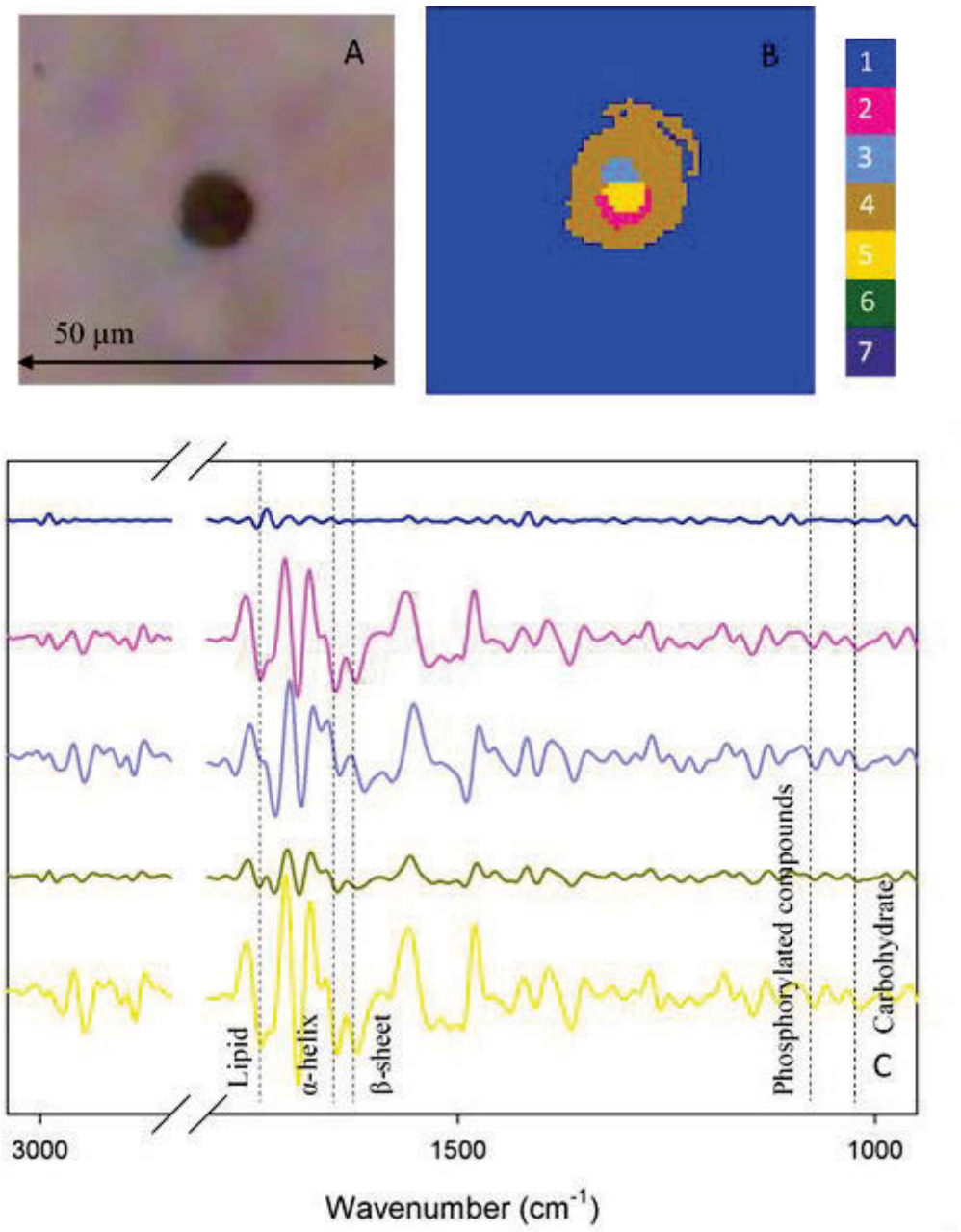

Figure 6.12: HCA mapping for a cell collected at 34 ºC (example 2). Light microscope image is shown in A. Groups are colour coded for the HCA map (B) and the average spectra (C). Dotted lines indicate band intensities used to build chemical images (Figure 6.6).

The HCA average spectra were analysed further by PCA in order to investigate the trends noticed above (Figure 6.13). These chemical groupings were classified based on their relative position within the cell; non-cellular, outer and middle. These groups were chosen based on patterns observed in the HCA images; a number of smaller chemical groups were encased in larger groups surrounding them. Lack of light microscopy resolution rendered a more specific classification difficult.

PCA models revealed that there was no clustering occurring for groups based on the temperature at which the cells were sampled (refer to Chapter 2.1.1). The best separation was achieved between the outer and middle groups once the non-cellular spectra had been removed from the model. Figure 6.13 shows scores and loadings for this PCA model. As shown, the variation between the two groups is largely explained by Principal Component 1 (PC-1). Since these spectra are second derivatives, the interpretation of the loadings is reversed. The α-helix and β-sheet protein structures are oppositely correlated in the loadings. This means that the groups around the outer edge of the cell contained a high β-sheet content, while groups within the middle of the cell tended towards a higher α-helix protein structure. This correlates with the distribution of protein secondary structure shown in chemical images (Figures 6.1-6.6).

The band at 1080 cm^{-1} was positively correlated in the loadings meaning that the clusters towards the centre of the cell contained a high degree of phosphorylated compounds. This trend was also found in lipids, with the lipid carbonyl and C-H stretching bands all positively correlated.

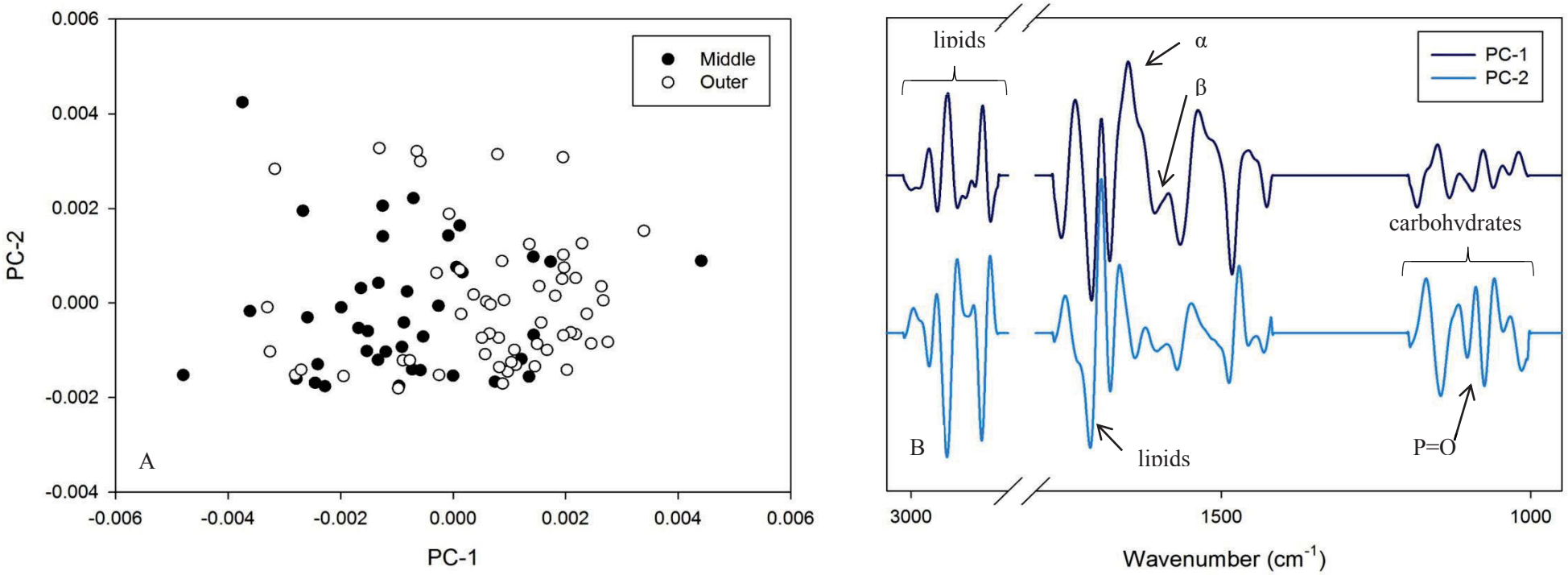

Figure 6.13: Scores (A) and loadings (B) for the PCA model for collated HCA loadings assigned to locations within cells.

6.4 Discussion

The data presented in this chapter is the outcome of a preliminary investigation of the benefits of this synchrotron technique and results show that this has significant promise with a number of modifications. It is possible, however, to describe a number of trends that can be correlated with macromolecular content and variation across the individual cells.

Comparing the chemical images, statistical images and PCA modelling, it is clear that a number of components cluster in specific areas and these might correlate with organelles within the cells. A possible method to distinguish between organelles in the absence of proper light microscopy reference images, is to use compounds known to congregate in certain areas within the cells. Chloroplasts are generally considered to be rich in lipids and the nucleus rich in protein. Previous FTIR spectroscopy imaging studies have noted that the highest concentration of lipid across an image, has been around the chloroplast. Protein content was also found to be highest at the nucleus [76]. PCA models revealed protein secondary structure clustered differently across the cells with α-helix congregating in the centre and β-sheet generally distributed across the cell. These clusters of α-helix structure could be correlated with the nucleus. This is particularly supported by the positively loaded phosphorylated compounds in PCA models indicating the centre of the cells contained more of these compounds. Comparison with TEM images, however, that the nucleus of these cells are small, and the HCA clusters are quite large [43], [140].

The discrepancy here could be simply due to a specific morphological characteristic of these cells and the method of spectra acquisition. *Symbiodinium* sp. cells are spherical

in shape. Since the spectra used to build the images were collected in transmission mode, the beam travelled in a cross section through the cell. This means that orientation of the *Symbiodinium* cells is different for each image. It would therefore be more effective to take prepared sections of the cells for analysis first by Transmission Electron Microscopy (TEM) as has been performed in previous studies [25], [140], [141]. Ultrastructural images of this nature could then be compared with FTIR spectroscopic images. TEM studies have also revealed lipids do not only congregate in concentrated quantities around chloroplasts. Lipid body formation has been noted as a result of exposure to elevated temperature [140]. These organelles could be the origin of the concentrated lipid appearing in the chemical images of this study, and not the chloroplasts.

As mentioned previously, the light microscopy capabilities of this beamline were limited for the size of the cells analysed, making comparison difficult. It was impossible to determine where specific organelles were appearing within the cells and assign clusters when forming the chemical images at a later date. This might have been avoided by preparing and marking slides before analysis at the synchrotron, but as the analysis was being performed overseas, it was decided that this approach was impractical.

It is important to note that drying may also complicate the structural elucidation of the cells. Whelen et al reported that drying samples changed the structure of the DNA contained within from B configuration to A [91]. At first glance, this may not seem vital, however when the high sensitivity of FTIR spectroscopy is taken in to account the complication can be significant. But in this case, since all cells were treated in exactly the same manner, comparisons between cells may still be made. It was also important in this project, to determine the protein content and structure across the cell. Regardless

of the identity of the organelles, the very fact that changes were observed can be considered of particular interest and worth further investigation.

Coupling the laboratory instruments to the increased power of synchrotron radiation has also allowed for the study of hydrated cells [64] and even live cells [76]. Subjecting cells to increases in temperature or light while *in situ* on the instrument, would allow for changes in cell structure to be monitored in real time. However, the addition of water to the cells results in loss of the information contained within the amide I protein band. This would not be ideal in the case of this thesis given that the secondary structure of proteins is of specific interest here.

Since the time of data collection, the SRC has been decommissioned. Before that, the IRENI beamline was the only facility in the world coupled to an FPA detector. Recent developments in technology of this nature have resulted in a new technique known as Nano-FTIR spectroscopy [139]. This involves coupling the intense light from the Advanced Light Source in Berkeley, California, to two different techniques; FTIR spectroscopy and infrared scattering-scanning near-field optical microscopy (IR s-SNOM). The combination of these two techniques results in images with resolution down to the nano-scale. This would undoubtedly provide much better resolution of macromolecular components within the *Symbiodinium* cells; however, nano-FTIR spectroscopic imaging is still very much in early stages of development.

The data presented in this chapter serves to highlight the need for further research in this particular area. The information contained within the macromolecular images of *Symbiodinium* will help resolve where structural changes will occur, and what implications these have on the overall health and function of the cells. The ability of this technique to discriminate between clusters of different macromolecular compounds

shows promise for this type of analysis; however, further development of current technology is needed before this area of research can become more widespread.

6.5 Conclusions

The results of this preliminary investigation of chemical imaging of *Symbiodinium* sp. are inconclusive. It is clear, looking at chemical images and HCA statistical images, that the spectra are different across the cell indicating ultra-structural variation. However, in the absence of resolved light microscopic images for comparison, it is impossible to determine which organelles are responsible for the clustering generated by the statistical images.

Further research is needed using TEM and nano-FTIR spectroscopic imaging techniques in order to obtain a detailed map of structural differences and response to environmental stress within the cells.

Chapter 7. General discussion and thesis summary

7.1 Introduction

Around the world, coral reef systems are under threat. The delicate balance between host and symbiotic dinoflagellate, *Symbiodinium*, has been the focus of a large amount of research; however, much is still left to be done in order to halt the decline of these vital ecosystems. Photosynthetic function and biochemical response of *Symbiodinium* under environmental stress are still in the process of being discovered. This thesis has aimed to add new insight into the biochemical processes within these dinoflagellates under increased environmental pressure.

Three main experiments investigating the macromolecular content and changes in the symbiotic dinoflagellate *Symbiodinium* were performed. Chapter 3 outlined the macromolecular content of two clades of *Symbiodinium* sp. grown under normal temperature and irradiance. In Chapter 4 the changes occurring once these cells were exposed to mild environmental sub-lethal stress factors was investigated, and in Chapters 5 and 6 the changes induced by extreme increases in temperature simulating bleaching were examined. The key findings from these experiments are summarised here, and directions for future research are suggested.

7.2 Structural changes

FTIR spectroscopic analysis of the *Symbiodinium* cells consistently revealed significant differences in lipid and protein structure. Before the commencement of this project, the change in structural components of the cells had not been examined before and so this thesis provides important information for the overall map of macromolecular content changes with *Symbiodinium* sp. Presented here is a summary of results from Chapters 3-6 and possible implications for environmental changes.

7.2.1 Lipids

Lipid saturation has been known to differ between the genetic clades of *Symbiodinium* sp. and the results provided in this thesis agree with previous findings [53], [55]. The data analysed in Chapter 3 revealed that the different clades of *Symbiodinium* grown under normal irradiance and temperature, differed significantly in their saturated lipid content. The pilot studies reported in that chapter found that clade A was the less thermally tolerant species, and this clade seemed to have a higher saturated lipid content than the more tolerant clade F. Lipid structure also differed in terms of a parameter called "disorder" [82], and is thought to give an indication of how membrane lipids are arranged. Clade F lipid disorder was significantly higher than clade A. It is possible that this means clade F membrane fluidity was higher than A and could therefore have some effect on environmental tolerance.

In Chapter 4 these two clades and their response to sub-lethal stress were further examined. It was found that, in general, the clade F lipid structure underwent more change in saturation, branching and disorder, than clade A. In addition to these findings, the different environmental treatments elicited different responses. Elevated light caused an increase in both saturation and branching for clade F, whereas temperature did not seem to affect either of these parameters. Lipid order was observed to increase under all treatments for clade F cells.

Cells' response to extreme temperature conditions was measured in Chapter 5. This time, clade A was observed to undergo the highest degree of change in relation to clade F cells. As temperature was increased, saturation, branching and order all changed significantly until conditions reached 34 ^{o}C. At this temperature, all the lipid parameters reverted back to the values measured initially. It was proposed that lipid

structural changes were correlated with a cell repair mechanism that failed at extremely high temperatures [21], [80].

7.2.2 Protein secondary structure

The amide I band, observed between ~1700-1600 cm^{-1} in the protein infrared spectra, contains important information about how proteins within a sample are folded. This information proved to be significant for interpretation of *Symbiodinium* sp. response to environmental stress. Secondary structure differences were first noted in Chapter 3 for cells grown under normal light and temperature conditions. Second derivatives revealed clade A contained a higher α-helix structure, whereas clade F displayed a higher degree of β-sheet structure. Given the difference in tolerance between these two clades, it was proposed that the increase in β-structural content was associated with protection against environmental stress.

In Chapter 4 this proposal was further investigated by looking at protein secondary structural changes in the clades of *Symbiodinium* exposed to mild environmental stress. In general, under light and temperature changes, β-sheet secondary structure increased over time. Under elevated irradiance, clade A showed no changes in structure and this was the only exception observed. The degrees of change in β-sheet structure differed between the clades, with clade F showing the highest increase under a combination of elevated light with temperature.

The extreme temperature conditions that cells were subjected to for the study discussed in Chapter 5, indicated that *Symbiodinium* sp health is somewhat dependent on protein secondary structure. PLS models built for clade A to predict maximum quantum yield of PSII using FTIR spectra, showed a direct correlation between F_v/F_m and protein secondary structure. As temperature was increased, the α-helix protein content

decreased and the β-sheet increased. A similar reversion back to initial values as observed for lipid structure (see previous section) was also shown for protein secondary structure at 34 ^{o}C. This reversion corresponded with a dramatic decline in maximum quantum yield of PSII.

FTIR spectroscopy chemical images presented in Chapter 6 revealed that, although there was a high degree of variation and clade A was not able to be assessed, α-helix and β-sheet protein structures were localised differently within the cells. It should be noted here that these results were inconclusive due to light microscopy limitations.

7.2.3 Significance in relation to photosynthetic health and repair

These previous observations indicated that lipid and protein secondary structure were involved in a repair mechanism in the cells. A correlation between F_v/F_m and structural parameters was also evident suggesting that the protein and lipid signal observed in FTIR spectra was obtained largely from chloroplast macromolecular content.

A previous analysis of protein crystallographic structures of the photosynthetic complexes [35], [36] led to the proposal made in Chapter 5 that the change in β-sheet protein structure was related to the protein subunit, PsbO. This subunit is largely responsible for stabilising the manganese complex, which is considered to be a potential initial site for damage to the thylakoid membranes [21]. Changes of this nature have been noted in a study analysing zooxanthellae *in hospite* and when expelled from the host organism [138]. The recently expelled symbionts consistently displayed a decreased maximum quantum yield of PSII. This drop in health was accompanied by a decrease in protein subunits and a decrease in active PSII complexes. All of these could be contributing to the changes in protein structure described in the previous chapters of this thesis.

Changes in lipid saturation and branching were also found to be specifically correlated to PSII repair. Previous research has suggested that lipid saturation plays a role in the repair of the D1 protein within the PSII complex and it is likely that this is what is observed in the results presented here [142]. It was also proposed that the structural differences observed were a result of changes in the lipid bilayer making up the thylakoid membranes. Further research is needed, specifically isolation of the thylakoid membranes, to clarify the mechanisms of these structural changes.

7.2.4 Significance in relation to field samples

The goal of this project was to establish a baseline for the analysis of *Symbiodinium* sp. from a macromolecular perspective. Using chemometric modelling, it is possible to build a database of the macromolecular content in all known species of the algal symbiont and how they respond to changes in climate. Since this was the beginning of these efforts, the samples analysed were exclusively grown in laboratory conditions. The benefits of this was to strictly control the nutrients received and used by the cultures so that all changes observed were in relation to induced climate fluctuations.

A significant drawback of this approach, however, is that symbionts grown in culture conditions in a laboratory have been shown to be very different to endosymbiotic *Symbiodinium* sp. isolated from their hosts. Pasaribu et al showed that the protein content of freshly isolated *Symbiodinium* was different to those grown in culture [140]. It would therefore be vital and of significant interest to investigate the protein structural changes occurring *in hospite*. Of particular note is a synchrotron-FTIR microscopy study by Peng et al in 2012 showed that macromolecular content differed significantly between endosymbiotic and cultured or “free-living” *Symbiodinium* [143]. This

research, however, may be affected by the use of transflectance slides, since it has been shown to cause interference in FTIR spectra [144].

As Klueter et al note in their metabolomics study, it is important to understand the metabolic profiles of *Symbiodinium* under strictly controlled conditions before moving onto the highly variable free-living and endosymbiotic, isolated samples [51]. However, this is an avenue of research that greatly needs to be conducted as an understanding of the algal symbionts' response to climate variability in the field would be of great value.

7.3 Macromolecular content and energy storage

Recent analyses of the macromolecular content of different clades of *Symbiodinium* sp. have revealed a number of differences. These can be seen as differences in compounds present, concentrations of compounds present and how these compounds change under environmental stress. FTIR spectroscopic analysis of the two clades analysed throughout this thesis revealed a number of changes occurring. Initial assessment of the macromolecular content of clades A and F in Chapter 3, revealed that there was no statistically significant difference in total content in cell grown under normal conditions. However, once mild environmental stress was introduced, the cells began to redistribute macromolecular content in response differences in temperature and irradiance.

Chapter 4 showed that the clades of *Symbiodinium* sp. increased lipid content in response to elevated light, and decreased in response to elevated temperature. Carbohydrate content for both clades decreased under elevated irradiance and increased when exposed to elevated temperature. These responses were correlated to previous research that reported clades of *Symbiodinium* sp. exhibited differences in energy

storage strategies. While both clades analysed in this thesis exhibited a similar response under mild stress, they appeared to consume lipid and store carbohydrates when exposed to high temperatures, and *vice versa* for elevated irradiance.

This response was further investigated under bleaching conditions in Chapter 5. Clade F carbohydrate content was shown to follow the trend noted in Chapter 4. Overall, these cells consumed lipid and stored carbohydrates under elevated temperature. Chemometric models indicated that the peak at ~1150 cm^{-1} often attributed to cellulose, contributes to the variation of factors used to build models. Interestingly, clade A did not exhibit any differences in carbohydrate content and the region between 1150-950 cm^{-1} was not shown to contribute at all to the chemometric models used to describe the macromolecular changes occurring as the temperature was gradually increased. The environmental conditions were clearly unfavourable for this clade and so it is possible that the cells were distributing energy towards the repair mechanism as discussed in the previous section.

Chemical images shown in Chapter 6 revealed interesting information about the spatial distribution of carbohydrates and lipids. The maps built using the 1020 cm^{-1} band, showed that carbohydrate content was generally evenly distributed across the cell, including the cellulose content at ~1150 cm^{-1}. Lipid content, however, was found to be generally localised to specific areas within the cells.

7.4 Summary of key findings

- More thermally tolerant clade F cells changed macromolecular content more when subjected to mild environmental stress than clade A. However, the reverse was found under bleaching conditions.

- Under normal growth conditions, protein and lipid structure differed between clades of *Symbiodinium* sp.
    - α-helix content was higher in the less tolerant clade A, while β-sheet content was higher in the more tolerant clade F
    - Clade A contained more saturated lipids than clade F
- Differences in protein and lipid structure were linked to maximum quantum yield of PSII for the less tolerant clade A.
    - This indicated change in thylakoid membrane structure occurs under extreme stress and decreased photosynthetic function
- The more tolerant clade F also exhibited an increase in β-sheet protein secondary structure without a corresponding decrease in maximum quantum yield.
    - Therefore, the change in thylakoid membrane structure is a pre-emptive measure and possibly related to repair processes.
- Clades of *Symbiodinium* store and use energy in different ways under changes in environmental conditions
    - Under elevated light, lipid is stored and carbohydrate consumed
    - Under elevated temperature, lipid is consumed and carbohydrate is stored
- Macromolecular compound groups (protein, lipid, carbohydrate and phosphorylated compounds) are distributed differently across *Symbiodinium* sp. cells.

7.5 Future research

The results discussed have produced a number of significant conclusions and some interesting areas for further investigation. Studies of macromolecular content changes within *Symbiodinium* clades often include zooxanthellae isolated from a host organism [52], [59]. It has been found that the biochemistry of cultured and *in hospite* *Symbiodinium* displays some differences largely due to the presence of the host nutrient exchange [59], [143]. However, as noted in Chapter 4, the biochemistry of the symbiont alone is incredibly complex. In order to gain a proper understanding of the macromolecular response to elevated stress factors, it is vital to control as many variables as possible. Given that a difference in external nutrient availability can change the macromolecular content, laboratory cultures provide this level of control. However, since the effects of temperature and irradiance increases have been investigated, it would be a logical next step to look at how these environmental factors are mitigated or antagonised by nutrient levels. It would also be of use to investigate the effect of heterotrophic feeding of the host as an increase in this feeding can negate coral bleaching [30].

An important measure of cellular energy usage is the rate of growth within a culture. As noted in Chapters 3 and 4, the cells analysed here displayed a high level of aggregation. This was seen to increase, the longer the cells were exposed to environmental stress. A reliable method for accurately counting cell suspension in *Symbiodinium* sp. is yet to be determined, however, the parameter would enable further analysis of energy usage within the sample sets presented here.

Measurements reported throughout this thesis were taken within the exponential phase of growth of the cells (~21 days). This meant that the cells were utilising energy in a

very different way to, say, those in the stationary phase of growth. This would have a significant effect on macromolecular content. It would therefore be important to analyse the response of these cells to similar environmental stress factors, but in the initial or stationary phases. This would ensure a comprehensive map of macromolecular change is developed.

The use of F/2 media is well documented in laboratory studies of microalgal cultures [51], [52], [133]. However, this media is replete with nutrients. Since corals are found in oligotrophic waters, this is generally not a good representation of the conditions in the field. Further research is therefore needed to determine the effect of different nutrient conditions on the response of these cells to temperature and light.

Exposure to extreme temperatures, as analysed in Chapter 5, revealed an interesting response in the less tolerant species of *Symbiodinium*. Clades of *Symbiodinium* have been shown to have different thylakoid membrane melt temperatures [53]. Since the more tolerant species did not display as significant a decrease in F_v/F_m it can be assumed that the temperature at which these cells were damaged was not reached. It therefore remains unknown as to whether the repair mechanism observed for clade A was universal or species-specific. Further analysis of multiple clades allowed to reach their thermal limits, would clarify this information.

Chapter 5 highlighted the need for isolation and analysis of cellular components within *Symbiodinium* sp. cells. As noted previously, the limitation for most metabolomics studies is that the techniques can only measure what macromolecular compounds are present and in what quantities. The locations in which these are found within the cells remains largely elusive using these methods alone. Various isolation protocols are available for extracting thylakoid membranes. Given the clear correlation between

maximum quantum yield of PSII and the FTIR spectra found in Chapter 5, isolation and analysis of the thylakoid membranes would be of particular interest.

The chemical images analysed in Chapter 6 highlighted a number of places for further study. The coupling of the laboratory FTIR spectrometer with the added power of synchrotron radiation significantly increased the spatial resolution, but it is clear that this increase was not enough. TEM images of cellular components within the cells illustrate the kind of resolution required [25], [26], [140], [141]. New techniques in development may provide the solution to this problem, allowing macromolecular component analysis at the nano-scale [139].

While FTIR spectroscopy provides a comprehensive macromolecular snapshot of the biochemistry within the *Symbiodinium* sp. cells, the complementary information provided by another vibrational spectroscopy technique would be invaluable. Raman spectroscopy exploits polarizability of bonds rather than polarity. It is therefore considered to provide complementary information to FTIR spectroscopy. It has specifically been used to analyse pigments such as β-carotene and chlorophyll in algae [145], [146]. However, Raman spectroscopy is highly susceptible to auto-fluorescence and chlorophyll in particular is known to interfere with Raman spectra. Use of a specialised near-infrared laser is necessary for analysis of these organisms. The combination of these two vibrational spectroscopic methods, along with sophisticated chemometric analysis of the data, would provide a complementary map of the macromolecular content of the cells.

This thesis aimed to investigate the function of two different types of *Symbiodinium* sp by mapping the macromolecular content of the cells using FTIR spectroscopy. Through a study of the response of these cells to differing levels of irradiance and temperature

stress, a number of vital observations have been presented and discussed. This will add to the overall understanding of the function of the coral symbiosis which will, in turn, bring us one step closer to saving these important ecosystems.

References

[1] J. M. Lough and M. J. van Oppen, “Introduction: coral bleaching - patterns, processes, causes and consequences,” in *Coral Bleaching: Patterns, Processes, Causes and Consequences*, M. J. H. van Oppen and J. M. Lough, Eds. Springer Berlin / Heidelberg, 2009, pp. 1–6.

[2] O. Hoegh-Guldberg, “Climate change and coral reefs: Trojan horse or false prophecy,” *Coral Reefs*, vol. 28, pp. 569–575, 2009.

[3] D. Allemand, C. Ferrier-Pagès, P. Furla, F. Houlbrèque, S. Puverel, S. Reynaud, É. Tambutté, S. Tambutté, and D. Zoccola, “Biomineralisation in reef-building corals: from molecular mechanisms to environmental control,” *Comptes Rendus Palevol*, vol. 3, no. 6–7, pp. 453–467, 2004.

[4] O. Hoegh-Guldberg, “Climate change, coral bleaching and the future of the world’s coral reefs,” *Mar. Freshw. Res.*, vol. 50, pp. 839–866, 1999.

[5] D. W. Souter and O. Linden, “The health and future of coral reef systems,” *Ocean Coast. Manag.*, vol. 43, pp. 657–688, 2000.

[6] G. De’ath, K. E. Fabricius, H. Sweatman, and M. Puotinen, “The 27–year decline of coral cover on the Great Barrier Reef and its causes,” *Proc. Natl. Acad. Sci.*, vol. 109, no. 44, pp. 17995–17999, 2012.

[7] M. P. Lesser, “Experimental biology of coral reef ecosystems,” *J. Exp. Mar. Bio. Ecol.*, vol. 300, no. 1–2, pp. 217–252, 2004.

[8] M. S. M. Gustafsson, M. E. Baird, and P. J. Ralph, “The interchangeability of autotrophic and heterotrophic nitrogen sources in Scleractinian coral symbiotic relationships: A numerical study,” *Ecol. Modell.*, vol. 250, pp. 183–194, 2013.

[9] M. P. Lesser, “Coral bleaching: causes and mechanisms,” in *Coral Reefs: An Ecosystem in Transition SE - 23*, Z. Dubinsky and N. Stambler, Eds. Springer Netherlands, 2011, pp. 405–419.

[10] E. A. Titlyanov and T. V Titlyanova, “Reef-Building Corals—Symbiotic Autotrophic Organisms: 1. General Structure, Feeding Pattern, and Light-Dependent Distribution in the Shelf,” *Russ. J. Mar. Biol.*, vol. 28, pp. S1–S15, 2002.

[11] E. Rosenberg, O. Koren, L. Reshef, R. Efrony, and I. Zilber-Rosenberg, “The role of microorganisms in coral health, disease and evolution,” *Nat. Rev. Microbiol.*, vol. 5, pp. 355–362, 2007.

[12] S. K. Davy, D. Allemand, and V. M. Weis, “Cell biology of cnidarian-dinoflagellate symbiosis.,” *Microbiol. Mol. Biol. Rev.*, vol. 76, no. 2, pp. 229–261, 2012.

[13] V. M. Weis, “Cellular mechanisms of Cnidarian bleaching: stress causes the collapse of symbiosis.,” *J. Exp. Biol.*, vol. 211, no. 19, pp. 3059–3066, 2008.

[14] E. A. Titlyanov and T. V Titlyanova, “Reef-Building Corals—Symbiotic Autotrophic Organisms: 2. Pathways and Mechanisms of Adaptation to Light,” *Russ. J. Mar. Biol.*, vol. 28, pp. S16–S31, 2002.

[15] L. Muscatine, J. W. Porter, and I. R. Kaplan, “Resource partitioning by reef corals as determined from stable isotope composition,” *Mar. Biol.*, vol. 100, no. 2, pp. 185–193, 1989.

[16] R. Grover, D. Allemand, and C. Ferrier-page, “Nitrate uptake in the scleractinian coral Stylophora pistillata,” vol. 48, no. 6, pp. 2266–2274, 2003.

[17] R. Grover, J.-F. Maguer, D. Allemand, and C. Ferrier-Pagès, “Uptake of dissolved free amino acids by the scleractinian coral Stylophora pistillata.,” *J. Exp. Biol.*, vol. 211, no. 6, pp. 860–865, 2008.

[18] R. Grover, J.-F. Maguer, D. Allemand, and C. Ferrier-Pagès, “Urea uptake by the scleractinian coral Stylophora pistillata,” *J. Exp. Mar. Bio. Ecol.*, vol. 332, no. 2, pp. 216–225, 2006.

[19] M. P. Lesser, “Using energetic budgets to assess the effects of environmental stress on corals: are we measuring the right things?,” *Coral Reefs*, vol. 32, no. 1, pp. 25–33, 2012.

[20] B. R. Gordon and W. Leggat, “Symbiodinium - Invertebrate symbioses and the role of metabolomics,” *Mar. Drugs*, vol. 8, no. 10, pp. 2546–2568, 2010.

[21] S. Takahashi and M. R. Badger, “Photoprotection in plants: A new light on photosystem II damage,” *Trends Plant Sci.*, vol. 16, no. 1, pp. 53–60, 2011.

[22] T. D. Ainsworth, O. Hoegh-Guldberg, S. F. Heron, W. J. Skirving, and W. Leggat, “Early cellular changes are indicators of pre-bleaching thermal stress in the coral host,” *J. Exp. Mar. Bio. Ecol.*, vol. 364, no. 2, pp. 63–71, 2008.

[23] R. Hill and S. Takahashi, “Photosystem II recovery in the presence and absence of chloroplast protein repair in the symbionts of corals exposed to bleaching conditions,” *Coral Reefs*, vol. 33, no. 4, pp. 1101–1111, 2014.

[24] N. N. Rosic, M. Pernice, S. Dove, S. Dunn, and O. Hoegh-Guldberg, “Gene expression profiles of cytosolic heat shock proteins Hsp70 and Hsp90 from symbiotic dinoflagellates in response to thermal stress: possible implications for coral bleaching.,” *Cell Stress Chaperones*, vol. 16, no. 1, pp. 69–80, 2011.

[25] M. Pernice, A. Meibom, A. Van Den Heuvel, C. Kopp, I. Domart-Coulon, O. Hoegh-Guldberg, and S. Dove, “A single-cell view of ammonium assimilation in coral–dinoflagellate symbiosis,” *ISME J.*, vol. 6, no. 7, pp. 1314–1324, 2012.

[26] M. Pernice, S. R. Dunn, L. Tonk, S. Dove, I. Domart-Coulon, P. Hoppe, A. Schintlmeister, M. Wagner, and A. Meibom, “A nanosims study of dinoflagellate functional diversity in reef-building corals.,” *Environ. Microbiol.*, vol. 17, no. 10, pp. 1–29, 2014.

[27] K. R. N. Anthony, D. I. Kline, G. Diaz-Pulido, S. Dove, and O. Hoegh-Guldberg, “Ocean acidification causes bleaching and productivity loss in coral reef builders,” *Proc. Natl. Acad. Sci.*, vol. 105, no. 45, pp. 17442–17446, 2008.

[28] S. Krief, E. J. Hendy, M. Fine, R. Yam, A. Meibom, G. L. Foster, and A. Shemesh, “Physiological and isotopic responses of scleractinian corals to ocean acidification,” *Geochim. Cosmochim. Acta*, vol. 74, no. 17, pp. 4988–5001, 2010.

[29] O. Hoegh-Guldberg and G. J. Smith, “The effect of sudden changes in temperature, light and salinity on the population density and export of zooxanthellae from the reef corals Stylophora pistillata Esper and Seriatopora hystrix Dana,” *J. Exp. Mar. Bio. Ecol.*, vol. 129, no. 3, pp. 279–303, 1989.

[30] A. H. Baird, R. Bhagooli, P. J. Ralph, and S. Takahashi, “Coral bleaching: the role of the host,” *Trends Ecol. Evol.*, vol. 24, no. 1, pp. 16–20, 2008.

[31] A. Mellis, “Photosystem-II damage and repair cycle in chloroplasts: What modulates the rate of photodamage in vivo?,” *Trends Plant Sci.*, vol. 4, no. 4, pp. 130–135, 1999.

[32] E.-M. Aro, “Dynamics of photosystem II: a proteomic approach to thylakoid protein complexes,” *J. Exp. Bot.*, vol. 56, no. 411, pp. 347–356, 2004.

[33] E. Tyystjärvi, “Photoinhibition of Photosystem II and photodamage of the oxygen evolving manganese cluster,” *Coord. Chem. Rev.*, vol. 252, no. 3–4, pp. 361–376, 2008.

[34] Y. Kato and W. Sakamoto, “Protein Quality Control in Chloroplasts: A Current Model of D1 Protein Degradation in the Photosystem II Repair Cycle,” *J. Biochem.*, vol. 146, no. 4, pp. 463–469, 2009.

[35] A. Zouni, H. T. Witt, J. Kern, P. Fromme, N. Krauss, W. Saenger, and P. Orth, “Crystal structure of photosystem II from Synechococcus elongatus at 3.8 A resolution.,” *Nature*, vol. 409, no. 1988, pp. 739–743, 2001.

[36] K. Ferreira, T. Iverson, K. Maghlaoui, J. Barber, and S. Iwata, “Architecture of the photosynthetic oxygen-evolving center,” *Nature*, vol. 303, pp. 1831–1838, 2004.

[37] S. Järvi, M. Suorsa, and E.-M. Aro, “Photosystem II repair in plant chloroplasts — Regulation, assisting proteins and shared components with photosystem II biogenesis,” *Biochim. Biophys. Acta - Bioenerg.*, vol. 1847, no. 9, pp. 900–909, 2015.

[38] Y. Kato and W. Sakamoto, “Phosphorylation of photosystem II core proteins prevents undesirable cleavage of D1 and contributes to the fine-tuned repair of photosystem II,” *Plant J.*, vol. 79, no. 2, pp. 312–321, 2014.

[39] M. X. Weber and M. Medina, “The role of microalgal symbionts (Symbiodinium) in holobiont physiology,” in *Genomic Insights into the Biology of Algae*, 1st ed., G. Piganeau, Ed. Elsevier Ltd: Academic Press, 2012, pp. 119–140.

[40] H. D. Freudenthal, “Symbiodinium gen. nov. and Symbiodinium microadriaticum sp. nov., a Zooxanthella: Taxonomy, Life Cycle, and

Morphology.*," *J. Protozool.*, vol. 9, no. 1, pp. 45–52, 1962.

[41] A. C. Baker, "Flexibility and specificity in coral-algal symbiosis: diversity, ecology, and biogeography of Symbiodinium," *Annu. Rev. Ecol. Evol. Syst.*, vol. 34, no. 1, pp. 661–689, 2003.

[42] F. Gómez, "A quantitative review of the lifestyle, habitat and trophic diversity of dinoflagellates (Dinoflagellata, Alveolata)," *Syst. Biodivers.*, vol. 10, no. 3, pp. 267–275, 2012.

[43] R. K. Trench, "The Physiology and Biochemistry of Zooxanthellae Symbiotic with Marine Coelenterates. I. The Assimilation of Photosynthetic Products of Zooxanthellae by Two Marine Coelenterates," *Proc. R. Soc. London B Biol. Sci.*, vol. 177, no. 1047, pp. 225–235, 1971.

[44] X. Pochon and R. D. Gates, "A new Symbiodinium clade (Dinophyceae) from soritid foraminifera in Hawai'i," *Mol. Phylogenet. Evol.*, vol. 56, no. 1, pp. 492–497, 2010.

[45] M. A. Coffroth and S. R. Santos, "Genetic diversity of symbiotic dinoflagellates in the genus Symbiodinium," *Protist*, vol. 156, no. 1, pp. 19–34, 2005.

[46] D. J. Suggett, S. Goyen, C. Evenhuis, D. T. Pettay, M. E. Warner, and P. J. Ralph, "Functional diversity of photobiological traits within the genus Symbiodinium appears to be governed by the interaction of cell size with cladal designation," *New Phytol.*, vol. 208, pp. 370–381, 2015.

[47] M. J. H. van Oppen, F. P. Palstra, a M. Piquet, and D. J. Miller, "Patterns of coral-dinoflagellate associations in Acropora: significance of local availability and physiology of Symbiodinium strains and host-symbiont selectivity.," *Proc. Biol. Sci.*, vol. 268, no. 1478, pp. 1759–1767, 2001.

[48] M. J. H. van Oppen, A. C. Baker, M. A. Coffroth, and B. L. Willis, "Bleaching resistance and the role of algal endosymbionts," in *Coral Bleaching: Patterns, Processes, Causes and Consequences*, M. J. H. Van Oppen and J. M. Lough, Eds. Springer Berlin / Heidelberg, 2009, pp. 83–103.

[49] L. Tonk, E. M. Sampayo, T. C. LaJeunesse, V. Schrameyer, and O. Hoegh-Guldberg, "Symbiodinium (Dinophyceae) diversity in reef-invertebrates along

an offshore to inshore reef gradient near Lizard Island, Great Barrier Reef," *J. Phycol.*, vol. 50, no. 3, pp. 552–563, 2014.

[50] R. Iglesias-Prieto, V. H. Beltran, T. C. LaJeunesse, H. Reyes-Bonilla, and P. E. Thome, "Different algal symbionts explain the vertical distribution of dominant reef corals in the eastern Pacific," *Proc. R. Soc. B Biol. Sci.*, vol. 271, no. 1549, pp. 1757–1763, 2004.

[51] A. Klueter, J. Crandall, F. Archer, M. Teece, and M. Coffroth, "Taxonomic and Environmental Variation of Metabolite Profiles in Marine Dinoflagellates of the Genus Symbiodinium," *Metabolites*, vol. 5, no. 1, pp. 74–99, 2015.

[52] L. Buxton, S. Takahashi, R. Hill, and P. J. Ralph, "Variability in the Primary Site of Photosynthetic Damage in Symbiodinium Sp. (Dinophyceae) Exposed To Thermal Stress," *J. Phycol.*, vol. 48, no. 1, pp. 117–126, 2012.

[53] E. Díaz-Almeyda, P. E. Thomé, M. El Hafidi, and R. Iglesias-Prieto, "Differential stability of photosynthetic membranes and fatty acid composition at elevated temperature in Symbiodinium," *Coral Reefs*, vol. 30, pp. 217–225, 2011.

[54] R. Hill, U. Schreiber, R. Gademann, A. W. D. Larkum, M. Kuhl, and P. J. Ralph, "Spatial Heterogeneity of photosynthesis and the effect of temperature-induced bleaching conditions in three species of corals," *Mar. Biol.*, vol. 144, pp. 633–640, 2004.

[55] D. Tchernov, M. Y. Gorbunov, C. De Vargas, S. N. Yadav, A. J. Milligan, M. Ha, and P. G. Falkowski, "Membrane lipids of symbiotic algae are diagnostic of sensitivity to thermal bleaching in corals," vol. 101, no. 37, pp. 13531–13535, 2004.

[56] T. F. Cooper, M. Lai, K. E. Ulstrup, S. M. Saunders, G. R. Flematti, B. Radford, and M. J. H. van Oppen, "Symbiodinium genotypic and environmental controls on lipids in reef building corals," *PLoS One*, vol. 6, no. 5, p. e20434, 2011.

[57] A. M. Jones and R. Berkelmans, "Tradeoffs to Thermal Acclimation : Energetics and Reproduction of a Reef Coral with Heat Tolerant Symbiodinium Type-D," *J. Mar. Biol.*, vol. 2011, 2011.

[58] D. M. Baker, J. P. Andras, A. G. Jordán-Garza, and M. L. Fogel, “Nitrate competition in a coral symbiosis varies with temperature among Symbiodinium clades.,” *ISME J.*, vol. 7, no. 6, pp. 1248–1251, 2013.

[59] L. H. Wang, H. K. Chen, C. S. Jhu, J. O. Cheng, L. S. Fang, and C. S. Chen, “Different strategies of energy storage in cultured and freshly isolated Symbiodinium sp.,” *J. Phycol.*, 2015.

[60] M. R. Viant and U. Sommer, “Mass spectrometry based environmental metabolomics: A primer and review,” *Metabolomics*, vol. 9, pp. 144–158, 2013.

[61] B. Gordon and W. Leggat, “Extraction protocol for non-targeted NMR and LC-MS metabolomics-based analysis of hard coral and their algal symbionts,” in *Metabollomics tools for natural product discovery: Mehods and protocols*, R. Ute, Ed. New York Humana Press, 2013, pp. 129–147.

[62] K. Stehfest, J. Toepel, and C. Wilhelm, “The application of micro-FTIR spectroscopy to analyze nutrient stress-related changes in biomass composition of phytoplankton algae,” *Plant Physiol. Biochem.*, vol. 43, no. 7, pp. 717–726, 2005.

[63] C. Jebsen, A. Norici, H. Wagner, M. Palmucci, M. Giordano, and C. Wilhelm, “FTIR spectra of algal species can be used as physiological fingerprints to assess their actual growth potential,” *Physiol. Plant.*, vol. 146, no. 4, pp. 427–438, 2012.

[64] O. Sackett, L. Armand, J. Beardall, R. Hill, M. Doblin, C. Connelly, J. Howes, B. Stuart, P. Ralph, and P. Heraud, “Taxon-specific responses of Southern Ocean diatoms to Fe enrichment revealed by synchrotron radiation FTIR microspectroscopy,” *Biogeosciences Discuss.*, vol. 11, no. 5, pp. 7327–7357, 2014.

[65] O. Sackett, K. Petrou, B. Reedy, A. De Grazia, R. Hill, M. Doblin, J. Beardall, P. Ralph, and P. Heraud, “Phenotypic Plasticity of Southern Ocean Diatoms: Key to Success in the Sea Ice Habitat?,” *PLoS One*, vol. 8, no. 11, p. e81185, 2013.

[66] D. Naumann, H. Helm, and H. Labischinski, “Microbiological characterisations by FT-IR spectroscopy,” *Nature*, vol. 351, pp. 81–84, 1991.

[67] A. P. Dean, D. C. Sigee, B. Estrada, and J. K. Pittman, “Using FTIR spectroscopy for rapid determination of lipid accumulation in response to nitrogen limitation in freshwater microalgae.,” *Bioresour. Technol.*, vol. 101, no. 12, pp. 4499–4507, 2010.

[68] H. Wagner, A. Jungandreas, A. Fanesi, and C. Wilhelm, “Surveillance of C-allocation in microalgal cells.,” *Metabolites*, vol. 4, no. 2, pp. 453–64, 2014.

[69] M. Igisu, Y. Ueno, M. Shimojima, S. Nakashima, S. M. Awramik, H. Ohta, and S. Maruyama, “Micro-FTIR spectroscopic signatures of Bacterial lipids in Proterozoic microfossils,” *Precambrian Res.*, vol. 173, no. 1–4, pp. 19–26, 2009.

[70] A. Domenighini and M. Giordano, “Fourier transform infrared spectroscopy of microalgae as a novel tool for biodiversity studies, species ideantification, and the assessment of water quality,” *J. Phycol.*, vol. 45, pp. 522–531, 2009.

[71] A. Barth, “Infrared spectroscopy of proteins,” *Biochim. Biophys. Acta*, vol. 1767, pp. 1073–1101, 2007.

[72] P. Heraud, S. Stojkovic, J. Beardall, D. McNaughton, and B. R. Wood, “Intercolonia variability in macromolecular composition in P-starved and P-replete Scenedesmus populations revealed by infrared microscpectroscopy,” *J. Phycol.*, vol. 44, no. 5, pp. 1335–1339, 2008.

[73] M. Kansiz, P. Heraud, B. R. Wood, F. Burden, J. Beardall, and D. McNaughton, “Fourier transform infrared microspectroscopy and chemometrics as a tool for the discrimination of cyanobacterial strains,” *Phytochemistry*, vol. 52, pp. 407–417, 1999.

[74] M. Giordano, M. Kansiz, P. Heraud, J. Beardall, B. Wood, and D. McNaughten, “Fourier transform infrared spectroscopy as a novel tool to investigate changes in intracellular macromolecular pools in the marine microalga Chaetoceros muellerii (Bacillariophyceae),” *J. Phycol.*, vol. 37, pp. 271–279, 2001.

[75] C. J. Hirschmugl, Z. El Bayarri, M. Bunta, J. B. Holt, and M. Giordano, “Analysis of the nutritional status of algae by Fourier transform infrared chemical imaging,” *Infrared Phys. Technol.*, vol. 49, no. 1–2, pp. 57–63, 2006.

[76] P. Heraud, B. R. Wood, M. J. Tobin, J. Beardall, and D. McNaughton, “Mapping

of nutrient-induced biochemical changes in living algal cells using synchrotron infrared microspectroscopy," *FEMS Microbiol. Lett.*, vol. 249, no. 2, pp. 219–225, 2005.

[77] E. Levenson, P. Lerch, and M. C. Martin, "Infrared imaging: Synchrotrons vs. arrays, resolution vs. speed," *Infrared Phys. Technol.*, vol. 49, no. 1–2, pp. 45–52, 2006.

[78] A. Imbs, D. Demidkova, Y. Latypov, and L. Pham, "Application of Fatty Acids for Chemotaxonomy of Reef-Building Corals," *Lipids*, vol. 42, no. 11, pp. 1035–1046, 2007.

[79] R. R. L. Guillard and J. H. Ryther, "Studies of Marine Planktonic Diatoms: I. Cyclotella nan hustedt, and Detonula confervacea (cleve) gran.," *Can. J. Microbiol.*, vol. 8, no. 2, pp. 229–239, Apr. 1962.

[80] R. Iglesias-Prieto, N. S. Govind, and R. K. Trench, "Apoprotein Composition and Spectroscopic Characterization of the Water-Soluble Peridinin-Chlorophyll a-Proteins from Three Symbiotic Dinoflagellates," *Proc. R. Soc. London. Ser. B Biol. Sci.*, vol. 246, no. 1317, pp. 275–283, 1991.

[81] J. Grdadolnik, "ATR-FTIR Spectroscopy: Its advantages and limitations," *Acta Chim. Slov.*, vol. 49, pp. 631–642, 2002.

[82] E. Staniszewska, K. Malek, and M. Baranska, "Rapid approach to analyze biochemical variation in rat organs by ATR FTIR spectroscopy," *Spectrochim. Acta - Part A Mol. Biomol. Spectrosc.*, vol. 118, pp. 981–986, 2014.

[83] H. Martens, J. P. Nielsen, and S. B. Engelsen, "Light scattering and light absorbance separated by extended multiplicative signal correction. Application to Near-infrared transmission analysis of powder mixtures," *Anal. Chem.*, vol. 75, no. 3, pp. 394–404, 2003.

[84] K. R. Bambery, B. R. Wood, and D. McNaughton, "Resonant Mie scattering (RMieS) correction applied to FTIR images of biological tissue samples," *Analyst*, vol. 137, no. 1, pp. 126–132, 2012.

[85] P. Bassan, A. Sachdeva, A. Kohler, C. Hughes, A. Henderson, J. Boyle, J. H. Shanks, M. Brown, N. W. Clarke, and P. Gardner, "FTIR microscopy of

biological cells and tissue: data analysis using resonant Mie scattering (RMieS) EMSC algorithm.," *Analyst*, vol. 137, no. 6, pp. 1370–1377, 2012.

[86] S. Takahashi, T. Nakamura, M. Sakamizu, R. van Woesik, and H. Yamasaki, "Repair machinery of symbiotic photosynthesis as the primary target of heat stress for reef-building corals," *Plant Cell Physiol.*, vol. 45, no. 2, pp. 255–521, 2004.

[87] R. Berkelmans and M. J. H. van Oppen, "The role of zooxanthellae in the thermal tolerance of corals: a 'nugget of hope' for coral reefs in an era of climate change," *Proc. R. Soc. B Biol. Sci.*, vol. 273, no. 1599, pp. 2305–2312, 2006.

[88] P. O. Souillac, C. R. Middaugh, and J. H. Rytting, "Investigation of protein/carbohydrate interactions in the dried state. 2. Diffuse reflectance FTIR studies," *Int. J. Pharm.*, vol. 235, no. 1–2, pp. 207–218, 2002.

[89] L. Pereira, A. M. Amado, A. T. Critchley, F. van de Velde, and P. J. a. Ribeiro-Claro, "Identification of selected seaweed polysaccharides (phycocolloids) by vibrational spectroscopy (FTIR-ATR and FT-Raman)," *Food Hydrocoll.*, vol. 23, no. 7, pp. 1903–1909, 2009.

[90] J. J. Mayers, K. J. Flynn, and R. J. Shields, "Bioresource Technology Rapid determination of bulk microalgal biochemical composition by Fourier-Transform Infrared spectroscopy," vol. 148, pp. 215–220, 2013.

[91] D. R. Whelan, K. R. Bambery, P. Heraud, M. J. Tobin, M. Diem, D. McNaughton, and B. R. Wood, "Monitoring the reversible B to A-like transition of DNA in eukaryotic cells using Fourier transform infrared spectroscopy," *Nucleic Acids Res.*, vol. 39, no. 13, pp. 5439–5448, 2011.

[92] K. R. N. Anthony, M. O. Hoogenboom, J. A. Maynard, A. G. Grottoli, and R. Middlebrook, "Energetics approach to predicting mortality risk from environmental stress: a case study of coral bleaching," *Funct. Ecol.*, vol. 23, no. 3, pp. 539–550, 2009.

[93] P. J. Edmunds and P. S. Davies, "Coral Reefs An energy budget for Porites porites (Scleractinia), growing in a stressed environment," *Coral Reefs*, vol. 8, pp. 37–43, 1989.

[94] R. Geider and J. La Roche, “Redfield revisited: variability of C:N:P in marine microalgae and its biochemical basis,” *Eur. J. Phycol.*, vol. 37, no. 1, pp. 1–17, 2002.

[95] K. R. Arrigo, “Marine microorganisms and global nutrient cycles,” *Nature*, vol. 437, pp. 349–355, 2005.

[96] S. J. Giovannoni and U. Stingl, “Molecular diversity and ecology of microbial plankton.,” *Nature*, vol. 437, no. 7057, pp. 343–8, 2005.

[97] J. Kong and S. Yu, “Fourier transform infrared spectroscopic analysis of protein secondary structures,” *Acta Biochim. Biophys. Sin. (Shanghai).*, vol. 39, no. 8, pp. 549–559, 2007.

[98] J. Cao, E. S. Ng, D. McNaughton, E. G. Stanley, A. G. Elefanty, M. J. Tobin, and P. Heraud, “Fourier transform infrared microspectroscopy reveals unique phenotypes for human embryonic and induced pluripotent stem cell lines and their progeny,” *J. Biophotonics*, vol. 7, no. 10, pp. 767–781, 2013.

[99] Z. Movasaghi, S. Rehman, and D. I. ur Rehman, “Fourier Transform Infrared (FTIR) Spectroscopy of Biological Tissues,” *Appl. Spectrosc. Rev.*, vol. 43, no. 2, pp. 134–179, 2008.

[100] J. N. Murdock and D. L. Wetzel, “FT-IR microspectroscopy enhances biological and ecological analysis of algae,” *Appl. Spectrosc. Rev.*, vol. 44, no. 4, pp. 335–361, 2009.

[101] S. Y. Oh, D. Il Yoo, Y. Shin, H. C. Kim, H. Y. Kim, Y. S. Chung, W. H. Park, and J. H. Youk, “Crystalline structure analysis of cellulose treated with sodium hydroxide and carbon dioxide by means of X-ray diffraction and FTIR spectroscopy,” *Carbohydr. Res.*, vol. 340, no. 15, pp. 2376–2391, 2005.

[102] D. A. Markell, R. K. Trench, and R. Iglesias-Prieto, “Macromolecules associated with the cell walls of symbiotic dinoflagellates,” *Symbiosis*, vol. 12, no. 1, pp. 19–31, 1992.

[103] T. S. Wakefield, M. A. Farmer, and S. C. Kempf, “Revised description of the fine structure of in situ ‘zooxanthellae’ genus Symbiodinium.,” *Biol. Bull.*, vol. 199, no. 1, pp. 76–84, 2000.

[104] L. Fujise, H. Yamashita, and K. Koike, “Application of calcofluor staining to identify motile and coccoid stages of Symbiodinium (Dinophyceae),” *Fish. Sci.*, vol. 80, no. 2, pp. 363–368, 2014.

[105] Y. Achituv, M. Ben-Zion, and L. Mizrahi, “Carbohydrate, lipid, and protein composition of zooxanthellae and animal fractions of the coral Pocillopora damicornis exposed to ammonium enrichment,” *Pacific Sci.*, vol. 48, no. 3, pp. 224–233, 1994.

[106] M. Rantalainen, O. Cloarec, J. K. Nicholson, E. Holmes, and J. Trygg, “OPLS discriminant analysis : combining the strengths of PLS-DA and SIMCA classification,” *J. Chemom.*, pp. 341–351, 2007.

[107] A. Barth, “The infrared absorption of amino acid side chains,” *Prog. Biophys. Mol. Biol.*, vol. 74, pp. 141–173, 2000.

[108] L. M. Miller, M. W. Bourassa, and R. J. Smith, “FTIR spectroscopic imaging of protein aggregation in living cells,” *Biochim. Biophys. Acta - Biomembr.*, vol. 1828, no. 10, pp. 2339–2346, 2013.

[109] J. M. Cardamone, “Investigating the microstructure of keratin extracted from wool: Peptide sequence (MALDI-TOF/TOF) and protein conformation (FTIR),” *J. Mol. Struct.*, vol. 969, no. 1–3, pp. 97–105, 2010.

[110] F. Bonnier, S. Rubin, L. Debelle, L. Ventéo, M. Pluot, B. Baehrel, M. Manfait, and G. D. Sockalingum, “FTIR protein secondary structure analysis of human ascending aortic tissues,” *J. Biophotonics*, vol. 1, no. 3, pp. 204–214, 2008.

[111] D. M. Byler and H. Susi, “Examination of the secondary structure of proteins by deconvolved FTIR spectra.,” *Biopolymers*, vol. 25, no. 3, pp. 469–487, 1986.

[112] Y. Yamamoto, “Quality control of photosystem II,” *Plant Cell Physiol.*, vol. 42, no. 2, pp. 121–128, 2001.

[113] K. R. N. Anthony, S. R. Connolly, and B. L. Willis, “Comparative analysis of energy allocation to tissue and skeletal growth in corals,” *Limnol. Oceanogr.*, vol. 47, no. 5, pp. 1417–1429, 2002.

[114] P. J. Edmunds, H. M. Putnam, R. M. Nisbet, and E. B. Muller, “Benchmarks in

organism performance and their use in comparative analyses.," *Oecologia*, vol. 167, no. 2, pp. 379–390, 2011.

[115] P. Heraud, E. S. Ng, S. Caine, Q. C. Yu, C. Hirst, R. Mayberry, A. Bruce, B. R. Wood, D. McNaughton, E. G. Stanley, and A. G. Elefanty, "Fourier transform infrared microspectroscopy identifies early lineage commitment in differentiating human embryonic stem cells," *Stem Cell Res.*, vol. 4, no. 2, pp. 140–147, 2010.

[116] J. Diaz, E. Ingall, C. Benitez-Nelson, D. Paterson, M. D. de Jonge, I. McNulty, and J. A. Brandes, "Marine Polyphosphate: A Key Player in Geologic Phosphorus Sequestration," *Science (80-.).*, vol. 320, no. 5876, pp. 652–655, 2008.

[117] O. Samek, A. Jonáš, Z. Pilát, P. Zemánek, L. Nedbal, J. Tříska, P. Kotas, and M. Trtílek, "Raman microspectroscopy of individual algal cells: sensing unsaturation of storage lipids in vivo," *Sensors*, vol. 10, no. 9, pp. 8635–8651, 2010.

[118] C. Nicolini, V. Erokhin, F. Antolini, P. Catasti, and P. Facci, "Thermal stability of protein secondary structure in Langmuir-Blodgett films," *Biochim. Biophys. Acta - Gen. Subj.*, vol. 1158, no. 3, pp. 273–278, 1993.

[119] A. Imbs, H. Luu, and L. Pham, "Intra- and interspecific variability of fatty acid composition of soft corals," *Russ. J. Mar. Biol.*, vol. 33, no. 1, pp. 67–70, 2007.

[120] B. Chen, D. Zhong, and A. Monteiro, "Comparative genomics and evolution of the HSP90 family of genes across all kingdoms of organisms.," *BMC Genomics*, vol. 7, no. 1, pp. 156–175, 2006.

[121] L. Pearl, C. Prodromou, and P. Workman, "The Hsp90 molecular chaperone: an open and shut case for treatment," *Biochem. J.*, vol. 410, pp. 439–453, 2008.

[122] J. Breton and E. Nabedryk, "Transmembrane orientation of α-helices and the organization of chlorophylls in photosynthetic pigment-protein complexes," *FEBS Lett.*, vol. 176, no. 2, pp. 355–359, 1984.

[123] E. Hofmann, P. M. Wrench, F. P. Sharples, R. G. Hiller, W. Welte, and K. Diederichs, "Structural basis of light harvesting by carotenoids: peridinin-

chlorophyll-protein from Amphidinium carterae," *Science (80-.).*, vol. 272, no. 5269, pp. 1788–1791, 1996.

[124] R. G. Hiller, A. M. Bardin, and E. Nabedryk, "The secondary structure content of pigment-protein complexes from the thylakoids of two chromophyte algae," *Biochim. Biophys. Acta - Bioenerg.*, vol. 894, no. 3, pp. 365–369, 1987.

[125] C. Büchel and G. Garab, "Molecular organisation of the chlorophyll a/c light-harvesting complex of Pleurochloris meiringensis (Xanthophyceae). Pigment binding and secondary structure of the protein," *J. Photochem. Photobiol. B Biol.*, vol. 42, no. 3, pp. 191–194, 1998.

[126] W. Z. He, W. R. Newell, P. I. Haris, D. Chapman, and J. Barber, "Protein secondary structure of the isolated photosystem II reaction center and conformational changes studied by Fourier transform infrared spectroscopy," *Biochemistry*, vol. 30, no. 18, pp. 4552–4559, 1991.

[127] S. Nahar, H. A. Tajmir-Riahi, and R. Carpentier, "A quantitative analysis of protein secondary structure of photosystem II particles and light-harvesting complex of chloroplast thylakoid membranes by FT-IR spectroscopy," *J. Mol. Struct.*, vol. 328, pp. 115–120, 1994.

[128] T. Schulte, S. Johanning, and E. Hofmann, "Structure and function of native and refolded peridinin-chlorophyll-proteins from dinoflagellates," *Eur. J. Cell Biol.*, vol. 89, no. 12, pp. 990–997, 2010.

[129] Y. Wu, D. A. Campbell, A. J. Irwin, D. J. Suggett, and Z. V Finkel, "Ocean acidification enhances the growth rate of larger diatoms," *Limnol. Oceanogr.*, vol. 59, no. 3, pp. 1027–1034, 2014.

[130] J. D. Leblond, M. Khadka, L. Duong, and J. L. Dahmen, "Squishy lipids: Temperature effects on the betaine and galactolipid profiles of a C18/C18 peridinin-containing dinoflagellate, Symbiodinium microadriaticum (Dinophyceae), isolated from the mangrove jellyfish, Cassiopea xamachana," *Phycol. Res.*, vol. 63, no. 3, pp. 219–230, 2015.

[131] Z. Dubinsky and P. Falkowski, "Light as a Source of Information and Energy in Zooxanthellate Corals," in *Coral Reefs: An Ecosystem in Transition*, Z.

Dubinsky and N. Stambler, Eds. Springer Netherlands, 2011, pp. 107–118.

[132] M. Tikkanen, N. R. Mekala, and E.-M. Aro, "Photosystem II photoinhibition-repair cycle protects Photosystem I from irreversible damage," *Biochim. Biophys. Acta - Bioenerg.*, vol. 1837, no. 1, pp. 210–215, 2014.

[133] R. Hill, K. E. Ulstrup, and P. J. Ralph, "Temperatrue induced changes in thylakoid membrane thermostability of cultured, freshly isolated and expelled zooxanthellae from scleractinian corals," vol. 85, no. 3, pp. 223–244, 2009.

[134] M. Tikkanen and E.-M. Aro, "Thylakoid protein phosphorylation in dynamic regulation of photosystem II in higher plants," *Biochim. Biophys. Acta*, vol. 1817, pp. 232–238, 2012.

[135] M. Tikkanen, M. Nurmi, S. Kangasjarvi, and E.-M. Aro, "Core protein phosphorylation facilitates the repair of photodamaged photosystem II at high light," *Biochim. Biophys. Acta*, vol. 1777, pp. 1432–1437, 2008.

[136] R. Hill, K. E. Ulstrup, and P. J. Ralph, "Temperature Induced Changes in Thylakoid Membrane Thermostability of Cultured, Freshly Isolated, and Expelled Zooxanthellae from Scleractinian Corals," *Bulletin of Marine Science*, vol. 85, no. 3. pp. 223–244.

[137] H. Popelkova and C. Yocum, "PsbO, the manganese-stabilizing protein: Analysis of the structure-function relations that provide insights into its role in photosystem II," *J. Photochem. Photobiol. BBiology*, vol. 104, pp. 179–190, 2011.

[138] J. Jeans, M. Szabó, D. a. Campbell, A. W. D. Larkum, P. J. Ralph, and R. Hill, "Thermal bleaching induced changes in photosystem II function not reflected by changes in photosystem II protein content of Stylophora pistillata," *Coral Reefs*, vol. 33, no. 1, pp. 131–139, 2014.

[139] H. A. Bechtel, E. A. Muller, R. L. Olmon, M. C. Martin, and M. B. Raschke, "Ultrabroadband infrared nanospectroscopic imaging," *Proc. Natl. Acad. Sci.*, vol. 111, no. 20, pp. 7191–7196, 2014.

[140] B. Pasaribu, L.-C. Weng, I.-P. Lin, E. Camargo, J. T. C. Tzen, C.-H. Tsai, S.-L. Ho, M.-R. Lin, L.-H. Wang, C.-S. Chen, and P.-L. Jiang, "Morphological

Variability and Distinct Protein Profiles of Cultured and Endosymbiotic Symbiodinium cells Isolated from Exaiptasia pulchella," *Sci. Rep.*, vol. 5, pp. 15353–15363, 2015.

[141] C. Kopp, M. Pernice, I. Domart-coulon, C. Djediat, J. E. Spangenberg, D. T. L. Alexander, M. Hignette, T. Meziane, and A. Meibom, "Highly Dynamic Cellular-Level Response of Symbiotic Coral to a Sudden Increase in Environmental Nitrogen," *MBio*, vol. 4, no. 3, pp. 1–9, 2013.

[142] E. Kanervo, Y. Tasaka, N. Murata, and E. M. Aro, "Membrane lipid unsaturation modulates processing of the photosystem II reaction-center protein D1 at low temperatures.," *Plant Physiol.*, vol. 114, no. 3, pp. 841–849, 1997.

[143] S. Peng, C. Chen, Y. Song, H. Huang, L. Fang, and Y. Lee, "Assessment of metabolic modulation in free-living versus endosymbiotic Symbiodinium using synchrotron radiation-based infrared microspectroscopy," no. November 2011, pp. 434–437, 2012.

[144] P. Bassan, J. Lee, A. Sachdeva, J. Pissardini, K. M. Dorling, J. S. Fletcher, A. Henderson, and P. Gardner, "The inherent problem of transflection-mode infrared spectroscopic microscopy and the ramifications for biomedical single point and imaging applications," *Analyst*, vol. 138, no. 1, pp. 144–157, 2013.

[145] M. Wagner, "Single-cell ecophysiology of microbes as revealed by Raman microspectroscopy or Secondary Ion Mass Spectrometry imaging," *Annu. Rev. Microbiol.*, vol. 63, pp. 411–429, 2009.

[146] A. Kudelski, "Analytical applications of Raman spectroscopy," *Talanta*, vol. 76, pp. 1–8, 2008.

Appendices

Appendix 1: Collated spectra analysed for Chapter 4

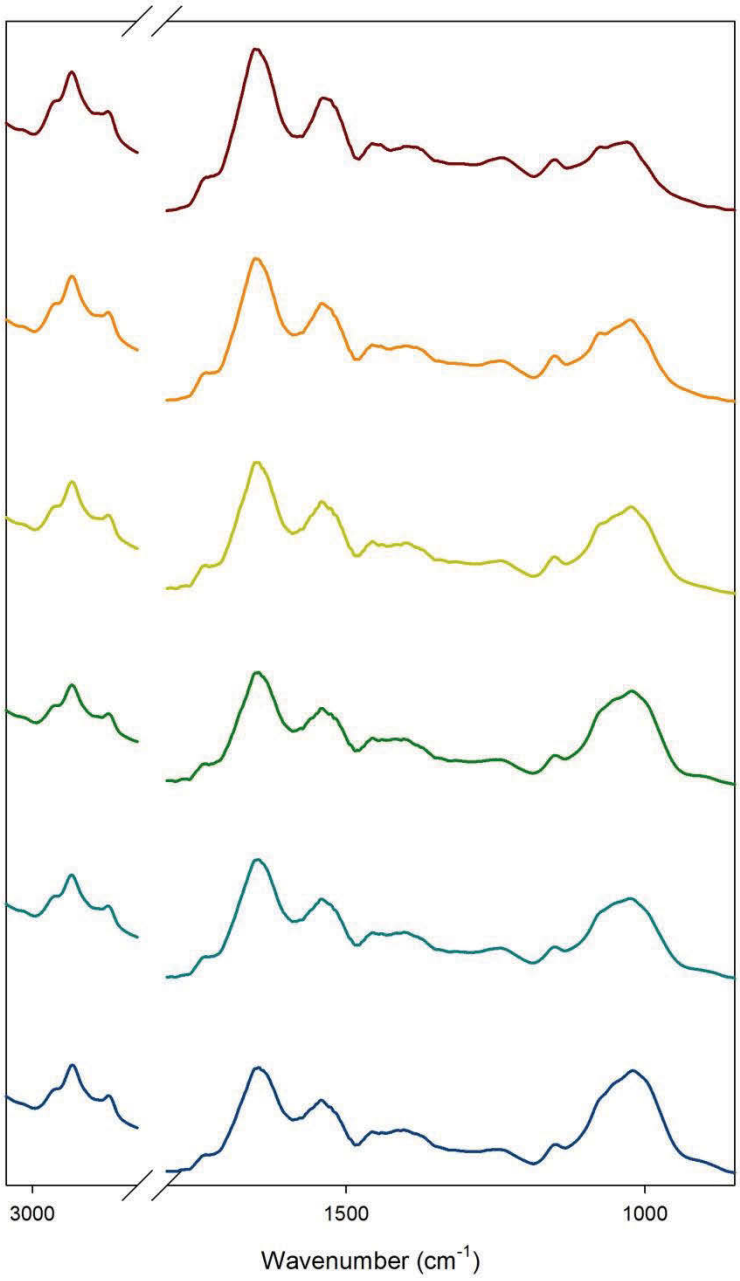

Figure A1.1: Spectra for clade A exposed to elevated light (top to bottom; T0-T5). Spectra are averages (n=12).

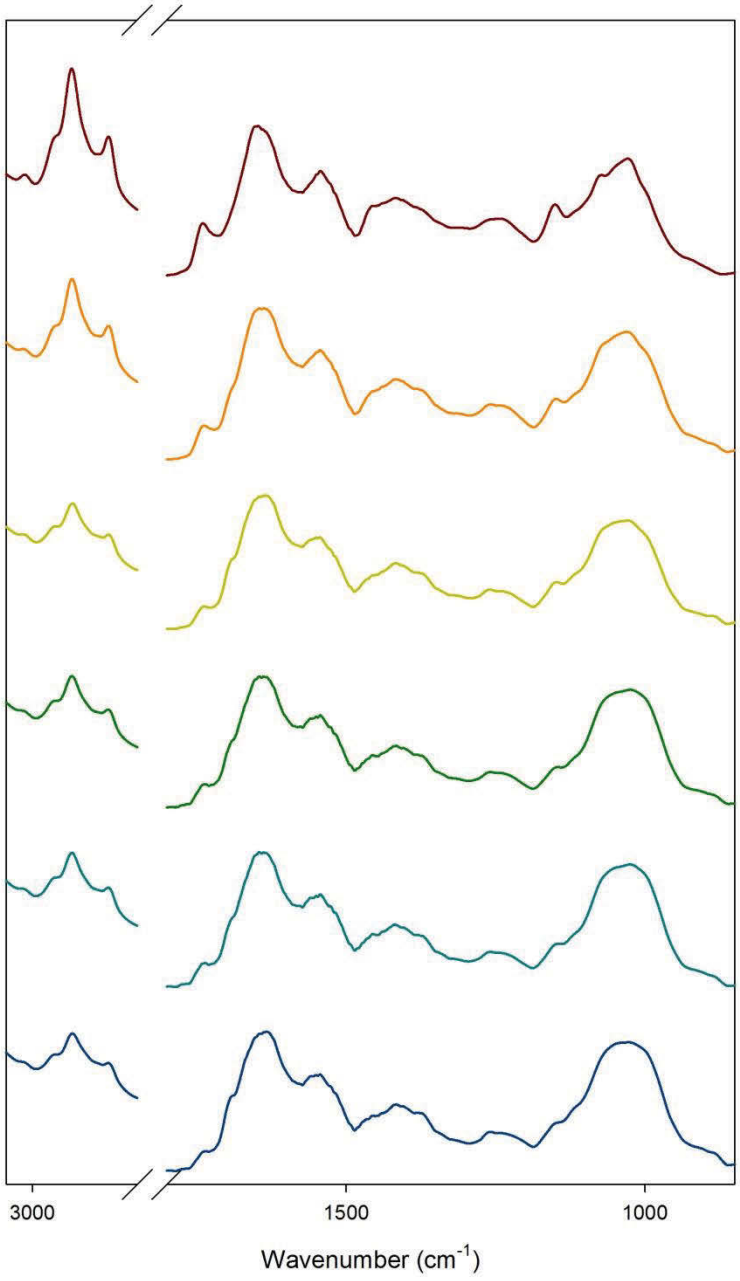

Figure A1.2: Spectra for clade F exposed to elevated light (top to bottom; T0-T5). Spectra are averages (n=12).

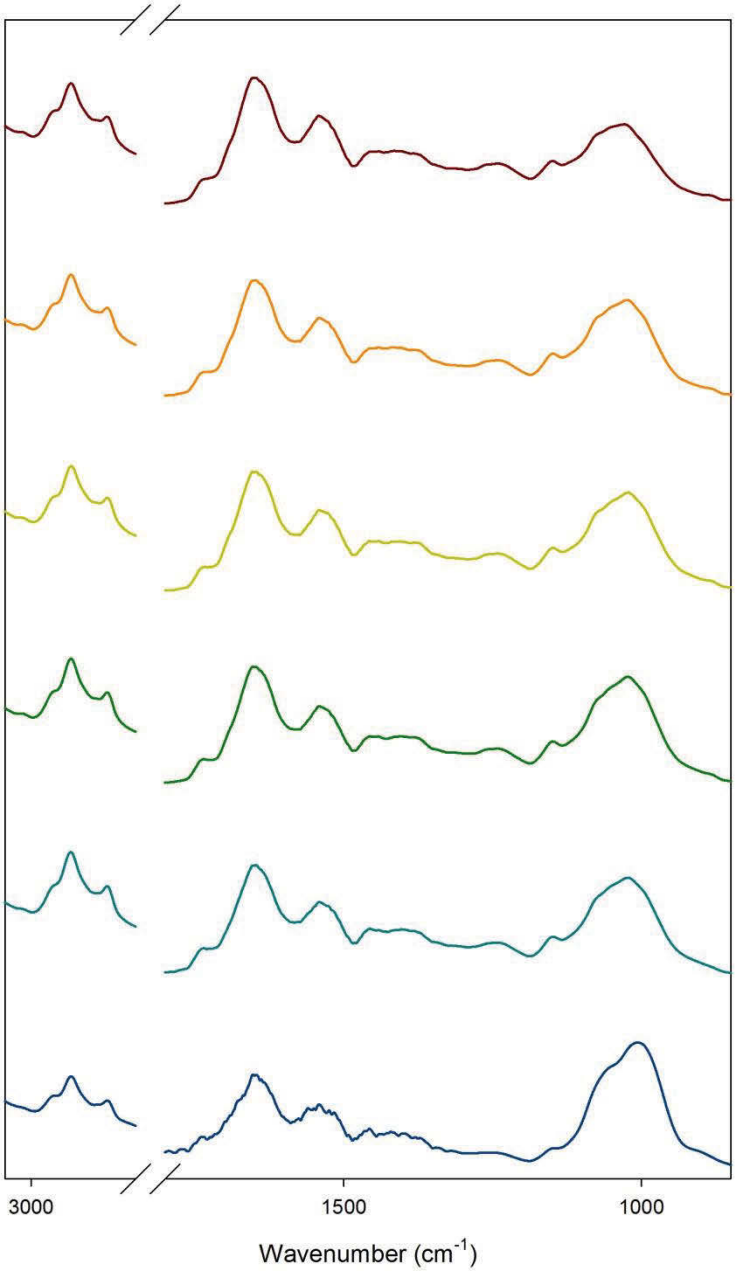

Figure A1.3: Spectra for clade A exposed to elevated temperature (top to bottom; T0-T5). Spectra are averages (n=12).

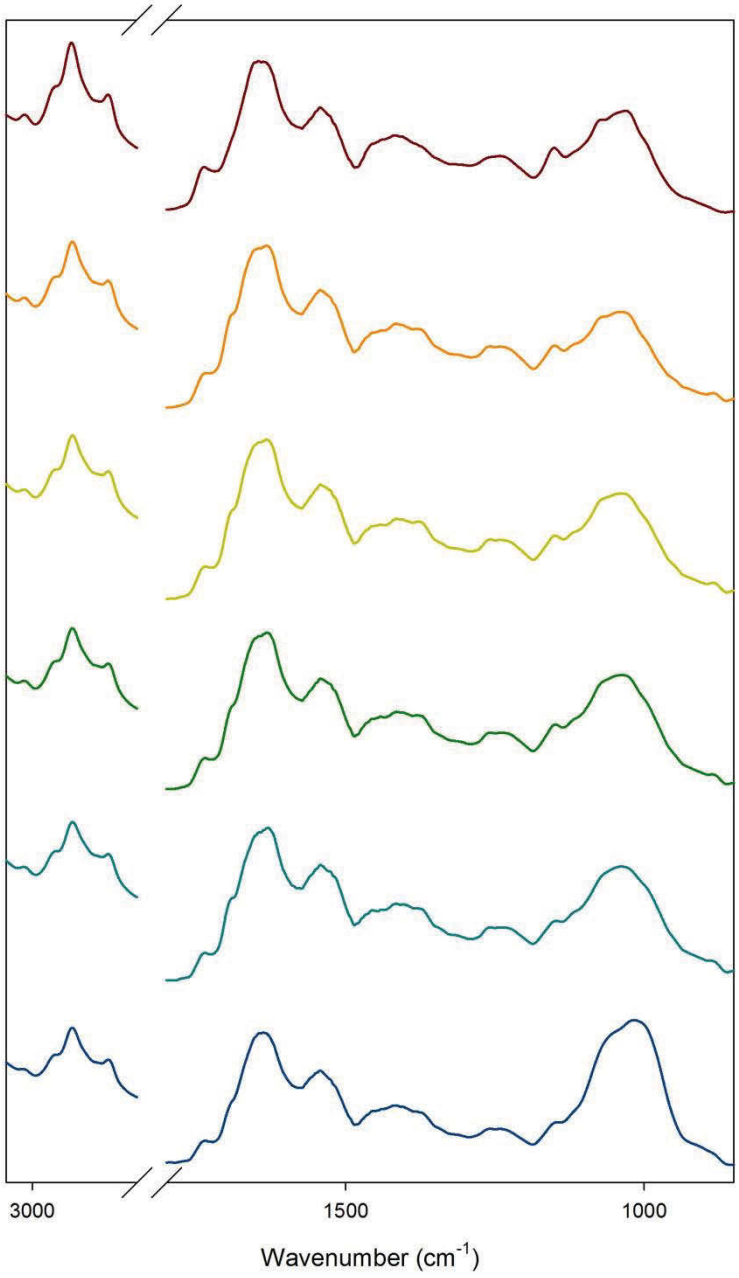

Figure A1.4: Spectra for clade F exposed to elevated temperature (top to bottom; T0-T5). Spectra are averages (n=12).

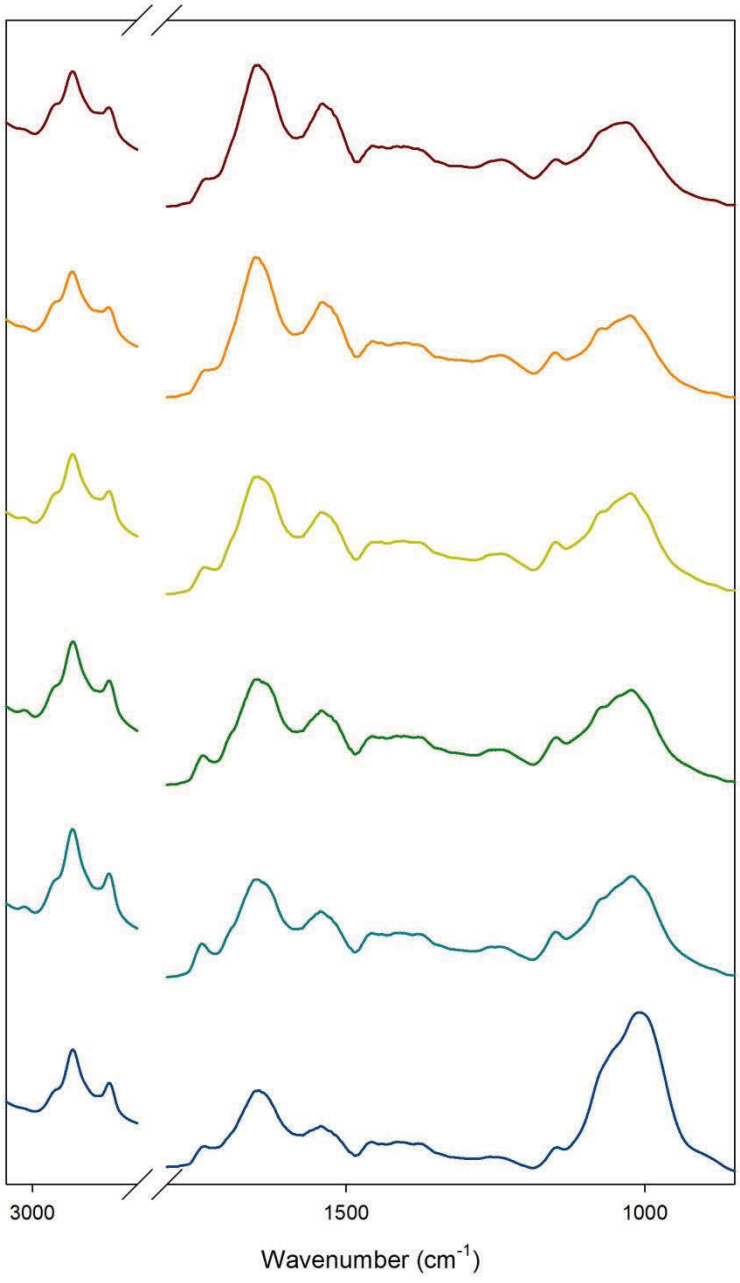

Figure A1.5: Spectra for clade A exposed to a combination of elevated light and temperature (top to bottom; T0-T5). Spectra are averages (n=12).

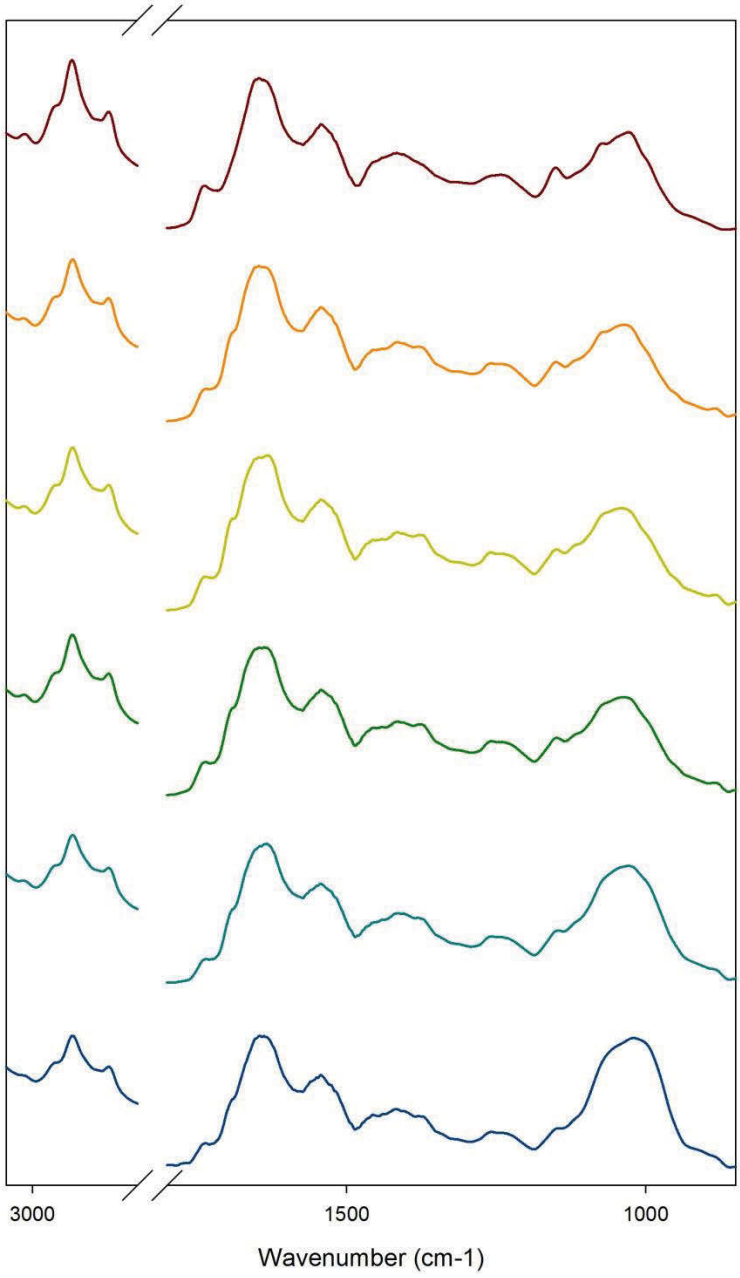

Figure A1.6: Spectra for clade F exposed to a combination of elevated light and temperature (top to bottom; T0-T5). Spectra are averages (n=12).

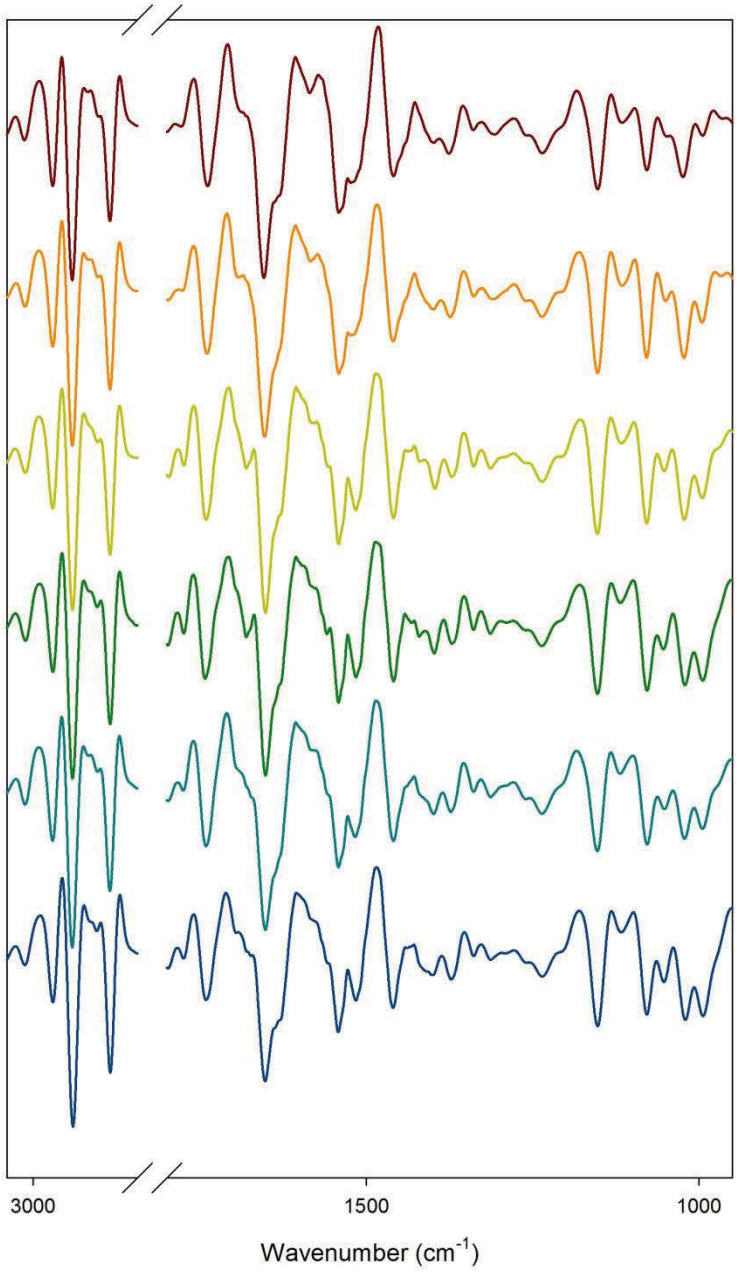

Figure A1.7: 2nd derivative spectra for clade A exposed to elevated light (top to bottom; T0-T5). Spectra are averages (n=12).

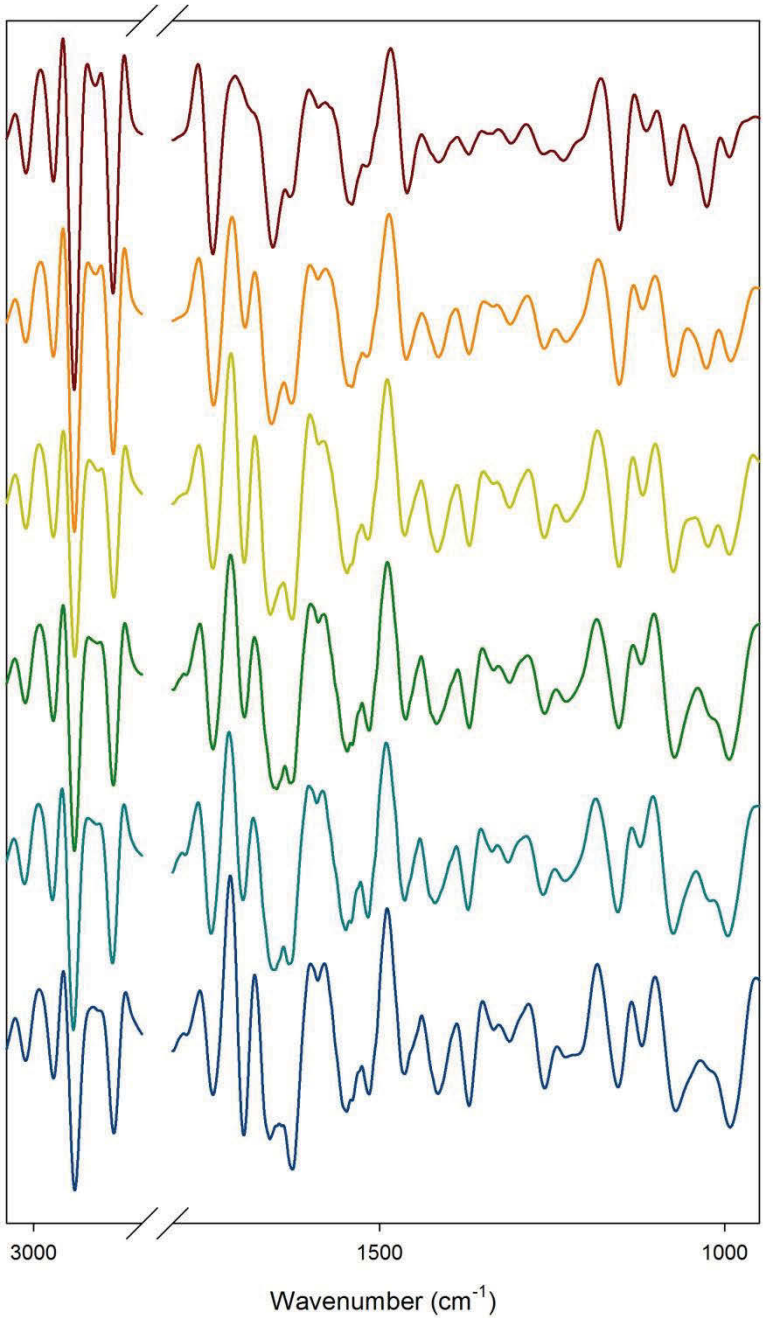

Figure A1.8: 2nd derivative spectra for clade F exposed to elevated light (top to bottom; T0-T5). Spectra are averages (n=12).

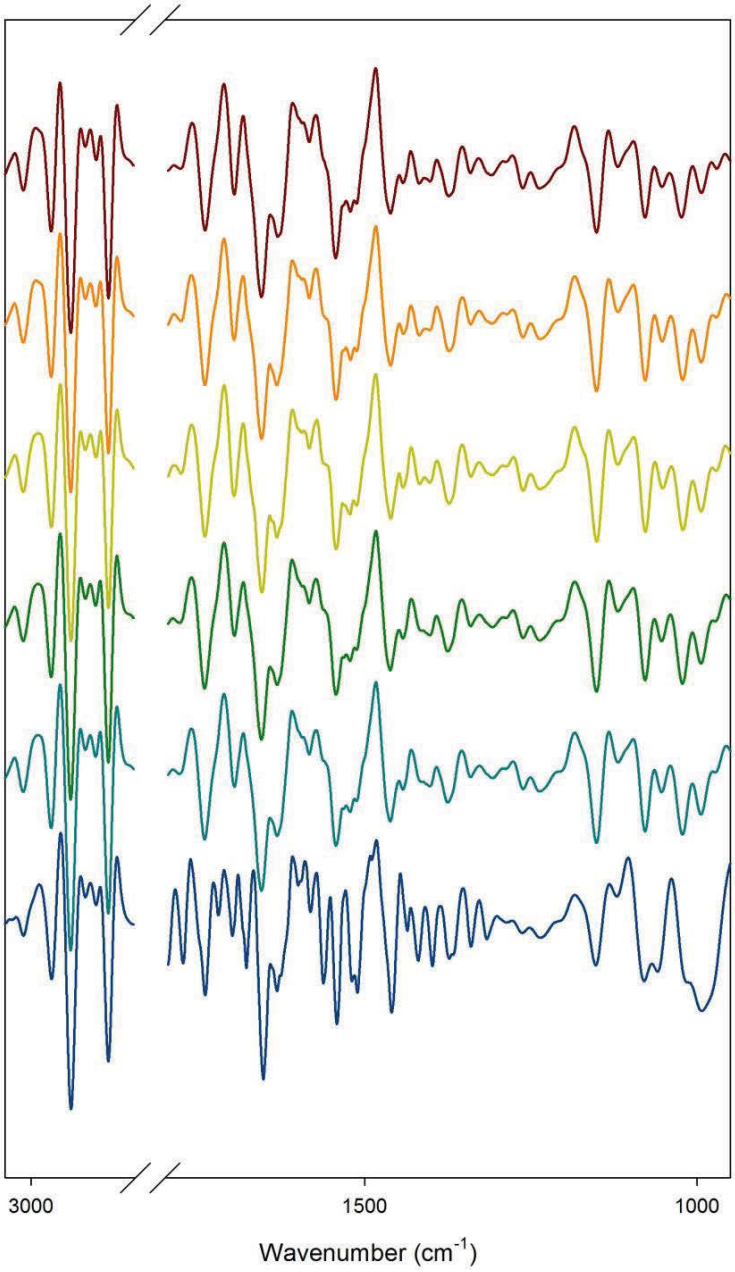

Figure A1.9: 2nd derivative spectra for clade A exposed to elevated temperature (top to bottom; T0-T5). Spectra are averages (n=12).

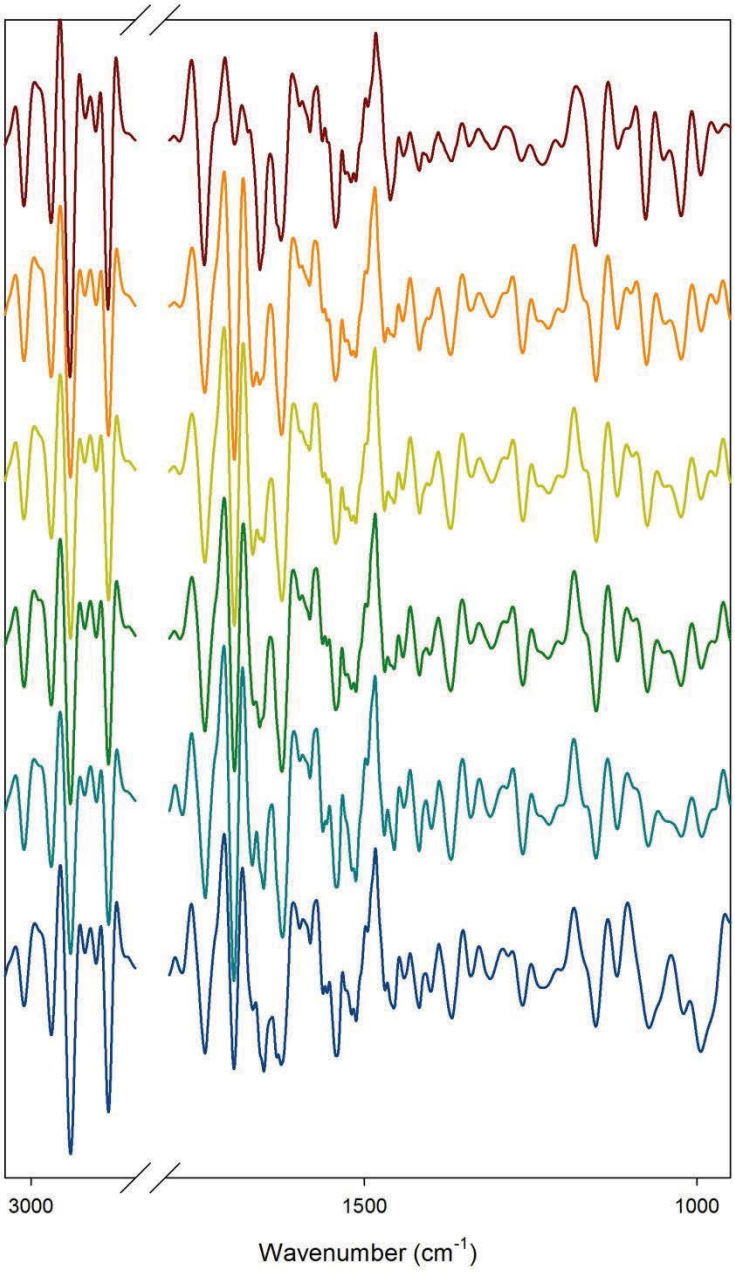

Figure A1.10: 2nd derivative spectra for clade F exposed to elevated temperature (top to bottom; T0-T5). Spectra are averages (n=12).

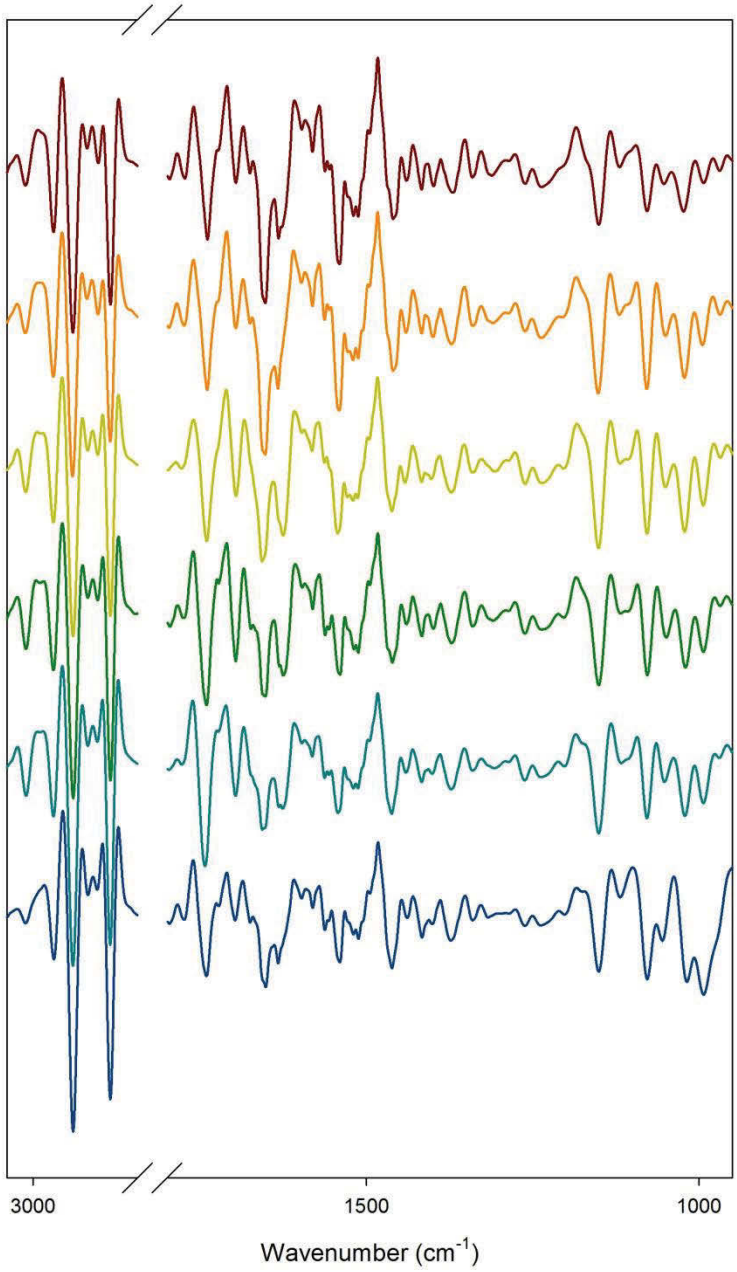

Figure A1.11: 2nd derivative spectra for clade A exposed to a combination of elevated light and temperature (top to bottom; T0-T5). Spectra are averages (n=12).

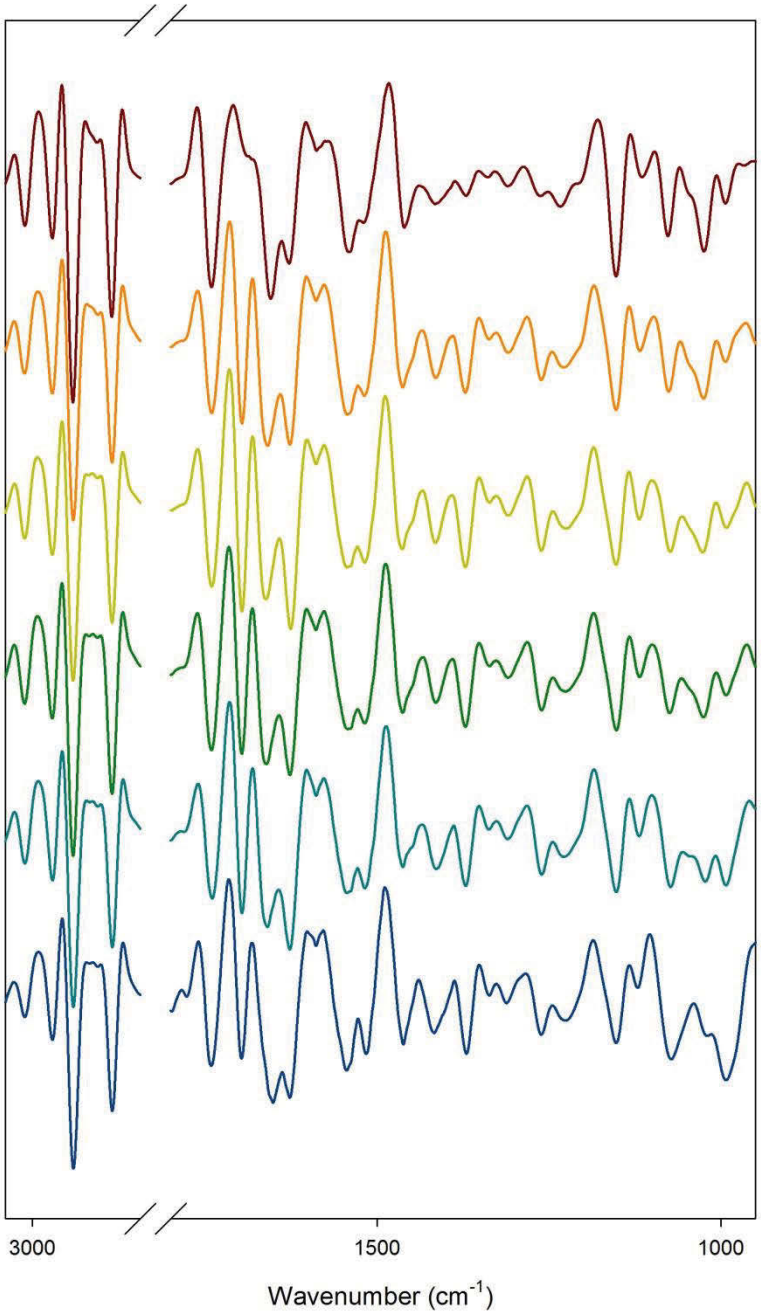

Figure A1.12: 2nd derivative spectra for clade F exposed to a combination of elevated light and temperature (top to bottom; T0-T5). Spectra are averages (n=12).

Appendix 2: Collated rmANOVA results for data presented in Chapter 4

Table A2.1: rmANOVA groups for clade A maximum quantum yield ($p<0.05$).

Treatment	T0	T1	T2	T3	T4	T5
Control	a	a	a	a		a
Elevated light	a	b	b	b	b	b
Elevated temperature	a	b	ab	ab	ab	ab
Elevated light and temperature	a	b	b	b	b	b

Table A2.2: rmANOVA groups for clade F maximum quantum yield ($p<0.05$).

Treatment	T0	T1	T2	T3	T4	T5
Control	a	a	a	a		a
Elevated light	a	a	a	a	a	b
Elevated temperature	a	a	a	a	a	a
Elevated light and temperature	a	a	a	a	ab	b

Table A2.3: rmANOVA groups for clade A protein content ($p<0.05$).

Treatment	T0	T1	T2	T3	T4	T5
Control	a	a	a	a		a
Elevated light	a	a	ab	b	ab	b
Elevated temperature	a	a	a	a	a	a
Elevated light and temperature	a	a	ab	ab	b	b

Table A2.4: rmANOVA groups for clade F protein content ($p<0.05$).

Treatment	T0	T1	T2	T3	T4	T5
Control	a	a	a	a		a
Elevated light	a	a	a	a	a	a
Elevated temperature	a	a	a	a	a	a
Elevated light and temperature	a	a	a	a	a	a

Table A2.5: rmANOVA groups for clade A carbohydrate content ($p<0.05$).

Treatment	T0	T1	T2	T3	T4	T5
Control	a	a	a	a		a
Elevated light	a	a	b	b	b	b
Elevated temperature	a	a	ab	ab	b	b
Elevated light and temperature	a	a	ab	ab	ab	b

Table A2.6: rmANOVA groups for clade F carbohydrate content ($p<0.05$).

Treatment	T0	T1	T2	T3	T4	T5
Control	a	a	a	a		a
Elevated light	a	a	ab	ab	ab	a
Elevated temperature	a	ab	a	a	a	a
Elevated light and temperature	a	a	a	a	a	a

Table A2.7: rmANOVA groups for clade A lipid content ($p<0.05$).

Treatment	T0	T1	T2	T3	T4	T5
Control	a	a	a	a		a
Elevated light	a	a	a	a	a	a
Elevated temperature	a	a	a	a	a	a
Elevated light and temperature	a	a	a	a	ab	a

Table A2.8: rmANOVA groups for clade F lipid content ($p<0.05$).

Treatment	T0	T1	T2	T3	T4	T5
Control	a	a	a	a		a
Elevated light	a	a	a	a	a	a
Elevated temperature	a	ab	b	b	b	b
Elevated light and temperature	a	a	a	a	a	b

Table A2.9: rmANOVA groups for clade A phosphorylated compounds content ($p<0.05$).

Treatment	T0	T1	T2	T3	T4	T5
Control	a	a	a	a		a
Elevated light	a	b	ab	ab	ab	b
Elevated temperature	a	a	a	a	a	a
Elevated light and temperature	a	ab	ab	ab	ab	b

Table A2.10: rmANOVA groups for clade F phosphorylated compounds content ($p<0.05$).

Treatment	T0	T1	T2	T3	T4	T5
Control	a	a	a	a		a
Elevated light	a	a	a	a	a	a
Elevated temperature	a	a	a	a	a	b
Elevated light and temperature	a	a	a	a	a	a

Table A2.11: rmANOVA groups for clade A unsaturated: saturated lipid content ratio ($p<0.05$).

Treatment	T0	T1	T2	T3	T4	T5
Control	a	a	a	a		a
Elevated light	a	a	b	b	b	b
Elevated temperature	a	a	a	a	a	b
Elevated light and temperature	a	a	a	b	b	a

Table A2.12: rmANOVA groups for clade F unsaturated: saturated lipid content ratio ($p<0.05$).

Treatment	T0	T1	T2	T3	T4	T5
Control	a	a	a	a		a
Elevated light	a	b	bc	c	c	c
Elevated temperature	a	b	b	b	c	c
Elevated light and temperature	a	ab	b	b	c	c

Table A2.13: rmANOVA groups for clade A lipid branching ($p<0.05$).

Treatment	T0	T1	T2	T3	T4	T5
Control	a	a	a	a		a
Elevated light	a	a	a	ab	b	a
Elevated temperature	a	a	ab	b	b	a
Elevated light and temperature	a	a	b	b	c	c

Table A2.14: rmANOVA groups for clade F lipid branching ($p<0.05$).

Treatment	T0	T1	T2	T3	T4	T5
Control	a	a	a	a		a
Elevated light	a	a	ab	ab	ab	b
Elevated temperature	a	a	a	a	a	a
Elevated light and temperature	a	ab	ab	ab	ab	b

Table A2.15: rmANOVA groups for clade A lipid disorder ($p<0.05$).

Treatment	T0	T1	T2	T3	T4	T5
Control	a	a	a	a		a
Elevated light	a	a	a	a	a	a
Elevated temperature	a	a	a	a	a	a
Elevated light and temperature	a	a	a	a	b	a

Table A2.16: rmANOVA groups for clade F lipid disorder ($p<0.05$).

Treatment	T0	T1	T2	T3	T4	T5
Control	a	a	a	a		a
Elevated light	a	b	b	b	b	c
Elevated temperature	a	b	b	b	b	ab
Elevated light and temperature	a	b	b	b	bc	c

Appendix 3: Collated spectra analysed in Chapter 5

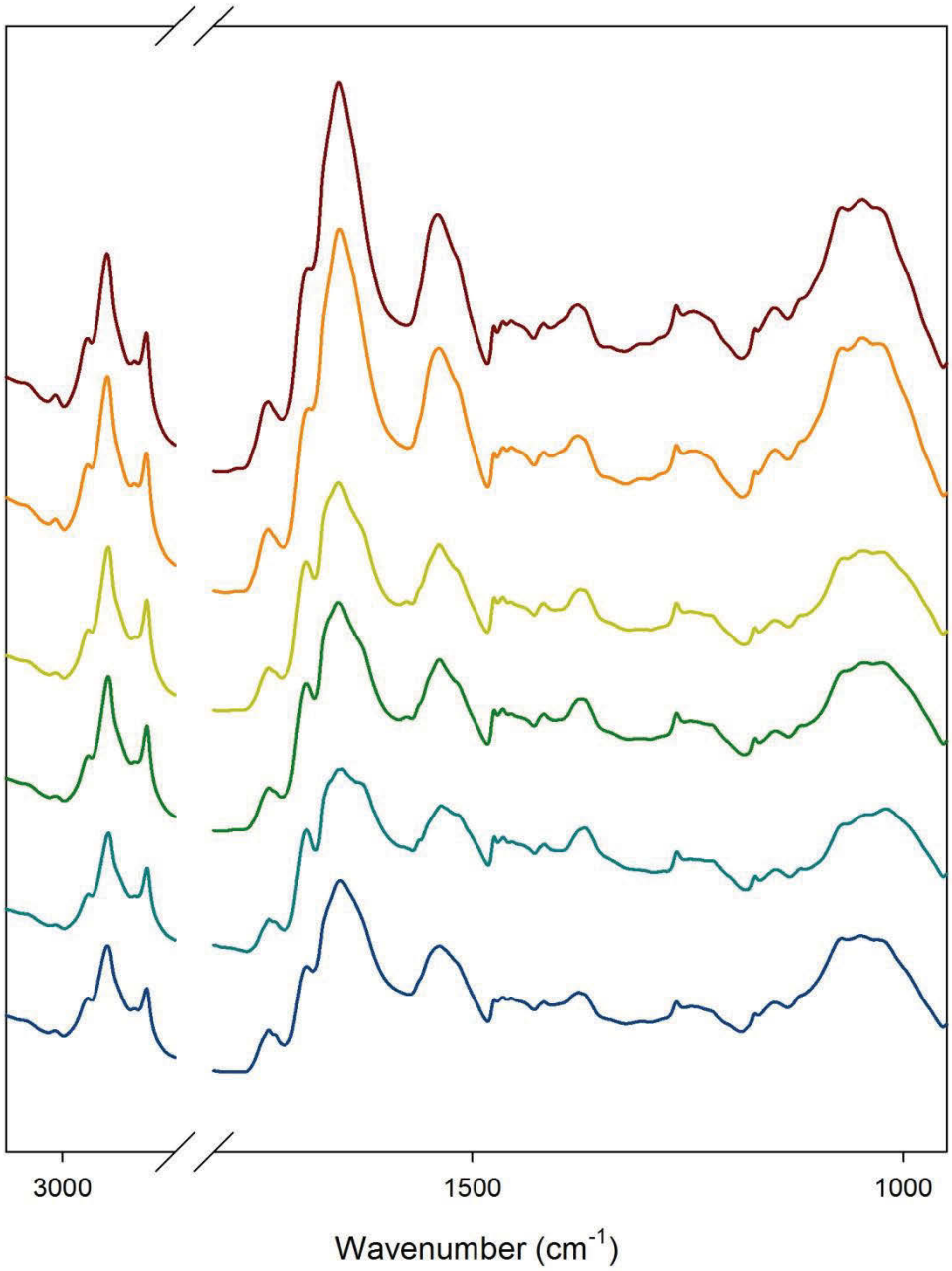

Figure A3.1: Spectra for Clade A exposed to a gradual increase in temperature (from top to bottom; T0-T5). Spectra are averages (n=16).

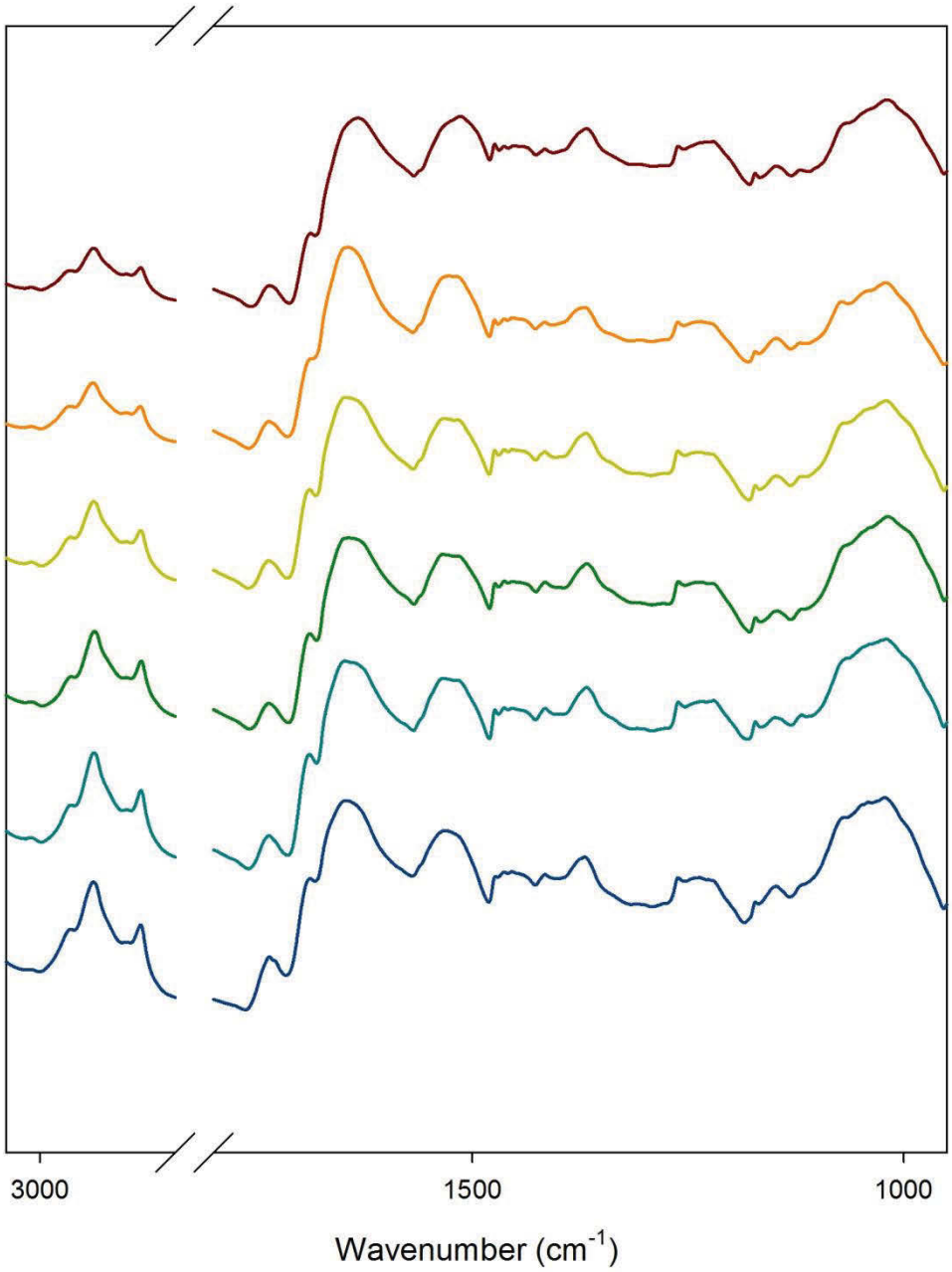

Figure A3.2: Spectra for Clade F exposed to a gradual increase in temperature (from top to bottom; T0-T5). Spectra are averages (n=16).

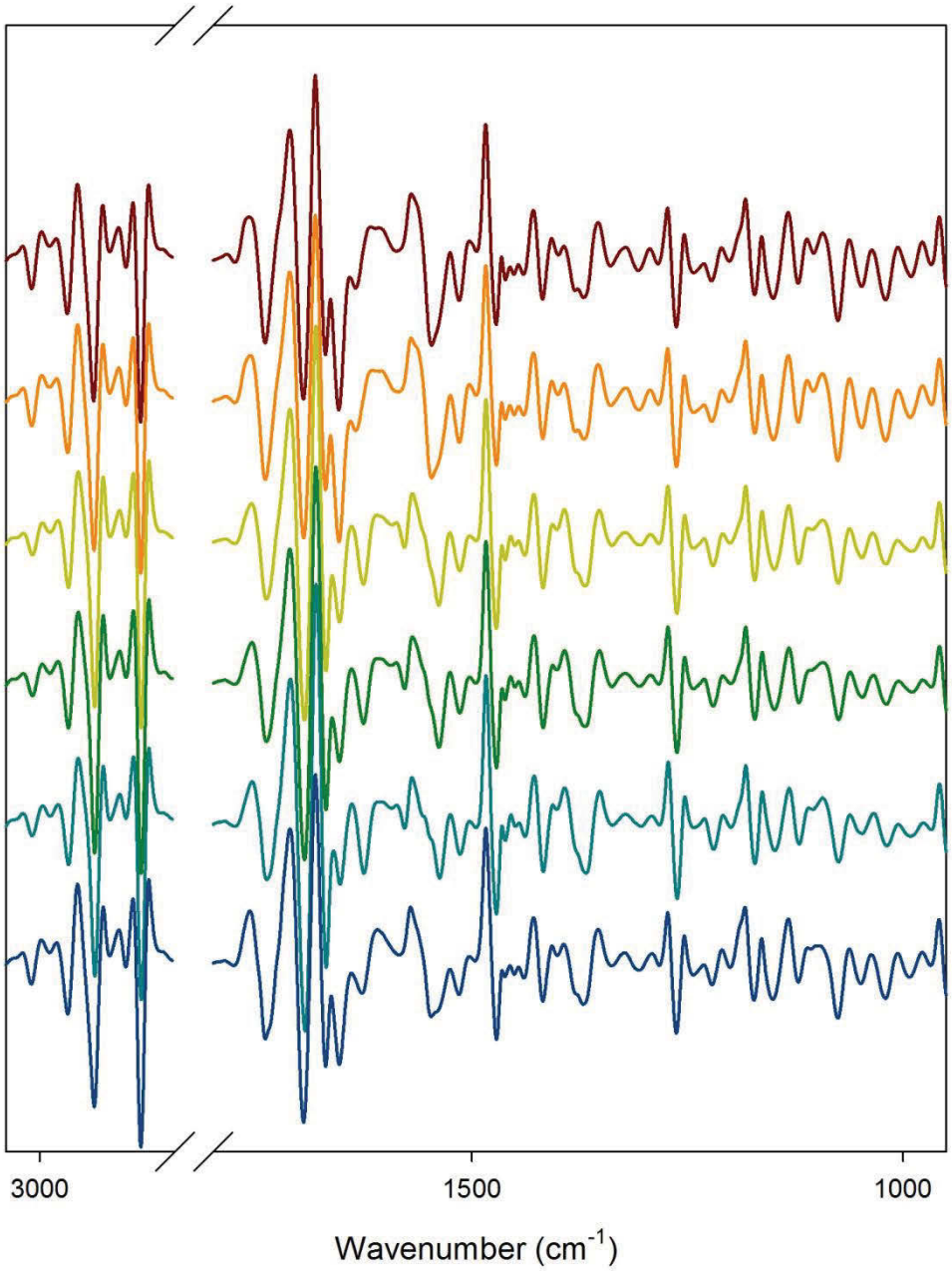

Figure A3.3: 2nd derivative spectra for Clade A exposed to a gradual increase in temperature (from top to bottom; T0-T5). Spectra are averages (n=16).

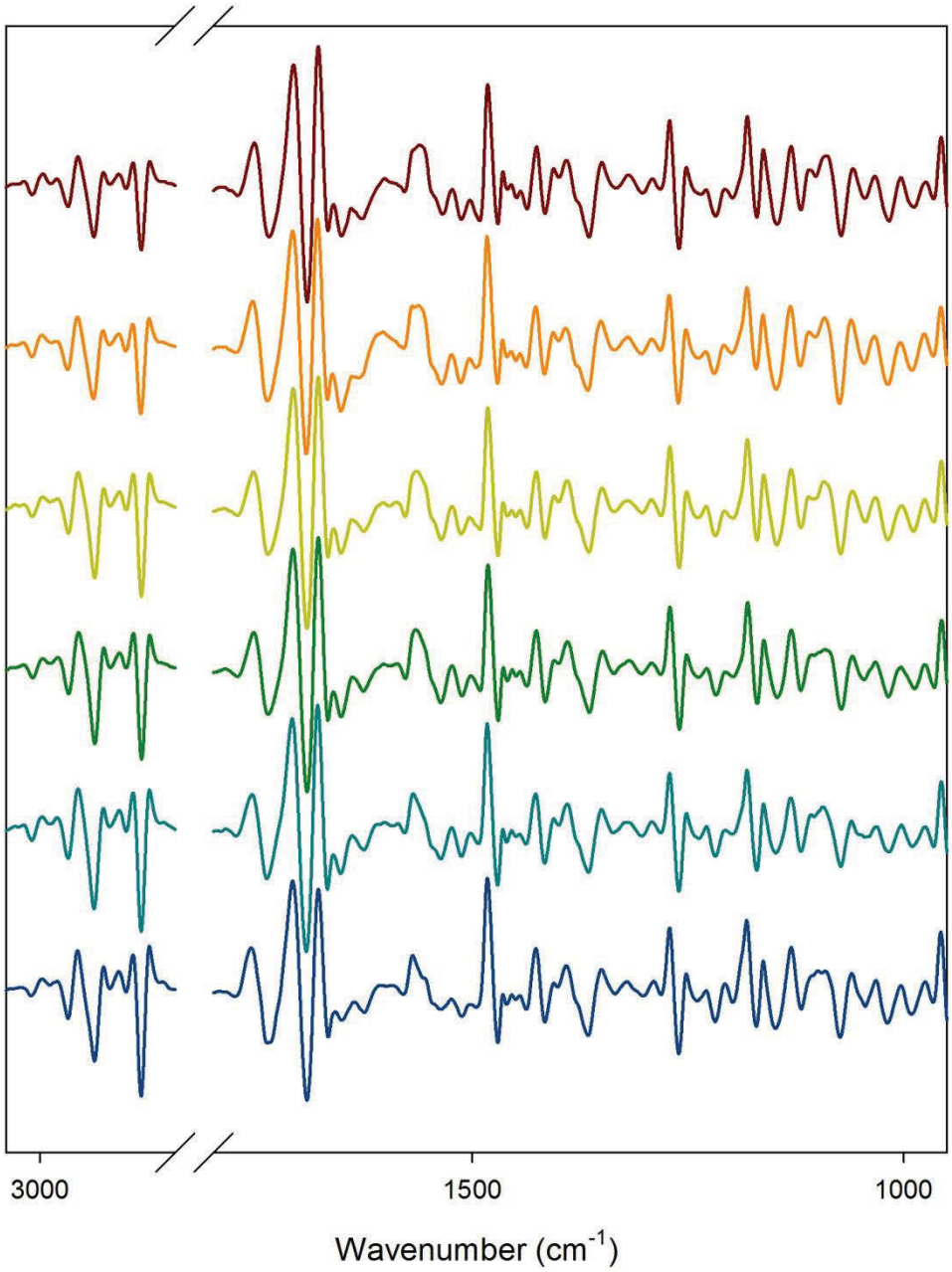

Figure A3.4: 2nd derivative spectra for clade F exposed to a gradual increase in temperature (from top to bottom; T0-T5). Spectra are averages (n=16).

Appendix 4: Collated rmANOVA results for data presented in Chapter 5

Table A4.1: rmANOVA groups for clade A cells subjected to gradual increase in temperature.

	T0	T1	T2	T3	T4	T5
F_v/F_m	a	a	a	a	b	b
Protein	a	a	a	a	a	a
Carbohydrate	a	a	a	a	a	a
Phosphorylated compounds	a	a	a	ab	a	b
Lipid	a	a	ab	b	b	ab
Lipid saturation	a	a	b	b	b	a
Lipid branching	a	a	b	b	b	a
Lipid disorder	a	a	ab	b	b	ab

Table A4.2: rmANOVA groups for clade F cells subjected to gradual increase in temperature.

	T0	T1	T2	T3	T4	T5
F_v/F_m	a	a	ab	a	ab	a
Protein	a	a	a	a	a	a
Carbohydrate	a	a	a	a	a	a
Phosphorylated compounds	a	a	a	a	a	b
Lipid	a	a	a	a	a	b
Lipid saturation	a	a	a	a	a	a
Lipid branching	a	a	ab	a	a	a
Lipid disorder	a	a	a	a	a	a